2006

Power system dynamic security analysis via decoupled time domain simulation and trajectory optimization

Dan Yang
Iowa State University

Power system dynamic security analysis via decoupled time domain simulation and trajectory optimization

by

Dan Yang

A dissertation submitted to the graduate faculty
in partial fulfillment of the requirements for the degree of
DOCTOR OF PHILOSOPHY

Major: Electrical Engineering

Program of Study Committee:

Venkataramana Ajjarapu, Major Professor
James D. McCalley
Zhengdao Wang
Zhijun Wu
Arne Hallam

Iowa State University

Ames, Iowa

2006

ProQuest Information and Learning Company
300 North Zeeb Road
P.O. Box 1346
Ann Arbor, MI 48106-1346

To my grandma

君子不器

TABLE OF CONTENTS

CHAPTER 1 INTRODUCTION 1

1.1 Background 1

1.1.1 Electric Power Industry 2

1.1.2 Power System Stability and Security 3

1.2 Literature Review 5

1.2.1 Static Analysis 5

1.2.2 Instability Identification for Small Disturbances 6

1.2.3 Control Strategies for Small Disturbances 9

1.2.4 Instability Identification for Large Disturbances 11

1.2.5 Control Strategies for Large Disturbances 12

1.3 Motivation 15

1.4 Organization 22

CHAPTER 2 POWER SYSTEM MODEL 23

2.1 Introduction 23

2.2 Power Flow 23

2.3 Synchronous Generator Model 25

2.4 Excitation System Model 26

2.5 Governor Model 27

2.6 Load Model 28

2.7 Power System DAE Model 29

CHAPTER 3 DECOUPLED TIME DOMAIN SIMULATION 31

3.1 Introduction 31

3.2 Conventional Explicit and Implicit Methods and Numerical Stability 32

3.2.1 Explicit Method 33

3.2.2 Implicit Method 34

3.2.3 Numerical Stability Analysis: Stiffness and A-Stability 34

3.3 Decoupled Method for ODE 38

3.4 Decoupled Method for DAE 42

3.4.1 Decoupled Forward Euler-Trapezoidal Method for DAE 42

3.4.2 Identification of Stiff Invariant Subspace 44

3.5 Numerical Examples 45

3.5.1 New England System Simulation Results 45

3.5.2 IEEE 118-bus System Simulation Results 50

3.6 Summary 54

CHAPTER 4 TRAJECTORY OPTIMIZATION 56

4.1 Introduction 56

4.1.1 Parameter Optimization Problems 57

4.1.2 Trajectory Optimization Problems 62

4.2 Formulation 64

4.3 Extended Penalty Function Equivalence 70

4.4 Numerical Solution of Boundary Value Problem 75

4.5 Numerical Examples 78

4.5.1 Trajectory Optimization Results for Simple Mathematical Example 78

4.5.2 Trajectory Optimization Results for 2-Bus System 80

4.5.3 Trajectory Optimization Results for 3-Bus System 92

4.5.4 Trajectory Optimization Results for New England System 101

4.5.5 Trajectory Optimization Results for IEEE 118-Bus System 110

4.6 Summary 115

CHAPTER 5 CONCLUSION 116

5.1 Contributions 116

5.2 Further Research Directions 117

REFERENCES 118

APPENDIX A: TRAJECTORY OPTIMIZATION WITH Vref CONTROL 132

APPENDIX B: SYSTEM DATA 134

ACKNOWLEDGEMENTS 149

LIST OF FIGURES

Fig. 1-1. Classification of Power System Stability 4

Fig. 1-2. Possible System Dynamic Responses after Disturbance 16

Fig. 1-3. Possible System Trajectories after Disturbance 17

Fig. 1-4. Dynamic Security Analysis Framework 21

Fig. 2-1. IEEE type DC-1 Excitation System 27

Fig. 2-2. Simplified Speed Governor and Prime Mover 28

Fig. 3-1. The Simulation Results by Explicit and Implicit Methods 36

Fig. 3-2. Stability Domain of Forward Euler and Trapezoidal Methods 37

Fig. 3-3. Case A Simulation Result by Forward Euler Method 46

Fig. 3-4. Case A Simulation Results by Decoupled and Implicit Methods 47

Fig. 3-5. Case B Simulation Results by Decoupled and Implicit Methods 48

Fig. 3-6. Case C Simulation Results by Decoupled and Implicit Methods 49

Fig. 3-7. Case D Simulation Result by Forward Euler Method 52

Fig. 3-8. Case D Simulation Results by Decoupled and Implicit Methods 53

Fig. 3-9. Case E Simulation Results by Decoupled and Implicit Methods 53

Fig. 3-10. Case F Simulation Results by Decoupled and Implicit Methods 54

Fig. 4-1. Trial and Error Method 60

Fig. 4-2. Model Predictive Control 61

Fig. 4-3. Power System Dynamical Optimization Concept 65

Fig. 4-4. Conceptual Dynamical Optimization Control Action 66

Fig. 4-5. Penalty Functions 73

Fig. 4-6. Optimal State Trajectories for Simple Mathematical Example 79

Fig. 4-7. Optimal Control Trajectory for Simple Mathematical Example 80

Fig. 4-8. Two-Bus Power System Diagram 81

Fig. 4-9. Trajectories after Disturbance without Control 82

Fig. 4-10. Optimal Trajectories with Reactive Power Compensation 86

Fig. 4-11. Constrained Optimal Trajectories with Reactive Power Compensation 88

Fig. 4-12. Optimal Trajectories with Delayed Reactive Power Compensation 89

Fig. 4-13. Control Amount with respect to Control Delay 90

Fig. 4-14. Optimal Trajectories with Load Control 91

Fig. 4-15. Optimal Trajectories with Combined Control 92

Fig. 4-16. Three-Bus Power System Diagram 93

Fig. 4-17. Trajectories after Disturbance without Control 93

Fig. 4-18. Bus Voltage Trajectories with Reactive Power Compensation 94

Fig. 4-19. Generator Relative Angle with Reactive Power Compensation 95

Fig. 4-20. Reactive Power Compensation Trajectory 95

Fig. 4-21. Bus Voltage Trajectories with Load Control 96

Fig. 4-22. Generator Relative Angle with Load Control 97

Fig. 4-23. Load Control Trajectory 97

Fig. 4-24. Bus Voltage Trajectories with Combined Control 98

Fig. 4-25. Generator Relative Angle with Combined Control 99

Fig. 4-26. Reactive Power Compensation Trajectory 99

Fig. 4-27. Load Control Trajectory 100

Fig. 4-28. Voltage Trajectory after Disturbance without Control 101

Fig. 4-29. Generator Angle Trajectory after Disturbance without Control 102

Fig. 4-30. Bus Voltage Trajectory with Reactive Power Compensation 104

Fig. 4-31. Generator Relative Angle Trajectory with Reactive Power Compensation 105

Fig. 4-32. Optimal Reactive Power Support Trajectories 105

Fig. 4-33. Optimal Reactive Power Support Trajectories 106

Fig. 4-34. Bus Voltage Trajectory 107

Fig. 4-35. Generator Relative Angle Trajectory 107

Fig. 4-36. Optimal Reactive Power Support Trajectories 108

Fig. 4-37. Optimal Reactive Power Support Trajectories 108

Fig. 4-38. Optimal Load Control Trajectories 109

Fig. 4-39. Bus Voltage Trajectory after Disturbance 111

Fig. 4-40. Generator Relative Angle Trajectory after Disturbance 111

Fig. 4-41. Optimal Bus Voltage Trajectory 112

Fig. 4-42. Optimal Generator Relative Angle Trajectory 113

Fig. 4-43. Optimal Reactive Power Compensation Trajectories 113

Fig. 4-44. Optimal Load Control Trajectories 114

Fig. A-1. Bus Voltage Trajectories with Vref Control 132

Fig. A-2. Generator Relative Angle with Vref Control 133

Fig. A-3. Generator Vref Control Trajectories 133

Fig. B-1. New England 39-Bus System One-Line Diagram..... 134

LIST OF TABLES

Table 3-1 Computational Time Comparison I 47

Table 3-2 Computational Time Comparison II 49

Table 3-3 Computational Time Comparison III 50

Table 3-4 The Summary of New England System Results 50

Table 3-5 The Summary of IEEE 118-bus System Results 54

Table 4-1 Control Amount with respect to Delay 89

Table 4-2 Comparison of Control Strategies 91

Table 4-3 Maximum Control Amount with respect to Delay 100

Table 4-4 Maximum Control Amount at All Buses 104

Table 4-5 Maximum Reactive Control Amount with respect to Delay 110

Table 4-6 Maximum Load Control Amount with respect to Delay 110

Table 4-7 Maximum Control Amount with respect to Delay 114

Table B-1 New England System Power Flow Data I 135

Table B-2 New England System Power Flow Data II 136

Table B-3 New England System Generator Data I 137

Table B-4 New England System Generator Data II 137

Table B-5 IEEE 118-Bus System Power Flow Data I 138

Table B-6 IEEE 118-Bus System Power Flow Data II 141

Table B-7 IEEE 118-Bus System Generator Data I 145

Table B-8 IEEE 118-Bus System Generator Data II 146

CHAPTER 1 INTRODUCTION

1.1 Background

Modern power system interconnections have become increasingly complex over the past hundred years. Electrical power and energy engineering has continuously evolved in terms of efficiency, economies of scale, and technology. As electric power industries change from vertically integrated utilities to electricity markets, challenges for the basic function of the industries – to produce and to deliver power safely and reliably – in this demanding business environment are being raised by new market structures and new technologies. Since security continues to be a basic requirement in power systems operation, power system stability and security analysis remains as an important research area.

Electric power engineering is a well established and mature discipline. Current developments in the field borrow from new technology developments in a number of associated sub-disciplines, including control theory, applied mathematics, economics, probability theory and risk analysis, computer engineering, software engineering, data structures, electronics, sensor technology, etc [1]. This dissertation is intended to solve power engineering problems in the area of stability and security through the application of applied mathematics.

1.1.1 *Electric Power Industry*

The commercial use of electricity began in the late nineteenth century when electric power was supplied by small isolated power generation companies. Over the past one hundred years, electric power has evolved into one of the largest industries in the world with interconnected systems of generation, transmission, and distribution. Among the incentives for interconnection in large geographic areas are scale of economy and supply redundancy. As power systems become larger in size, the increasing complexity of the power industry results in challenging problems with respect to power system security.

During the past few decades, power industries all over the world have experienced several major system failures. In the 1965 Northeast blackout in North America, east coast interconnection separated into several disjoint areas and 30 million people lost power [2]. Other major system failures occurred in New York, on the west coast, and in the Midwest United States. During the August 14, 2003 Northeast blackout in North America, power supply for 50 million people was interrupted, with financial losses estimated to be between 4 billion and 6 billion U.S. dollars [3, 4]. In the same year, system failures also occurred in several European countries, and one of them affected even more people than the one in North America [5].

Another significant advancement in the power industry is the development of the electricity market. The power industry has traditionally been dominated by vertically integrated monopolies. Since the 1990s, competition and market-based operation have been gradually introduced by deregulation of the power industry. This restructuring also brings in an institutional change in the industry [6]. Independent System Operator (ISO) is established

to monitor system operation under market mechanism. The service for the system security may be procured from the market operation. In the long run, market forces may drive new technology serving system security for the power industry.

1.1.2 *Power System Stability and Security*

In general, power system stability is similar to the stability of any dynamic system, and has fundamental mathematical underpinnings [7]. Power system stability is a single problem; it is still useful to provide physically motivated classification of power system stability. Power system stability can be classified into several sub-areas based on the following consideration [8]:

- The physical nature of the instability problems: rotor angle stability, frequency stability and voltage stability
- The size of the disturbance considered: small-disturbance stability and large-disturbance stability
- The time span needed to be taken into consideration: short-term stability and long-term stability

The classification of power system stability according to different criteria is shown in Fig. 1-1 in the IEEE/CIGRE report [7].

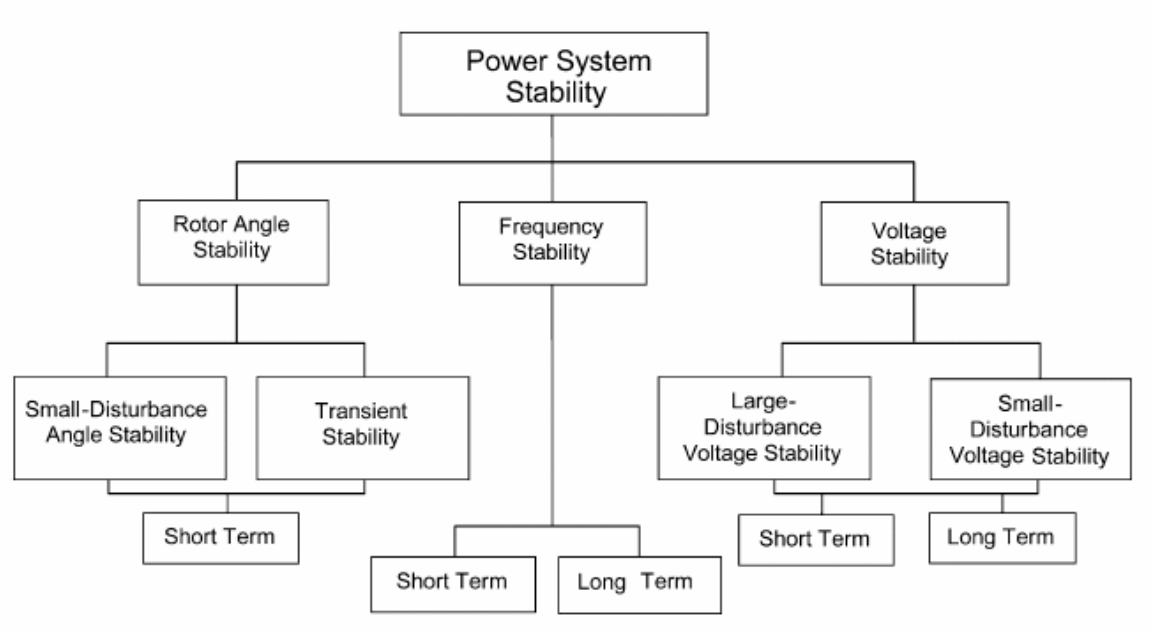

Fig. 1-1. Classification of Power System Stability

The classification of power system stability has been based on a number of diverse considerations, making it difficult to select clearly distinct categories and to provide rigorous definitions, and overlap may occur among different stability definitions. Thus, it is important to keep in mind overall stability of the system. The proposed definition of power system stability in [7] is the following:

- "Power system stability is the ability of an electric power system, for a given initial operating condition, to regain a state of operating equilibrium after being subjected to a physical disturbance, with most system variables bounded so that practically the entire system remains intact."

Security of a power system refers to the degree of risk in its ability to survive imminent disturbances or contingencies without interruption of customer service. Security analysis relates to determination of the robustness of the power system relative to such imminent

disturbances. For a power system subjected to small and large disturbances, it is important that, when the changes are completed, the system settles to new operating conditions such that no physical constraints are violated. This implies that, in addition to the existence of new operating conditions, the system must also survive the transition to these conditions. There are two main categories of power system security analysis: static security analysis and dynamic security analysis. In static security analysis, only steady-state analysis is involved, while in dynamic security analysis, power system dynamic response is examined. Stability analysis is thus an integral component of system security analysis.

1.2 Literature Review

1.2.1 *Static Analysis*

In static analysis, power system dynamics are not considered. The focus of static analysis is the system steady state, which may or may not be reached through governing dynamics following disturbances. In certain situations such as voltage stability subject to small disturbances, static analysis may be a good approximation and can be effectively used to estimate system stability limits, and to screen a large number of system conditions and scenarios. Therefore, techniques for static analysis are also used in stability analysis in certain areas.

The role of static analysis can be further classified into solution-finding and solution-optimization. The solution-finding problems aim to find the power system steady state for given system conditions, and such an approach is usually referred to as power flow analysis. The solution-optimization problems attempt to obtain the best steady state solution for a

given the objective function by adjusting system conditions, and this type of analysis is usually called optimal power flow. The underlying techniques for static analysis include numerical methods for equations solution and mathematical optimization theory [9, 10].

1.2.2 *Instability Identification for Small Disturbances*

The small disturbances in power system analysis refer to small perturbations to the initial operating condition. If system security can be maintained, a new operating condition can be reached subject to such small perturbations. Stability problems resulting from small disturbances may be voltage related or rotor angle related. For angle related small disturbance stability, also called small-signal rotor angle stability, the analysis can be performed based on the linearization of the system equations [7]. For small disturbance voltage stability, methods such as bifurcation theory can be used to study the inherently nonlinear phenomenon for voltage collapse [11]. Bifurcation theory [12, 13] is a mathematical tool with which to analyze voltage stability subject to small disturbances [14, 15].

In bifurcation theory, equilibrium behaviors of dynamical systems are studied using a slowly changing parameter, with qualitative changes occurring when the parameter reaches a bifurcation point. When bifurcation theory is applied to power systems, such systems are represented by dynamic equations and small disturbance such as a load increment is usually chosen as the slow varying power system parameter. As power system parameter varies slowly, the stability of the equilibrium may encounter sudden changes, which are often associated with system failures.

Saddle node bifurcation and Poincare-Andronov-Hopf bifurcation (or Hopf bifurcation) are two important bifurcations in power system dynamics. In saddle node bifurcation, a stable equilibrium disappears as the results of parameter change, with a consequence of system states collapse, for example, voltage collapse. Prior to encountering the saddle node bifurcation point, there are two system equilibriums: one stable and the other unstable. At the saddle node bifurcation point, these two equilibriums coalesce into one equilibrium and the system Jacobian matrix at this equilibrium has a simple zero eigenvalue. Beyond the saddle node bifurcation point, no system equilibrium exists. In the Hopf bifurcation, a stable equilibrium becomes oscillatory unstable as the result of the parameter change, with a consequence of system state oscillation. At the Hopf bifurcation point, the system Jacobian at equilibrium has a pair of purely imaginary eigenvalues.

Since, at the bifurcation points, system stability will be lost, system security can be analyzed by identification of the bifurcation points. Before these bifurcation points are reached, the system operation is secure when subject to small disturbances, and therefore the bifurcation points indicates a system operating limit. Load margin is a concept strongly associated with the stability limit. Load margin is defined as the difference between the load level at the stability limit and the current operating load level. When the system approaches the stability limit, the load margin tends to reduce to zero. Therefore, the identification of the stability limit is often referred to in the literature as the calculation of the load margin.

In many cases, the identification of the stability limit or the bifurcation point, especially saddle node bifurcation points, can be done approximately by the static analysis such as power flow. The continuation method is a path-following method for analyzing smooth

parameter change [16], and it is applied to power systems to identify the system stability limit. The continuation method is used in [17-20] to identify the saddle node bifurcation point based on power flow analysis. The continuation method with a transmission line branch selected as a parameter is investigated in [21], and the power transfer limit among different areas due to stability constraint is studied in [22]. The continuation method is applied to power system dynamical equations in [23]. In addition to the continuation method, the direct method is also applied to identify the saddle node bifurcation point in [19, 24, 25].

The oscillatory stability limit associated with the Hopf bifurcation point is presented in [26] using an iterative method, with the Hopf bifurcation point obtained through eigenvalue calculation.

In the calculation of bifurcation points or stability limit, the parameter path must be pre-specified. If the parameter path is changed, the stability limit also changes. In [27], a method is proposed for identifying the closest bifurcation point or the smallest stability limit among all the possible load paths. This algorithm is based on iterative and direct methods through the use of normal vectors.

Accurate identification of the stability limit requires relatively high computational costs, and it is sometime desirable to find sensitivities or indices for the stability limit with greater computational efficiency. These sensitivities or indices can often give proximity information about the distance of the current operating point from the stability limit.

Sensitivity Factor and Voltage Sensitivity Factor are easily-computed indices used in the power industry to detect voltage stability problems [15]. In [28] a minimum singular value is proposed as the proximity index for voltage stability, and an efficient algorithm for singular

value calculation is given in [29]. The Voltage Instability Proximity Index is another stability indicator based on the fact that the number of power system solutions decreases as the system approaches stability limit. The test function [30] is a stability indicator based on the system Jacobian matrix with quadratic shape of the load margin. The reduced determinant method is proposed in [31] to produce a voltage stability index based on reduction of the power flow Jacobian with respect to the critical bus of the system. The Tangent Vector Index is an indicator with behavior similar to that of the test function with a reduced determinant resulting in less computational cost [32]. Other voltage stability indices such as Jacobian determinant, Voltage Controllability Index [33], and voltage profile index also exist. Each of these indices has its own advantages and disadvantages. In general, those indices with high accuracy tend to have high computational costs, while those indices with poorer prediction ability can be calculated efficiently. As a compromise, several indices may be jointly used in a practical application.

1.2.3 *Control Strategies for Small Disturbances*

The control strategy for mitigation of voltage stability subject to small disturbances aims to improve the system stability limit or load margin by adjusting system control resources. More specifically, the control strategy may specify control actions to satisfy a given stability limit, or give the maximum stability limit as constrained by the available control resources. The methods used vary from simple controls based on sensitivities to controls incorporating more complex mathematical formulation. Usually the control methods based on sensitivities have relatively low computational costs and relatively poor accuracy, and the complex controls tend to yield more accurate solutions with higher computational costs.

In the simple method, sensitivities are used to quickly identify control resources. The difference between the sensitivities for instability identification and those for control lies in the fact that the sensitivities for instability identification estimate the distance between the current operating condition and stability limit without considering control actions, while the sensitivities with respect to control resources give the estimation of the stability limit change or stability limit index change under the control adjustment.

The stability limit index change with respect to the control parameter is given in [34]. In the proposed method, a minimum singular value is chosen as the stability limit index, and the effects of capacitor compensation and generation rescheduling on the stability limit index are examined. The sensitivities of control resources can also be directly derived to the stability limit or load margin. A first order sensitivity with respect to load margin is derived in [35]. In [36], sensitivities of the load margin with respect to arbitrary control parameters are given. The control effect of emergency load shedding, reactive power support, variation in load increment direction, generation re-dispatch, changes of load model and load composition, and varying transmission line susceptance are demonstrated. The method is further expanded to apply to study the post-contingency stability limit change line [37]. The load margin sensitivities are sensitivities associated with the saddle node bifurcation point. In [38], the stability limit with respect to system parameters of Hopf bifurcation is presented, and the comparison between sensitivities of saddle node bifurcation and Hopf bifurcation is given.

In addition to sensitivity based control strategy, control methods can also be obtained from direct stability limit improvement using optimization techniques and the continuation method. In [39], the problem of improving the stability limit is directly formulated as a

mathematical optimization problem. The objective in the optimization problem is chosen as the load margin. In [40], the stability limit is enhanced as the solution produced by a multiple-stage optimization method. At each stage, sensitivity information is used to estimate the optimal direction; and the estimation is updated by the dynamic programming at each succeeding stage. For given control resources, the load margin can be traced by the continuation method from the initial stability limit to the new stability limit [41].

1.2.4 *Instability Identification for Large Disturbances*

Time domain simulation or dynamical simulation is the basic numerical tool for analysis of dynamical systems. Since power systems are dynamical systems, time domain simulation is also a fundamental method for power system instability identification subjected to large disturbances. Power system dynamic responses may be examined using time domain simulation by general purpose numerical methods suitable for application to dynamical systems [42-48].

In addition to time domain simulation, in certain cases instability identification may also be determined by direct methods. The basic idea of such direct methods goes back to Lyapunov, and according to [8], their application to power systems began as early as the 1940s and has remained a challenging problem up until the present time. In the direct methods, an energy function is required for power systems, and an estimate of the critical energy is subsequently needed. The initial energy of the power system subject to the disturbance can be estimated and compared with the critical energy. In the direct method, stability can be maintained if the initial energy is less than the critical energy. Direct methods were originally applied to angle stability [49-51], and later expanded to voltage stability [52,

53]. Despite the significant accomplishments of applying direct methods during decades of research efforts, the construction of an energy function for general power system models remains an open problem, and the instability identification of a power system subjected to large disturbances is typically explored using time domain simulation [7].

1.2.5 *Control Strategies for Large Disturbances*

The simplest control strategies for large disturbance are based on a measure of local information such as voltage. Under-voltage load-shedding proposed in [54] is such a mechanism to for mitigation of voltage instability problems. Since the voltage level may decline following initial disturbances, voltage decay is measured and compared with pre-specified trigger conditions. A given amount of load at the pre-specified buses is automatically shed once these trigger conditions are satisfied. The concept and implementation of under-voltage load-shedding is simple, but performance is not always guaranteed. For example, too much load shedding at nearby locations in a very short time may lead to undesirable high voltage. Therefore, the scheme design is based on extensive dynamic simulations, and the coordination among control elements such as load shedding locations, amount, and time can be quite difficult.

The simplest control strategies for large disturbance are based on the measure of local information such as voltage. Under voltage load shedding is such a mechanism to mitigate voltage instability problem proposed in [54]. As voltage level may decline following the initial disturbances, voltage decay is measured and compared with the pre-specified trigger conditions. A given amount of load at the pre-specified buses is automatically shed once the trigger conditions are satisfied. The concept and implementation of under voltage load

shedding is simple, but the performance is not always guaranteed. For example, too much load shedding at the nearby locations in very close time may lead to undesirable high voltage. Therefore, the design of the scheme is based on the extensive dynamical simulations, and the coordination among control elements such as load shedding locations, amount, and time is quite difficult.

Since local measurement may not be good enough to guarantee system performance, more sophisticated control mechanisms are needed. These strategies may use a combination of dynamic simulation and optimization techniques or transform the difficult problem into another form using existing optimization methods.

In [55], an approach to load-shedding control of voltage using sensitivity and simulation instability is given. The sensitivity is first derived from the Jacobian matrix with respect to control variables, and a control amount is then estimated to satisfy post-disturbance stability based on the sensitivity. The method can be further expanded into simulations using trial-and-error methods. The basic idea is to narrow the amount of control needed through iteration and to use dynamical simulation to verify the control effect. In [56], the sensitivity information is used to rank load buses for load-shedding. Next a binary search based on the time domain simulation results is used to determine the minimal amount of load shedding at a given time. The binary search persists in building a smaller and smaller interval of load shedding amount such that upper bound of the interval is stable system response and the lower bound is unstable system response. In the search procedure, the load shedding locations and time is pre-specified, and the only decision variables are the load shedding amounts. At each step, the mid-point of the search interval is tested through dynamical

simulation and taken as the new upper or lower bound according to the simulation results. In the simulation a large load shedding amount P1 is first identified such that system equilibrium can be recovered through dynamical simulation, and then a small amount of load shedding P2 is examined such that instability cannot be prevented. The best load shedding amount should lie between P2 and P1. In the next iteration, the midpoint amount of the load shedding (P1+P2)/2 is tested, and the range containing the minimum load-shedding amount is reduced by half. The search procedure ends until the range is sufficiently small. Trial and error simulation methods are very time-consuming for large power systems, and transient behaviors such as voltage dip or sag are not considered in these methods.

In another approach, search and optimization techniques with modal predictive control are used to determine control strategies. System responses are predicted based on current states and for several different candidate control sequences. In [57], a tree-search method is employed to determine the best control strategy among all the control candidates. For example, from initial state point A at certain time T_0, the future states at T_0+T_p can be predicted as different trajectories with different control. The tree-search method is similar to those used in chess computers where each node in the tree corresponds to one possible control action. In [58], the selection of the optimum control action in the complex optimization problem is achieved by evolutionary programming. In [59], linear programming techniques are applied at each step to determine the control actions. In modal predictive control, power system dynamic behavior is usually approximated by straight lines between discrete times, and the time interval is usually selected to be quite large, for example, 30-60

seconds in [58]. Therefore, short-term power systems dynamic behavior is not represented using large time horizons and straight line approximation.

In [60] the difficult problem of control for dynamical systems is transformed into a traditional nonlinear optimization problem. The transformation is based on discrete time formulation, and the subsequent control strategies are obtained from the solution of the transformed problem. However, the transformation tends to give an inaccurate solution compared with the true solution, and the inaccuracy is due to the introduction of pseudo-minima from the transformation [61].

1.3 Motivation

Identification and mitigation of power system instability plays an important role in the dynamic security analysis. Power systems are routinely subjected to various physical disturbances, which may lead to voltage or angle stability problems. Depending on disturbance severity, power systems may either approach a new equilibrium or lose stability. In Fig. 1-2, conceptual power system dynamic response after large disturbance is illustrated.

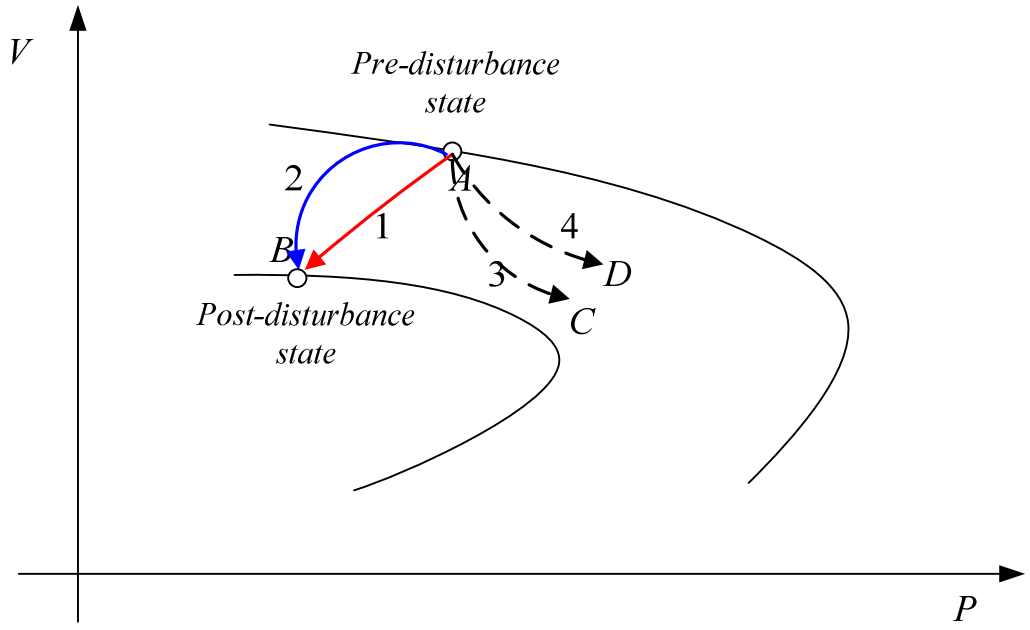

Fig. 1-2. Possible System Dynamic Responses after Disturbance

The initial power system operating point is at point A, and post-disturbance analysis shows that point B is an equilibrium point. However, the existence of equilibrium for the post-disturbance power system cannot guarantee that system states will be attracted to point B. The actual trajectory of system states may move away from point B, e.g., towards point C or point D after a certain time (dashed lines in the figure). In such cases, the system will eventually become unstable and proper control must be applied to save system. Under control actions, power system states may move towards the desirable post-disturbance point B. But the path from pre-disturbance point A to post-disturbance point B may not be unique. Several possible paths (solid lines in the figure) may exist because of different controls. Among all these possible paths, some paths may not be physically feasible due to physical constraint violations. For example, control actions such as generation and load re-dispatch may cause transmission line flow limit violations, or control actions such as reactive power

compensation may demand more resource than that physically available. After eliminating trajectories with such constraints violations, there may still be remaining multiple trajectories left connecting point A to point B. It is desirable to find a best trajectory with best control from pre-disturbance state to post-disturbance state among all the possible trajectories. Under such best control, the power system can be restored to new stable states with minimum objective function or cost function. Fig. 1-3 conceptually shows possible time trajectories after disturbance. Dashed lines in the figure represent unstable system trajectories. The blue solid line is a stable transition from point A to point B with state variable violation (for example, voltage dip), while the red line is a stable transition with minimum cost.

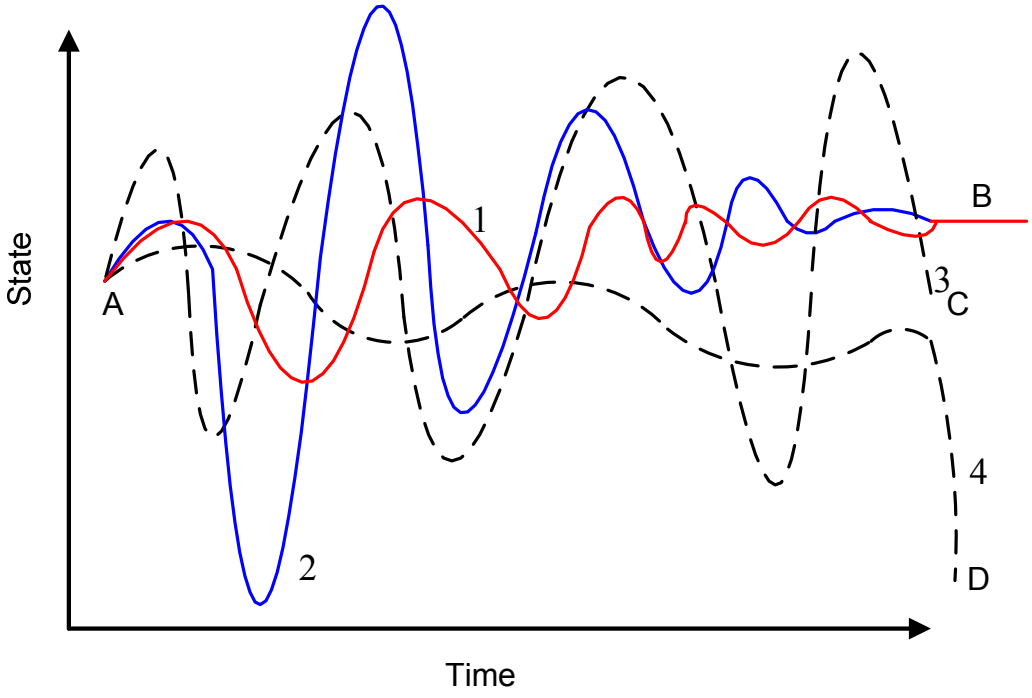

Fig. 1-3. Possible System Trajectories after Disturbance

In power system dynamic security analysis, the first step is to identify system dynamic response for a given disturbance or contingency; and then to consider the control strategy

required to restore post disturbance system equilibrium. Power system response to large disturbances is typically studied by time domain simulation, but such simulations are time consuming for large power systems, and developing a fast simulation method is often quite a challenging problem.

Once unstable system responses have been identified, the next problem is how to bring the power system back into equilibrium state. Control strategies incorporating power system dynamics are often time dependent [14, 62], and there are three important elements for control strategies: locations, amount, and time. The coordination among these three important aspects has not been completely solved based on the existing methods found in the literature. A control strategy based on trial and error simulation usually pre-specifies two control aspects such as locations and time, and then considers only the control amount as the decision variable. Modal predictive control typically ignores short term dynamic behaviors by using a simplified system dynamic response prediction. The transformed nonlinear optimization technique is plagued with inaccurate solutions. Incorporation of accurate power system dynamics into optimization techniques, especially short term dynamics, remains an open problem.

In dynamic security analysis, in addition to the requirement that a new operating condition must be restored after the disturbances, system transient behavior also plays an important role in security analysis. There are two major concerns for the system transition: power quality and cascading events. Electric power supplies are subject to quality constraints. For example, the voltage and frequency level should be maintained within a specified narrow range under normal operating conditions. Under disturbances, system voltage and frequency

may be allowed to vary over a larger range, but are still limited. A limit violation such as voltage sag or voltage dip may cause damage to equipment and/or degraded service. Cascading events is the other problem with extremely huge potential impact triggered by system transitions. There exist many relaying and protection schemes for monitoring power system status and protecting component. In some cases the relays may be triggered by the post disturbance transition, and subsequently the protection scheme may unnecessarily trip system devices such as transmission lines. Such initial actions may lead to more transitions which trigger more protective actions. The cascading events may result in large area system failure such as in the 2003 Northeast blackout of North America. Therefore, transient behavior such as voltage profile variation following the disturbance and control resource limits should be considered in the analysis.

Dynamic security analysis requires advances in both time domain simulation method and optimization methods. These two methodologies are are closely associated. The stability of power systems under large disturbances is typically explored using time domain simulations. Since power systems often have thousands of components, dynamical simulation can be very time consuming. Advances in time domain simulation algorithms can improve computational efficiency and permit handle more contingencies and larger systems. Results from time domain analysis can also help to decide on a time scale for the instabilities and control strategies, but it is difficult to find a best control strategy from simulations alone; an optimization method may pave the way for a theoretical solution with rigorous justification. The research effort described here attempts to develop an integrated framework with both

fast time domain simulation method and comprehensive optimization technique for system dynamics.

The overall framework of the proposed research work is illustrated in Fig. 1-4. The basic philosophy used is security assessment and control. The data input includes power system dynamic data and a critical disturbance or contingency list. The procedure can be divided into 2 phases: security observation and control action. Security assessment is the first phase, and followed by control action in the second phase. In the first phase, for a given disturbance, system post-disturbance behavior is studied through time domain simulation. Once instability is found, the time scale of the system dynamic response is identified using the results of advanced time domain simulation. Time scale and post-disturbance equilibrium are taken as inputs for the second phase. In this phase, trajectory optimization theory is applied to power system dynamical optimization. Optimal conditions can be formulated incorporating post-disturbance equilibrium and system dynamics. The state and control constraints are considered by using penalty function equivalence. The mathematical formulation of the necessary conditions is a boundary value problem that can be solved by finite difference methods. The output is the best control strategy with which to mitigate instabilities.

In the proposed research, decoupled time domain simulation [63, 64] and trajectory optimization are integrated for dynamic security analysis. A decoupled dynamical simulation method based on invariant subspace partition can reduce the required simulation time. Trajectory optimization theory provides a theoretical framework for power system dynamical optimization. Trajectory optimization can find the best trajectory and control actions with which to minimize a scalar objective function subject to end point and path constraints. Its

application to power systems can provide the best transition from pre-disturbance equilibrium to post-disturbance equilibrium.

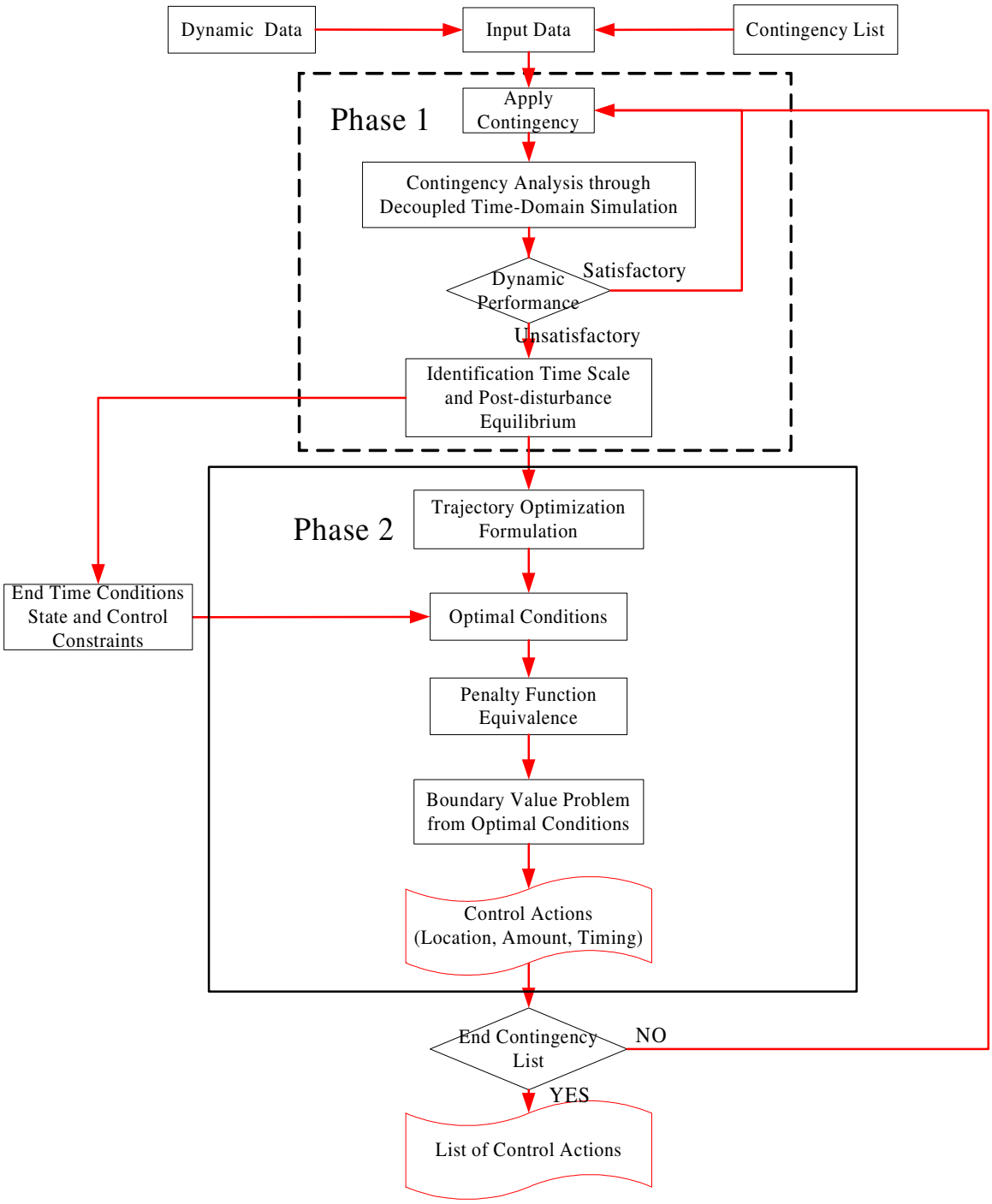

Fig. 1-4. Dynamic Security Analysis Framework

1.4 Organization

The rest of the dissertation is organized as follows.

The mathematical model for power system dynamic security analysis is given in chapter 2. This chapter is an overview of mathematical models for power systems in the dissertation.

Decoupled time domain simulation algorithm is proposed for power system security analysis in chapter 3. The decoupled method is an efficient algorithm with numerical stability, and fast instability identification can be achieved via the decoupled method.

In chapter 4, trajectory optimization theory is utilized to solve power system optimization problem constrained by dynamics. The solution from the trajectory optimization provides the coordination control strategy among control locations, amount, and time to regain a new operating equilibrium subject to transitional constraints.

The conclusions and further research directions are given in chapter 5.

CHAPTER 2 POWER SYSTEM MODEL

2.1 Introduction

In this chapter, power system models are described for a variety of power system components. The representation consists of both static and dynamic characteristics. Based on the detailed representation for each component, a generic mathematical formulation is given for the power system dynamic security analysis. This chapter is an overview of mathematical models for power systems in the dissertation. These basic mathematical models [8, 65] are also used in the research work in [66-68].

2.2 Power Flow

Power flow is the model for power system network. Power system variables are studied from a set of algebraic equations. The compact form of the power flow equations is as follows.

$$g(y) = 0 \tag{2.1}$$

In the formulation (2.1), algebraic variables y represent the solution of power flow. The algebraic equations g represent network equations. At each bus of the power system, power injection is balanced. The network equations g can be expanded into the nonlinear forms consisting of both real power and reactive power balance.

$$\begin{cases} 0 = P_{gi} - P_{li} - P_{ti} \\ 0 = Q_{gi} - Q_{li} - Q_{ti} \end{cases} \tag{2.2}$$

where

P_{gi} : Real power generation at bus *i*

P_{li} : Real power load at bus *i*

P_{ti} : Net real power injection at bus *i*

Q_{gi} : Reactive power generation at bus *i*

Q_{li} : Reactive power load at bus *i*

Q_{ti} : Net reactive power injection at bus *i*

The real and reactive power generations are determined by the inherent characteristics of the generator. The real and reactive loads are determined by the load characteristics. The net real and reactive power injections are constrained by the physical characteristics, which are represented by the following equations.

$$\begin{cases} P_{ti} = \sum_{k}^{n} V_i V_k Y_{ik} \cos(\theta_i - \theta_k - \varphi_{ik}) \\ Q_{ti} = \sum_{k}^{n} V_i V_k Y_{ik} \sin(\theta_i - \theta_k - \varphi_{ik}) \end{cases} \tag{2.3}$$

The variables V and θ are bus voltage and angle respectively, and these variables belong to the unknown variables *y* in (2.1) for power flow analysis. The variables Y and φ are given parameters from power system model representing bus connections.

In the power flow analysis, it is usually assumed that generation and load variables are given. By solving a set of nonlinear equations, power system static states such as bus voltages and angles can be determined from power flow analysis.

2.3 Synchronous Generator Model

Two-axis generator model [65] [69] is used to describe synchronous generator. The mathematical formulation of the synchronous machine is given as:

$$\dot{\delta} = (\omega_i - \omega_m)\omega_0 \tag{2.4}$$

$$\dot{\omega}_i = M_i^{-1}[P_{mi} - D_i(\omega_i - \omega_m) - (E_{qi}^{'} - X_{di}^{'} I_{di})I_{qi} - (E_{di}^{'} + X_{qi}^{'} I_{qi})I_{di}] \tag{2.5}$$

$$\dot{E}_{qi}^{'} = T_{d0i}^{-1}[E_{fdi} - E_{qi}^{'} - (X_{di} - X_{di}^{'})I_{di}] \tag{2.6}$$

$$\dot{E}_{di}^{'} = T_{q0i}^{-1}[-E_{di}^{'} + (X_{qi} - X_{qi}^{'})I_{qi}] \tag{2.7}$$

In the two-axis generator model (2.4)-(2.7), δ is the generator angle, ω is the generator angular speed; $E_d^{'}$ and $E_q^{'}$ are transient direct axis (*d* axis) and quadrature axis (*q* axis) EMF respectively. The variables I_d and I_q are *d* axis and *q* axis current respectively, and the parameter variables T_{d0} and T_{q0} are *d* axis and *q* axis open circuit time constants. X_d and X_q represent synchronous *d* axis and *q* axis reactances; $X_d^{'}$ and $X_q^{'}$ represent synchronous *d* axis and *q* axis transient reactances; M_i is the machine inertia constant and D_i is the machine damping constant.

Interface voltage equations to the network are given as follows:

$$E_{qi}^{'} = V_i \cos(\delta_i - \theta_i) + R_{si} I_{qi} + X_{di}^{'} I_{di} \tag{2.8}$$

$$E_{di}^{'} = V_i \sin(\delta_i - \theta_i) + R_{si} I_{di} - X_{qi}^{'} I_{qi} \tag{2.9}$$

where V and θ are bus voltage and angle, and R_s is armature resistance of the machine.

The machine currents I_d and I_q can be eliminated by solving the generator interface equations to the network. Hence,

$$I_{di} = [R_{si} E_{di}^{'} + E_{qi}^{'} X_{qi}^{'} - R_{si} V_i \sin(\delta_i - \theta_i) - X_{qi}^{'} V_i \cos(\delta_i - \theta_i)] A_i^{-1} \tag{2.10}$$

$$I_{qi} = [R_{si} E_{qi}^{'} + E_{di}^{'} X_{di}^{'} - R_{si} V_i \cos(\delta_i - \theta_i) - X_{di}^{'} V_i \sin(\delta_i - \theta_i)] A_i^{-1} \tag{2.11}$$

$$A_i = R_{si}^2 + X_{di}^{'} X_{qi}^{'} \tag{2.12}$$

2.4 Excitation System Model

The simplified IEEE type DC-1 excitation system [8] is shown in Fig. 2-1 to represent excitation system. The mathematical model is as follows.

$$\dot{E}_{fdi} = T_{ei}^{-1} [V_{ri} - (K_{ei} + S_{ei}(E_{fdi})) E_{fdi}] \tag{2.13}$$

$$\dot{V}_{ri} = T_{ai}^{-1} [-V_{ri} + K_{ai}(V_{refi} - V_i - R_{fi})] \tag{2.14}$$

$$\dot{R}_{fi} = T_{fi}^{-1} [-R_{fi} - (K_{ei} + S_{ei}(E_{fdi})) K_{fi} E_{fdi} / T_{ei} + K_{fi} V_{ri} / T_{ei}] \tag{2.15}$$

where V_{ref} is the reference voltage of the automatic voltage regulator (AVR); V_r and R_f are the outputs of the AVR and exciter soft feedback; E_{fd} is the voltage applied to generator field winding; T_a, T_e and T_f are AVR, exciter and feedback time constants; K_a, K_e and K_f are gains of AVR, exciter and feedback; $V_{r,\min}$ and $V_{r,\max}$ are the lower and upper limits of V_r.

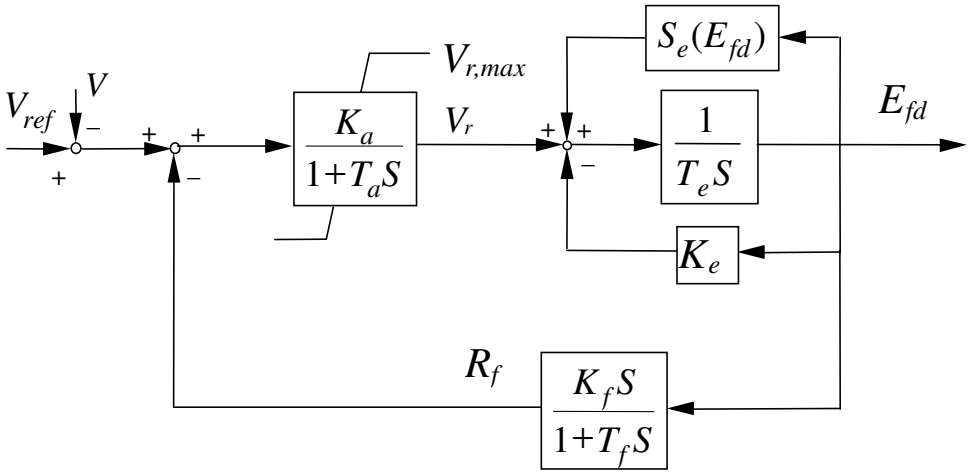

Fig. 2-1. IEEE type DC-1 Excitation System

2.5 Governor Model

A simplified prime mover and speed governor is shown in Fig. 2-2. Two differential equations are used to describe the dynamics of the governor.

$$\dot{P}_{mi} = T_{chi}^{-1}(\mu_i - P_{mi}) \tag{2.16}$$

$$\dot{\mu}_i = T_{gi}^{-1}[P_{gsi} - (\omega_i - \omega_{ref})/R_i - \mu_i] \tag{2.17}$$

In the formulation, the variable P_{gs} is the designated real power generation; P_m is the mechanical power of the prime mover and μ is the steam valve or water gate opening; R is the governor regulation constant representing the inherent speed-droop characteristic; ω_{ref} is the governor reference speed; T_{ch} and T_g are the time constants related to the prime mover and speed governor respectively; $\mu_{\min}$ and are the lower and upper limits of μ.

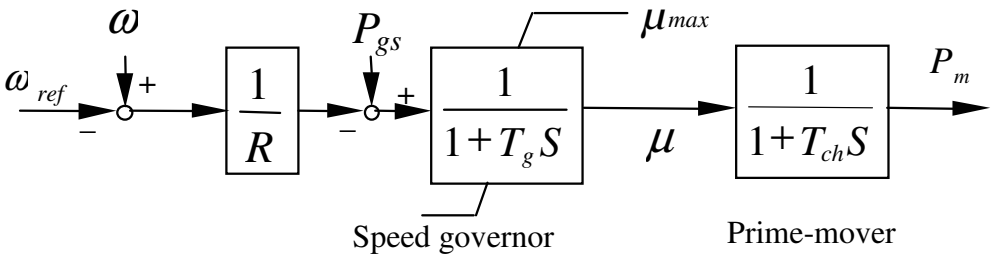

Fig. 2-2. Simplified Speed Governor and Prime Mover

2.6 Load Model

Load model may be voltage and frequency dependent. In power system analysis, common load models can be constant power model, constant current model, and constant impedance model. The representation for these load models are shown as follows.

Constant Power Load:

$$P_{li} = P_{li0} \qquad Q_{li} = Q_{li0} \tag{2.18}$$

Constant Current Load:

$$P_{li} = P_{li0}(V_i / V_{i0}) \qquad Q_{li} = Q_{li0}(V_i / V_{i0}) \tag{2.19}$$

Constant Impedance Load:

$$P_{li} = P_{li0}(V_i / V_{i0})^2 \qquad Q_{li} = Q_{li0}(V_i / V_{i0})^2 \tag{2.20}$$

The generic load model may be the combination of constant power, constant current, and constant impedance loads. The generic load model may also have frequency dependent component. The mathematical formulation of the generic load model is given in (2.21).

$$\begin{cases} P_{li} = P_{li0}[K_{p1} + K_{p2}(V_i / V_{i0}) + K_{p3}(V_i / V_{i0})^2](1 + K_{freqpi}(\omega_m - 1)) \\ Q_{li} = Q_{li0}[K_{q1} + K_{q2}(V_i / V_{i0}) + K_{q3}(V_i / V_{i0})^2](1 + K_{freqqi}(\omega_m - 1)) \end{cases} \tag{2.21}$$

In (2.21), P_l and Q_l are the real and reactive power; P_{l0} and Q_{l0} are the real and reactive power consumed by the load at the nominal voltage V_{i0}; parameters K_{p1}, K_{p2}, K_{p3} indicate the components of constant power, constant current, and constant impedance load for real power; parameters K_{q1}, K_{q2}, K_{q3} indicate the components of constant power, constant current, and constant impedance load for reactive power; parameters K_{freqp} and K_{freqq} are the load changing factors with respect to system frequency.

2.7 Power System DAE Model

Since there are both differential equations and algebraic equations in power systems, power systems can be represented generally by Differential Algebraic Equations (DAE). The mathematical formulation is as follows.

$$\begin{cases} \dot{x} = f(x, y) \\ 0 = g(x, y) \end{cases} \tag{2.22}$$

The differential equation *f* represents governing dynamics of power systems, which is associated with generators, excitation systems, and speed governor. The differential variables *x* consist of the states of dynamic components. The algebraic equation *g* represents the network power balance of power systems. The algebraic states *y* include bus voltages and bus phase angles. The values of the algebraic variables can be changed instantaneously, while differential variables cannot jump from one state value to another state value without transition time.

In power system analysis, there exist also control and parameter variables. To incorporate these additional variables, DAE system in (2.22) can be rewritten as the following form:

$$\begin{cases} \dot{x} = f(x, y, u) \\ 0 = g(x, y, u) \end{cases} \tag{2.23}$$

In the above equations, variable u is the control and parameter variable which may be used to control or tune power system performance.

Power system dynamic security problems are studied based on the mathematical model. The study of dynamic responses subject to the disturbances can be achieved through dynamical simulation, or time domain simulation of the power system mathematical model, which is shown in chapter 3. The control strategies for power system dynamics are also based on the mathematical model with the application of the trajectory optimization theory, which is shown in chapter 4.

CHAPTER 3 DECOUPLED TIME DOMAIN SIMULATION

3.1 Introduction

In this chapter, decoupled time domain simulation method [63, 64] is presented for power system dynamic security assessment. Time domain simulation or dynamical simulation is an important tool for power system dynamic analysis. As power system behaviors are subject to governing dynamics, time domain simulation is typically used to explore power system responses following the disturbances.

A set of differential and algebraic equations (DAE) are numerically solved to study the transient behavior of power systems. Power systems networks typically include thousands of generators, exciters, governors, loads, transformers and other devices, where each individual component may need several differential and algebraic equations to represent, thus the total number of differential and algebraic equations of a real power system can be formidably large.

Time domain simulations for the dynamical systems such as power systems include step-by-step numerical integration of DAEs. The numerical error introduced in each step can be measured via the local truncation error. To improve the accuracy, small step size and higher order approximations are usually required. The error accumulated in each step may also yield qualitatively wrong results, and numerical stability analysis is needed to guarantee the correctness.

Power system simulations involve various system components whose time constants vary in a large range. As a result, time domain simulations face numerical problems related to stiffness caused by different time scales. A considerable amount of effort has been spent to solve large scale stiff problems in the literature [42-48]. In power system literature, mathematical algorithms are applied to study power system dynamic responses, and typically no mathematical analysis with proof is provided.

Numerical integration methods can be classified into two categories: explicit methods and implicit methods. The explicit methods involve fixed point iteration and are computationally efficient, but have numerical stability problem when dealing with stiff problems. The implicit methods involve solving nonlinear equations at each step. The implicit methods are slow but stable. Implicit methods are commonly used for solving power system dynamical simulation in the literature.

In this chapter a new method which combines explicit methods and implicit methods to solve the time domain simulation is proposed. The main motivation is to propose an algorithm to take advantage of both the methods: efficiency and numerical stability. In the dynamical simulation process, the large-scale differential and algebraic equations are decoupled into two parts to treat them separately based on invariant subspace partition to achieve the goals.

3.2 Conventional Explicit and Implicit Methods and Numerical Stability

Consider a general ODE system with a given initial condition as described by (3.1):

$$\begin{cases} \dot{x} = f(x) \\ x(0) = x_0 \end{cases} \tag{3.1}$$

To solve the above initial value problem (IVP) the following two approaches are commonly employed [70-75].

3.2.1 *Explicit Method*

Explicit methods typically replace the ordinary differential equations by nonlinear recursive mappings

$$x_{k+1} = g(x_k) \tag{3.2}$$

Here the recursion is to be understood in the sense that from some initial value x_0 the states $x_1, x_2, \cdots$ are generated as long as they remain in the domain of definition of the mapping.

Some of the methods under this category include: forward Euler method, explicit Runge-Kutta methods, and Adams-Bashforth methods.

The forward Euler method is formulated as:

$$x_{k+1} = x_k + hf(t_k, x_k) \tag{3.3}$$

The 4$^{\text{th}}$-order Runge-Kutta method is formulated as:

$$\begin{aligned} K_1 &= f(t_k, x_k) \\ K_2 &= f(t_k + h/2, x_k + hK_1/2) \\ K_3 &= f(t_k + h/2, x_k + hK_2/2) \\ K_4 &= f(t_k + h, x_k + hK_3) \\ x_{k+1} &= x_k + h(K_1 + 2K_2 + 2K_3 + K_4)/6 \end{aligned} \tag{3.4}$$

The advantage of explicit methods is that at each simulation step, the next step value can be directly calculated from previous results. Thus explicit methods are very efficient with fixed point iteration techniques.

3.2.2 *Implicit Method*

The implicit methods use both current state and past state to solve the initial value problem. As a result, a set of nonlinear equations needs to be solved at each individual step which causes higher computational burden compared with the explicit methods.

Backward Euler method, trapezoidal method, implicit Runge-Kutta method, Adams-Moulton methods, backward differential formulae methods are part of the whole family of the implicit methods.

The backward Euler method is formulated as:

$$x_{k+1} = x_k + hf(t_{k+1}, x_{k+1}) \tag{3.5}$$

The trapezoidal method is formulated as:

$$x_{k+1} = x_k + h[f(t_k, x_k) + f(t_{k+1}, x_{k+1})]/2 \tag{3.6}$$

In the formulae of implicit methods, the next step state cannot be obtained directly, and Newton method is usually used to solve the nonlinear equations in the implicit methods. However, the implicit methods have better numerical stability properties than explicit methods despite their slow computational performance.

3.2.3 *Numerical Stability Analysis: Stiffness and A-Stability*

Power systems usually have components with vastly different time scales. The problems of such systems are described as being stiff: the time constants of the various physical

processes differ greatly (from tens of milliseconds for fast transients up to one hundred seconds for slow adjustments). Physically speaking the stiffness is caused by the presence of different time scale components; while mathematically speaking, the stiffness of the problem is associated with the existence of both large and small eigenvalues. The quotient of the largest and the smallest eigenvalues can be considered as the stiffness ratio to measure the degree of stiffness [73].

The numerical methods may produce qualitatively wrong results for stiff problems due to the error accumulations in the simulation steps. It is crucial that the numerical methods correctly identify whether the system is stable or unstable. In some cases the numerical solution may indicate unstable behavior for the case where the actual system is stable and vice versa. Explicit methods may require a significant reduction of the step size to maintain numerical stability such that the step size is smaller than the step size needed to represent the solution accurately. The required step size for explicit methods to guarantee numerical stability may be too small for practical implementation. The implicit methods are necessary to guarantee the numerical stability for stiff systems

A simple example given in [73] is used to show the difference between explicit and implicit methods for stiff systems.

$$\begin{cases} \dot{x}_1 = -100x_1 + x_2 \\ \dot{x}_2 = -0.1x_2 \end{cases} \tag{3.7}$$

The initial value is $(-3,-1)^T$, and the step size is chosen as 0.1. The eigenvalues of (3.7) are -100 and -0.1, which are both negative; therefore, the system trajectory should converge to the origin as time goes into infinity. To obtain the time response both forward Euler

method and trapezoidal method are applied. The result by forward Euler method is shown in Fig. 3-1a. Actually in this case the forward Euler iterates grow geometrically in magnitude if step size is greater than 0.02, in contrast with the asymptotic behavior of the true solution. The simulation result by trapezoidal method is shown in Fig. 3-1b. which demonstrates proper stable behavior.

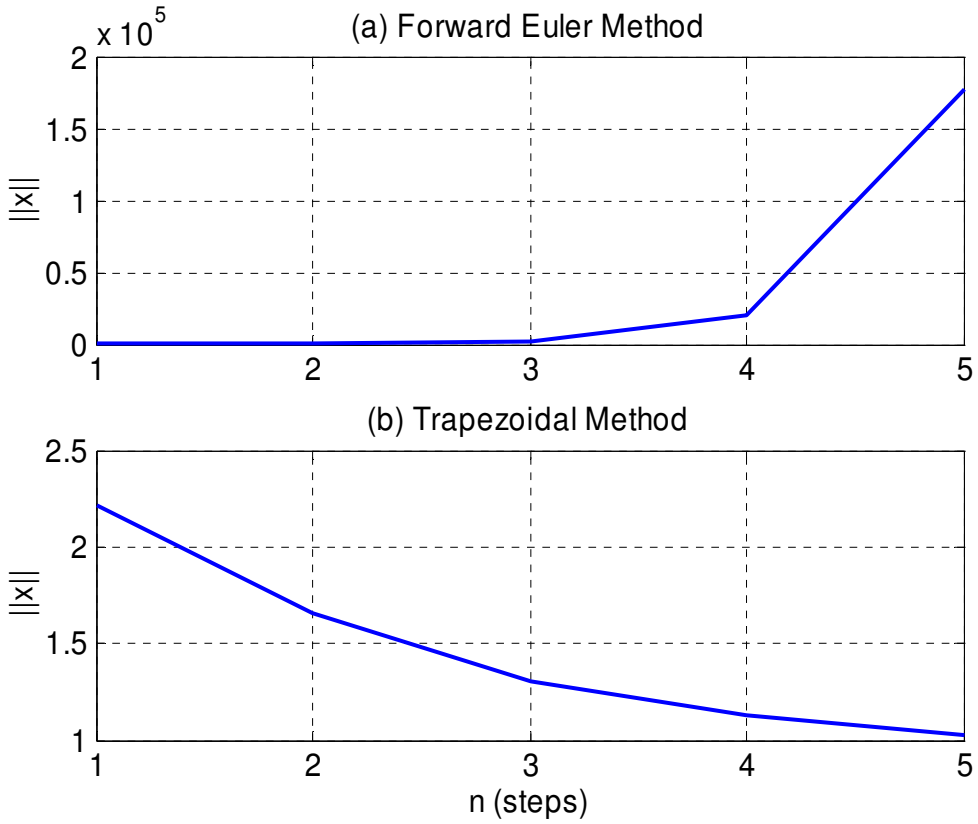

Fig. 3-1. The Simulation Results by Explicit and Implicit Methods

To analyze possible instability caused by numerical methods, the concepts of A-stability and stability domain are proposed in the literature. Suppose that a given numerical method is applied with a step size h>0 to the linear test system $\dot{x} = \lambda x$, the stability domain of the underlying numerical method is the set of all numbers hλ such that x_n approach zero as $n \to \infty$.

In other words, the stability domain is the set of all hλ for which the correct asymptotic behavior is recovered, provided that the linear system is stable.

A method is *A-stable* if x_n approach zero as $n \to \infty$ for all values of the step size h when this method is applied to the equation $\dot{x} = \lambda x$ for all $\lambda \in \mathbf{C}$ with $\mathrm{Re}(\lambda)<0$. Note that for this equation, the exact solution also goes to zero. In other words for $\mathrm{Re}(\lambda)<0$ the solution of corresponding differential equations should be stable for any positive value of h. It implies that the stability domain includes the whole left half plane. Thus whether a method is A-stable or not can be judged from the stability domain. The stability domains of the forward Euler and trapezoidal method are shown in Fig. 3-2. The forward Euler method is not A-stable while trapezoidal method is A-stable. It is proven that no explicit Runge-Kutta method may be A-stable [73]. In general, an A-stable linear multi-step method is necessarily implicit but not every implicit method is A-stable.

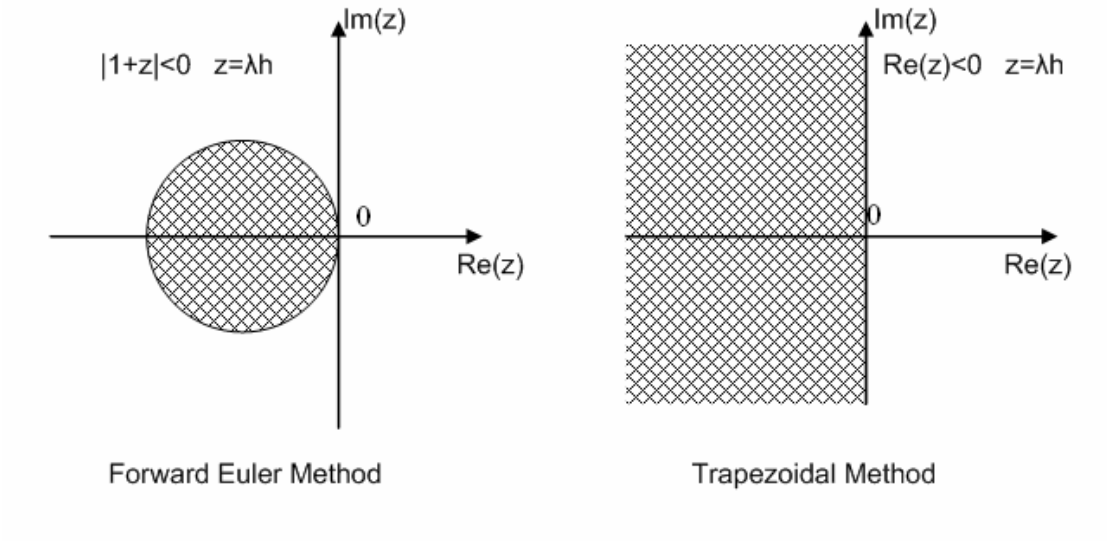

Fig. 3-2. Stability Domain of Forward Euler and Trapezoidal Methods

One of the drawbacks of A-stability is that the stability domain may include part of the right half plane, thus the real unstable phenomena will be simulated as a stable one. The spurious damping is called hyper stability [42]. Hyper stability can be avoided by reducing the step size during the simulation on the basis of the experience of the end user or the evaluation of eigenvalues.

3.3 Decoupled Method for ODE

Since power systems are stiff problems, implicit methods are commonly used to simulate the dynamic behavior. Each integration step of a stiff equation involves the solution of a nonlinear equation which leads to a set of linear problems involving the Jacobian of the system. As a result, the methods for solving stiff systems spend most of the time solving systems of linear equations. The numerical stability properties of the time domain simulation algorithms are determined by the eigenvalues of the linearized matrix, and frequently the eigenvalues which cause stiff problems are only a small portion of the whole spectra. It seems inefficient to solve these problems only with implicit methods. If the problem can be partitioned into a stiff part and a non stiff part such as

$$\begin{cases} \dot{x}_s = f_s(x_s, x_n) \\ \dot{x}_n = f_n(x_s, x_n) \end{cases} \tag{3.8}$$

where f_s, f_n are stiff and non stiff equations with variables x_s and x_n respectively, the system can be treated with an implicit method for the stiff equations and an explicit method for the non stiff equations [71].

In the numerical stability analysis of the algorithms, it is required that eigenvalues are located inside the stability domain to yield convergence behavior. If some eigenvalues are outside the stability domain of explicit methods, numerical stability may not be revealed by the dynamical simulation. However, the numerical results can be corrected by treating those outside eigenvalues differently. The decoupled method is based on the idea of separating stiff eigenvalues from the others.

From the geometric viewpoint, the solutions of the ODE and DAE systems are points or vectors in the multi-dimensional space. This space can be divided into two or more subspaces and the solution vectors can be decomposed into corresponding two or more sub-vectors in each subspaces. Thus, by decomposing the space into a number of small subspaces, the solution vectors can be divided into sub-vectors and the original ODE and DAE systems can be decoupled into several small dimensional systems.

Denote $\lambda_1, \cdots, \lambda_m, \lambda_{m+1}, \cdots, \lambda_n$ be the eigenvalues of linearized n-dimensional matrix $A = D_x f(x)$, and suppose only first m eigenvalues are located outside the stability domain of an explicit method. Let $\mathbf{P}$ be the invariant subspace corresponding to these m eigenvalues and let Z_1 be an orthonormal basis in $\mathbf{P}$. Thus Z_1 is $n \times m$ matrix which satisfies the following conditions:

$$AZ_1 = Z_1\Lambda_1 \tag{3.9}$$

$$Z_1^T Z_1 = I_m \tag{3.10}$$

where I_m is $m \times m$ identity matrix, and Λ_1 is a square matrix with m eigenvalues outside the stability domain.

Furthermore, there exists an orthogonal complement **Q** such that **Q** = **P**$^{\perp}$. And let Z_2 be the orthonormal basis in **Q**, then

$$Z_2^T Z_2 = I_{n-m} \tag{3.11}$$

And since **Q** is an orthogonal complement, it follows that

$$Z_1^T Z_2 = 0 \;\; Z_2^T Z_1 = 0 \tag{3.12}$$

Therefore, the *n*-dimensional space can be represented by the direct sum of **P** and **Q** where Z_1 and Z_2 are the corresponding basis respectively. Moreover, $n \times n$ dimension matrix $Z_1 Z_1^T$ and $Z_2 Z_2^T$ are the orthogonal projectors into the two subspaces according to the definition in [76].

Because $Z_1 Z_1^T$ and $Z_2 Z_2^T$ are the orthogonal projectors, any vector in the full space can be projected into two subspaces by multiplying the projectors on the left. In other words, once the projections in these two subspaces are known, the original vector in the full space can be recovered. Let *p* and *q* be the vectors in *m*-dimensional and (*n*-*m*)-dimensional subspaces, and the original *n*-dimensional vector *x* can be recovered from *p* and *q* by setting $p = Z_1^T x$ and $q = Z_2^T x$.

Proposition 1: For each vector x in R^n space, there exist unique vector $p \in R^m$ and $q \in R^{n-m}$ such that $x = Z_1 p + Z_2 q$.

Proof:

Since $Z_1^T (Z_1 Z_1^T + Z_2 Z_2^T) = Z_1^T Z_1 Z_1^T + Z_1^T Z_2 Z_2^T = Z_1^T$, therefore $(Z_1 Z_1^T + Z_2 Z_2^T) = I_n$.

Let $p = Z_1^T x$, $q = Z_2^T x$, thus $Z_1 p + Z_2 q = Z_1 Z_1^T x + Z_2 Z_2^T x = (Z_1 Z_1^T + Z_2 Z_2^T) x = x$. □

Since the vector in the original *n*-dimensional space can be decomposed into the sum of two small dimension vectors, the original system can be split into two sub systems according to Lyapunov-Schmidt decomposition:

$$f^P(p,q) = Z_1^T f(Z_1 p + Z_2 q) \tag{3.13}$$

$$f^Q(p,q) = Z_2^T f(Z_1 p + Z_2 q) \tag{3.14}$$

And the ODE system equations can be decoupled into two systems

$$\begin{cases} \dot{p} = f^P(p,q) = Z_1^T f(Z_1 p + Z_2 q) \\ \dot{q} = f^Q(p,q) = Z_2^T f(Z_1 p + Z_2 q) \end{cases} \tag{3.15}$$

By solving the above equations, variables p and q can be calculated separately, and the original states are given as $x = Z_1 p + Z_2 q$.

For the decoupled systems, the second set of equations $Z_2^T f(Z_1 p + Z_2 q)$ has the derivative $Z_2^T A Z_2$. It is desirable if the eigenvalues are still in the stability region of the explicit methods. And we have the following conclusion:

Proposition 2: The matrix $Z_2^T A Z_2$ has the remaining *n-m* eigenvalues $\lambda_{m+1}, \cdots, \lambda_n$.

Proof is given in [77, 78]. □

Equation (3.15) has the desired form as (3.8) and the all the eigenvalues of the second equation set are inside the stability domain of explicit method. Therefore, an explicit method

can be applied to solve the second set of equations and an implicit method can be applied to solve the first set of equations. To eliminate the need for Z_2, let $v = Z_2 q$, thus

$$\dot{v} = Z_2 Z_2^T f(Z_1 p + v) = (I - Z_1 Z_1^T) f(Z_1 p + v)$$

The new system is

$$\begin{cases} \dot{p} = Z_1^T f(Z_1 p + v) \\ \dot{v} = (I - Z_1 Z_1^T) f(Z_1 p + v) \end{cases} \tag{3.16}$$

3.4 Decoupled Method for DAE

The simulation of differential algebraic equation systems involves solving of a set of differential equations and a set of algebraic equations simultaneously. The solutions of differential equations and algebraic equations can be obtained either separately or simultaneously. The decoupled method can be applied to the differential equations in similar way as applied to ODE systems. To demonstrate the approach forward Euler method is chosen as an example of explicit method and trapezoidal method as an example of the implicit method. Also we denote the number of differential equations as *n*, the number of the algebraic equations as *l*, and the dimension of stiff invariant subspace **P** as *m*.

3.4.1 *Decoupled Forward Euler-Trapezoidal Method for DAE*

Similar to the ODE system, the DAE system can be decomposed into the following form

$$\begin{cases} \dot{p} = Z_1^T f(Z_1 p + v) \\ \dot{v} = (I - Z_1 Z_1^T) f(Z_1 p + v) \\ 0 = g(p, v, y) \end{cases} \tag{3.17}$$

The initial conditions are given as

$$\begin{cases} x(0) = x_0 \\ y(0) = y_0 \\ p(0) = Z_1^T x_0 \\ v(0) = (I - Z_1 Z_1^T) x_0 \end{cases} \tag{3.18}$$

The decoupled forward Euler-Trapezoidal method is formulated as:

$$\begin{cases} v_{k+1} = v_k + h(I - Z_1 Z_1^T) f(Z_1 p_k + v_k) \\ p_{k+1} = p_k + h Z_1^T [(f(Z_1 p_k + v_k) + f(Z_1 p_{k+1} + v_{k+1})]/2 \\ 0 = g(p_{k+1}, v_{k+1}, y_{k+1}) \end{cases} \tag{3.19}$$

The first set of equations can be solved via fixed point iteration, and the second and third sets of the equations actually are nonlinear equation and Newton method is needed to solve it. The second and third equation sets are reformulated as:

$$\begin{cases} p_{k+1} - \frac{1}{2} h Z_1^T f(Z_1 p_{k+1} + v_{k+1}) = p_k + \frac{1}{2} h Z_1^T f(Z_1 p_k + v_k) \\ g(p_{k+1}, v_{k+1}, y_{k+1}) = 0 \end{cases} \tag{3.20}$$

where the unknowns are p_{k+1} and y_{k+1}.

Whereas the full implicit method needs to solve the following nonlinear equation set

$$\begin{cases} x_{k+1} - hf(x_{k+1})/2 = x_k + hf(x_k)/2 \\ g(x_{k+1}, y_{k+1}) = 0 \end{cases} \tag{3.21}$$

The dimension of the full implicit method is *n+l* while the dimension of the decoupled system is *m+l*. Since *m*<<*n*, the dimension of the nonlinear systems can be significantly reduced.

3.4.2 *Identification of Stiff Invariant Subspace*

To identify the basis Z_1 of invariant subspace **P**, it is only required to identify the a few eigenvectors of corresponding eigenvalues instead of all of the eigenvectors. As for the forward Euler method, the stability domain boundary is a circle which has the center (-1/h, 0) and radius 1/h for eigenvalue λ. Thus the stiff invariant subspace is associated with eigenvalues outside the circle. Because the algorithms for dominant eigenvalues calculation such as Arnoldi method tend to converge to eigenvalues with largest moduli, it is not straightforward to directly identify the invariant subspace if the center of the circle is not the origin. The remedy is to shift the stability domain to the right direction so that the origin becomes the center of the shifted circle by shifting the linearized matrix *A*.

Proposition 3: Let (λ_i, v_i) be the eigen-pair of *n*-by-*n* matrix *A*, then $(\lambda_i + 1/h, v_i)$ is the eigen-pair of matrix $A + I/h$.

Proof: Let λ_i , v_i be the corresponding eigen-pair to matrix A, thus $Av_i = \lambda_i v_i$. Then $Av_i + v_i/h = \lambda_i v_i + v_i/h$, that is $(A + I/h)v_i = (\lambda_i + 1/h)v_i$. Therefore $\lambda_i + 1/h$ is the eigenvalue of $A + I/h$. □

Now the original problem is transformed into the new problem to find out a few eigenvalues outside a circle of the matrix $A + I/h$. These eigenvalues can be computed efficiently by the Arnoldi method.

3.5 Numerical Examples

3.5.1 *New England System Simulation Results*

Numerical examples of New England power system is demonstrated here. New England system has 39 buses and 10 generators. There are 9 differential states for each generator. As there are 9 states for each generator, and the total number of differential states and algebraic states are 90 and 78 respectively. The step size during the simulation is chosen as 0.025 second. The stiff invariant subspace is calculated at the initial state with dimension as 19, thus the dimension of the nonlinear equation system is 97 for the decoupled method (19 stiff differential states and 78 algebraic states), while the dimensions of the nonlinear equation systems are 78 and 168 for the explicit method and implicit method respectively. The computational time for stiff invariant subspace is 0.235 seconds.

In the following section, several disturbances and control actions are considered to demonstrate both the accuracy and computational efficiency of decoupled method for New England system. Here is a summary of the cases:

Case A: Line outage

Case B: Line outage with load variation

Case C: Line outage with load variation and shunt capacitor compensation

The contingency in case A is transmission line trip between bus 6 and bus 7 at 0.05 second, and the simulation duration is 20 seconds. The actual post-disturbance behavior is that the system stability can be maintained. The simulation results of decoupled method and

full implicit method yield stable cases; however, full explicit method fails to give correct answer. Full explicit method (forward Euler method) diverges at about 1.1 second as shown in Fig. 3-3. Before explicit method diverges, an oscillatory behavior can be observed from the result which is only due to numerical error instead of real system response.

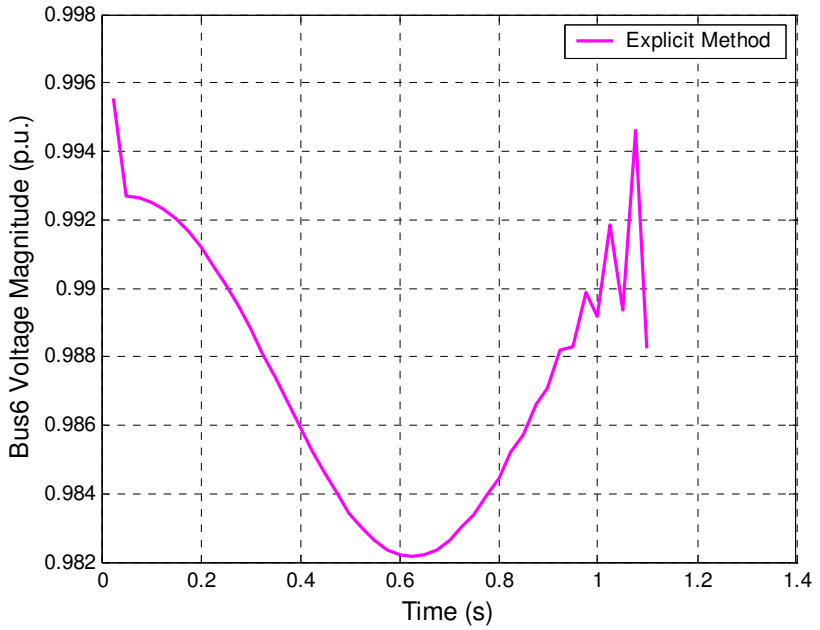

Fig. 3-3. Case A Simulation Result by Forward Euler Method

The simulation results of decoupled method and full implicit method give the stable system behaviors as shown in Fig. 3-4. Both methods give stable post disturbance behavior and the results from two methods match very well.

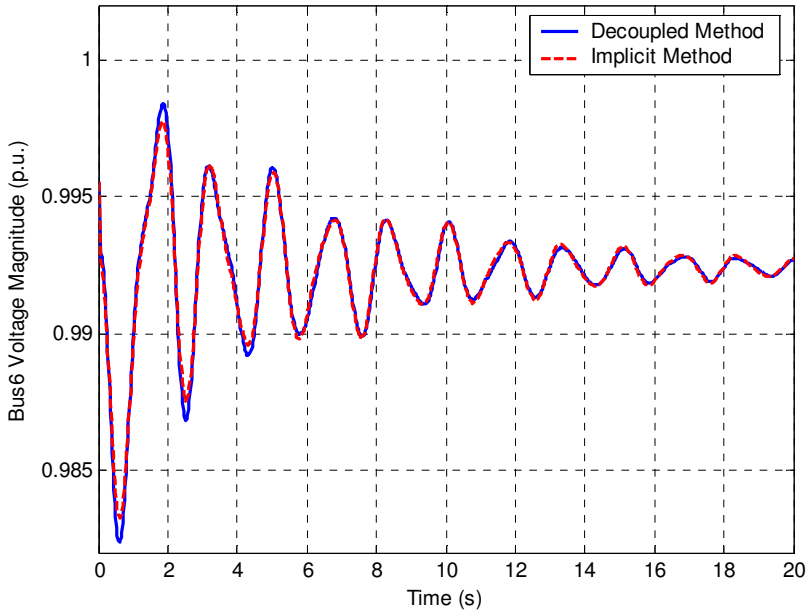

Fig. 3-4. Case A Simulation Results by Decoupled and Implicit Methods

The computational time of decoupled method, explicit method and full implicit method in case A is shown in Table 3-1 (N/A means dynamical simulation cannot be finished due to numerical divergence under the given step size; the maximum step size for forward Euler method to give similar results as trapezoidal method is 0.002 second and the simulation time is about 2800 seconds under such step size). It shows that decoupled method requires much less time than implicit method to finish the dynamic simulation.

TABLE 3-1 COMPUTATIONAL TIME COMPARISON I

Methods	CPU Time (s)
Explicit Method	N/A
Implicit Method	745
Decoupled Method	405

The disturbances in case B are both loss of transmission line and load increment. Line between bus 6 and bus 7 is tripped off at 0.05 second as in case A, and the system loads also increase by 10 percent per second until the end of simulation (5 seconds duration). The effect of continuous load increment will cause system instability in this case. Here also explicit method experiences convergence problems and provides the wrong result during the simulation; while decoupled method and implicit method yield correct system behaviors as shown.

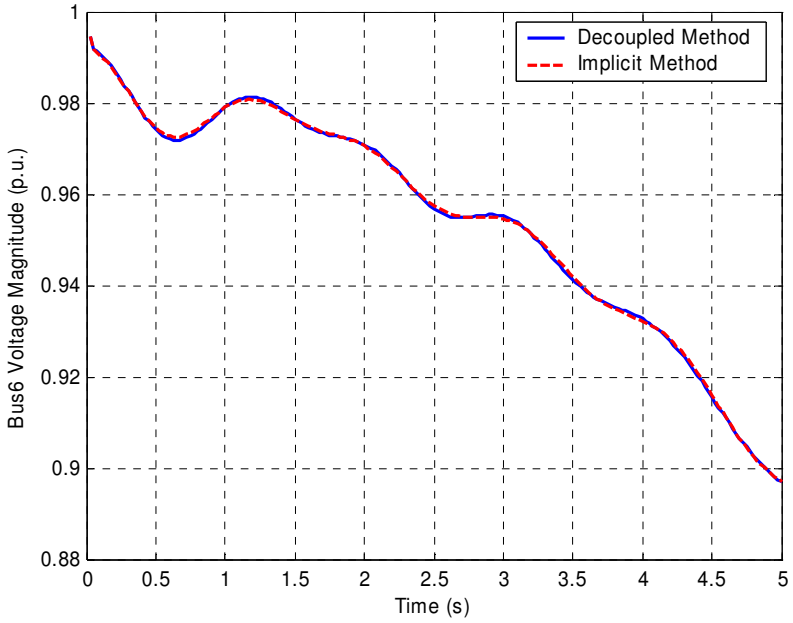

Fig. 3-5. Case B Simulation Results by Decoupled and Implicit Methods

The computational time of decoupled method and full implicit method in case B is shown in Table 3-2. The decoupled method is almost twice as fast as the implicit method.

TABLE 3-2 COMPUTATIONAL TIME COMPARISON II

Methods	CPU Time (s)
Implicit Method	230
Decoupled Method	130

In case C, the transmission line between bus 6 and bus 7 is tripped at 0.05 second and system loads increase by 10 percent in the 1st second. At 1 second (right after the end of load variation), a 250KVARs shunt capacitor is switched on at bus 7. The dynamical response of decoupled method and implicit method is shown in Fig. 3-6.

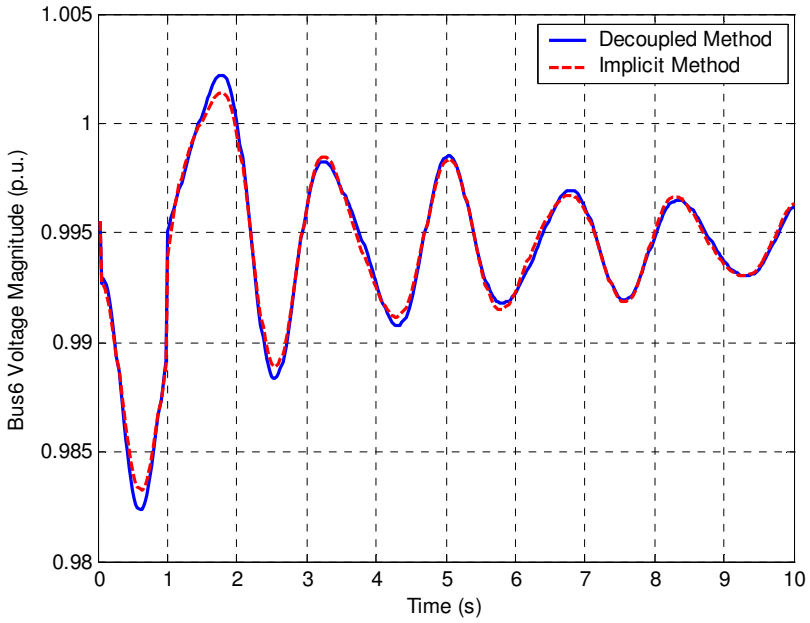

Fig. 3-6. Case C Simulation Results by Decoupled and Implicit Methods

The computational time of decoupled method and implicit method in case C is shown in Table 3-3.

TABLE 3-3 COMPUTATIONAL TIME COMPARISON III

Methods	CPU Time (s)
Implicit Method	442
Decoupled Method	252

The simulation results summary of the above cases are given in Table 3-4. It includes the dimension of the nonlinear equations for decoupled and implicit methods, computational time and the computational errors between decoupled and implicit methods. The dimension of stiff subspace is 19, and the computational time of decoupled method includes 0.235 seconds for the stiff subspace computation. The computational error in Table 3-4 is defined as the infinity norm of the difference between implicit method and decoupled method.

TABLE 3-4 THE SUMMARY OF NEW ENGLAND SYSTEM RESULTS

Cases	Nonlinear Equations Dimension		Computational Time (s)		Computational Error
	Implicit	Decoupled	Implicit	Decoupled	
Case A	168	97	745	405	9.4689 e-004
Case B	168	97	230	130	9.0860 e-004
Case C	168	97	442	252	12.0000 e-004

3.5.2 *IEEE 118-bus System Simulation Results*

IEEE 118-bus system has 118 buses and 48 generators, and the total number of differential states and algebraic states are 432 and 236 respectively. The step size during the simulation is chosen as 0.025 second. The stiff invariant subspace is calculated at the initial state with dimension as 31, thus the dimension of the nonlinear equation system is 267 for the decoupled method (31 stiff differential states and 236 algebraic states), while the

dimensions of the nonlinear equation systems are 236 and 668 for the explicit method and implicit method respectively. The computational time for stiff invariant subspace is 1.062 seconds.

Three cases are considered in IEEE 118-bus system. Here is a summary of the cases:

Case D: Line outage. In case D, the transmission line between bus 85 and bus 89 is tripped off at the time of 0.05 second. The simulation duration is 2 seconds.

Case E: Line outage with shunt capacitor compensation. In case E, line 85-89 is tripped off at the same time as in case D; after the line trip contingency, a 250KVARs shunt is switched on at bus 85 at the time of 0.5 second. The simulation duration is 2 seconds.

Case F: Three-phase short circuit. In case F, a three-phase short-circuit fault occurs at the middle point of line 85-89 at the time of 0.05 second. The fault duration is 0.1 second (6 cycles for 60Hz system), and the fault is cleared at the time of 0.15 second by opening line 85-89.

The simulation results in case D are plotted in Fig. 3-7 and Fig. 3-8. In Fig. 3-7, the results by explicit method show oscillatory behavior near 1 second which is only due to numerical error accumulation. The simulation results by both decoupled method and implicit method are shown in Fig. 3-8, and both methods give similar results while decoupled method requires much less time.

The simulation results in case E and case F are given in Fig. 3-9 and Fig. 3-10. Decoupled method and implicit method also give very close results.

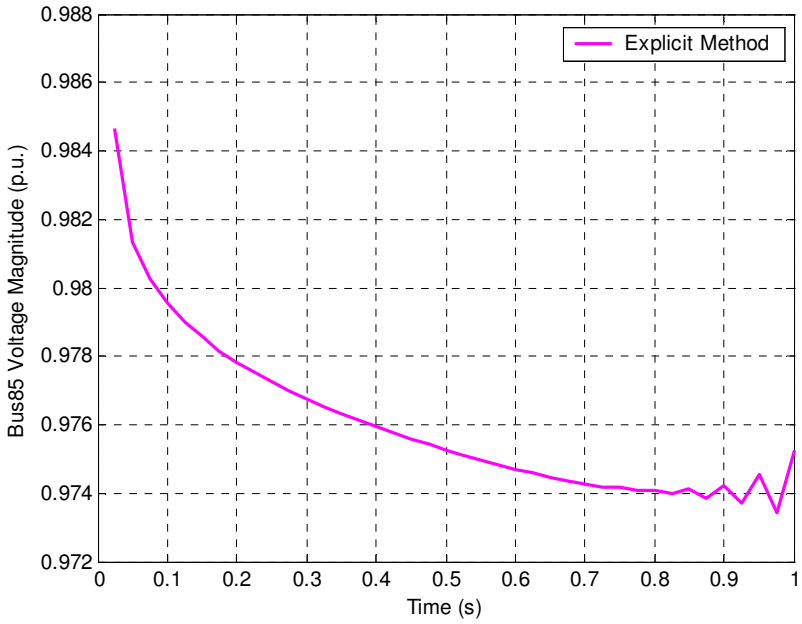

Fig. 3-7. Case D Simulation Result by Forward Euler Method

The simulation results summary of the above IEEE 118-bus system cases are given in Table 3-5. It includes the dimension of the nonlinear equations for decoupled and implicit methods, computational time and the computational errors between decoupled and implicit methods. The dimension of stiff subspace is 31, and the computational time of decoupled method includes 1.062 seconds for the stiff subspace computation. The computational error is the infinity norm of the difference between implicit method and decoupled method.

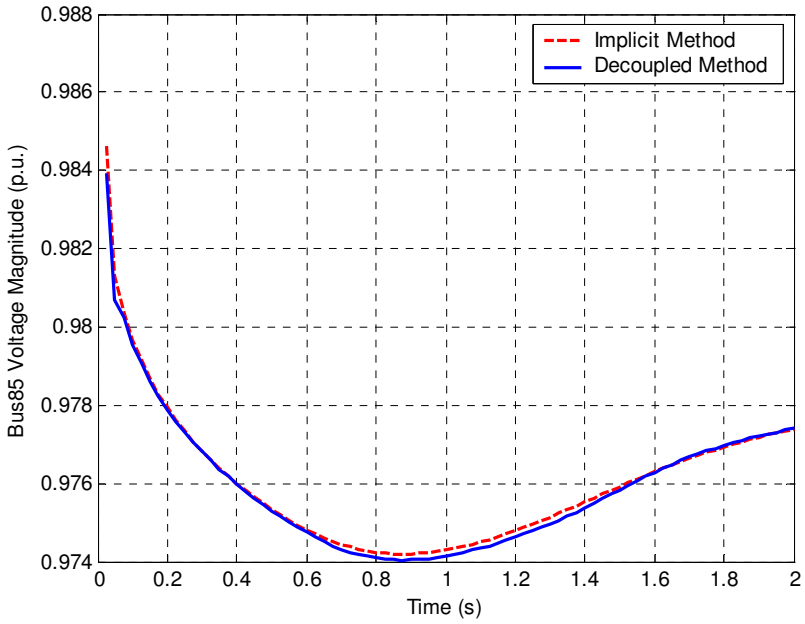

Fig. 3-8. Case D Simulation Results by Decoupled and Implicit Methods

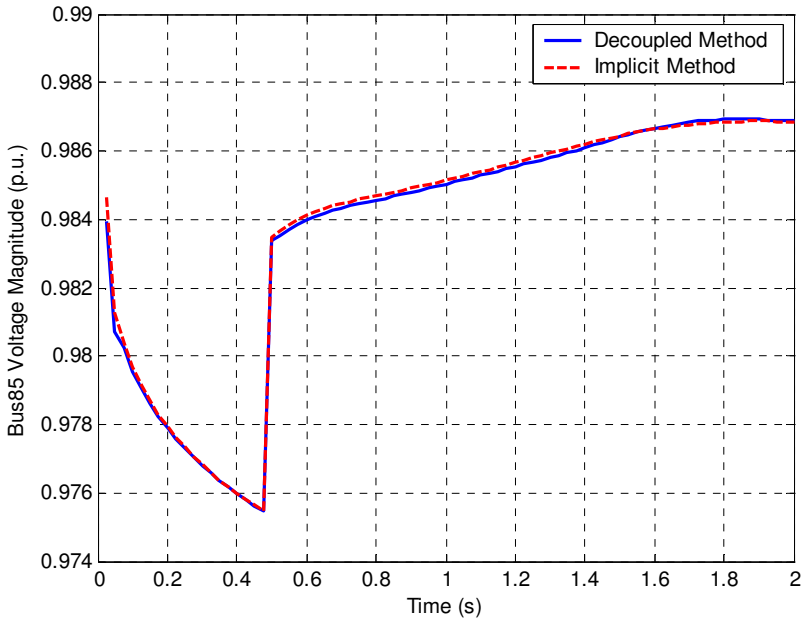

Fig. 3-9. Case E Simulation Results by Decoupled and Implicit Methods

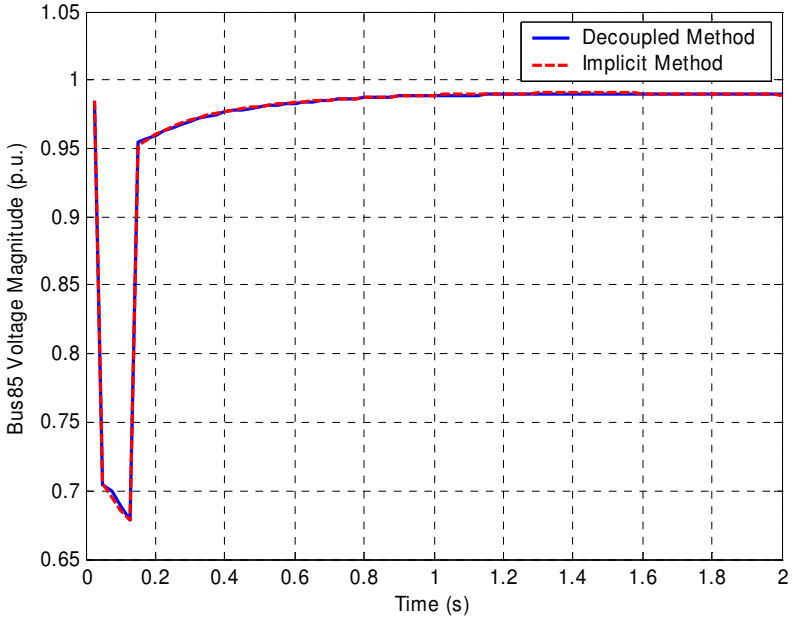

Fig. 3-10. Case F Simulation Results by Decoupled and Implicit Methods

TABLE 3-5 THE SUMMARY OF IEEE 118-BUS SYSTEM RESULTS

Cases	Nonlinear Equations Dimension		Computational Time (s)		Computational Error
	Implicit	Decoupled	Implicit	Decoupled	
Case D	668	267	956	247	6.9335 e-004
Case E	668	267	997	246	6.9335 e-004
Case F	668	267	998	299	49.0000 e-004

3.6 Summary

In this chapter, a decoupled method is proposed to improve the computational efficiency of the power system dynamical simulation. The method combines the advantages of explicit

and implicit methods. The original power system equations are decoupled into two parts which correspond to the stiff and non-stiff subspaces. For the stiff invariant subspace, the implicit method is applied to achieve numerical stability and the explicit method is employed to handle non-stiff invariant subspace for the computational efficiency. As a result, the new hybrid method is both numerically stable and efficient. In the next chapter, optimization method for dynamical systems will be formulated to prevent system instabilities based on the simulation results from the time domain simulation.

CHAPTER 4 TRAJECTORY OPTIMIZATION

4.1 Introduction

Power system behaviors subject to disturbances such as potential failure can be identified by dynamical simulation such as decoupled dynamical simulation algorithm introduced in the previous chapter. Once potential system failure has been identified, the next step is to find a control method with which to mitigate system failure. This chapter proposes an optimization method incorporating system dynamics for providing optimal control strategies with which to prevent system failure caused by disturbances.

Control strategies may be simply based on steady state analysis using optimal power flow calculations to minimize cost or maximize distance to a collapse point. However, the complexity of power systems requires an additional consideration of dynamics, since traditional steady state analysis may not be sufficient to judge power system dynamical behavior. For example, power flow analysis only considers the existence of system equilibrium. Equilibrium may exist for the post disturbance power system, but loss of stability may still occur due to lack of attraction towards the post disturbance equilibrium. Since power systems are dynamic, power system control strategies are time dependent, and the representation of a dynamic system model should be taken into account for optimal control guarding against system failure. The coordination over time of control amounts at a variety of locations for power system security is quite a challenging problem. Often it is

found that system collapse can be prevented by applying a small amount of control resource, so it is important to discover the optimal control strategy by considering the system dynamics.

From the viewpoint of mathematical optimization, problems with optimization can be classified into parameter optimization problems and trajectory optimization problems. In the formulation of parameter optimization problems, feasible regions are represented by algebraic conditions, while system dynamics are represented in the formulation of trajectory optimization problems. The formulation of parameter optimization and trajectory optimization is given in the following sections.

4.1.1 *Parameter Optimization Problems*

Parameter optimization problems, or static optimization problems, involve finding the best values of an objective function in the feasible regions represented by algebraic conditions. Such problems may be either unconstrained or constrained. In the unconstrained case, the feasible regions of the control variables are unbounded, while in the constrained case, a set of algebraic inequality and inequality conditions are imposed to describe the allowed range of the control variables.

The general formulation of parameter optimization problems is as follows.

$$\min \quad L(x,u)$$

subject to

$$0 = c(x,u)$$

$$0 \le d(x,u)$$

The objective $L(x,u)$ defines the performance index to be optimized, while the equality constraints $c(x,u)$ and $d(x,u)$ define the feasible regions of the problems.

Optimal power flow is the application of parameter optimization problem to power systems. The aim of optimal power flow is to find the best power system control variables with which to optimize the power system performance index while satisfying the power system steady state constraints. The performance index in the optimal power flow may be the total cost or the total system loss, and the constraints of the optimal power flow consist of power flow equations and other conditions such as voltage profiles.

Parameter optimization problems can be further classified according to different criteria. The classification of linear and nonlinear optimization problems is based on whether there are nonlinear conditions in the formulation. In linear optimization problems, both objective and constraints are linear, while nonlinear optimization problems include nonlinear conditions. Nonlinear optimization problems may have a general formulation and some special formulations, such as quadratic nonlinear optimization problems that have quadratic objective function and linear constraints. Relative to the existence of discrete variables, parameter optimization problems can be categorized as continuous problems and discrete problems. The difference between global optimization and local optimization comes from the contrast between the global solution and the local solution. There are also a variety of numerical optimization techniques for parameter optimization problems, including simplex method, sequential quadratic programming, interior point method, active set method, and branch-and-bound method [79].

Control strategies for dynamic security analysis in the literature either use a combination of dynamical simulation and optimization techniques or transform a difficult problem with system dynamics into the form of parameter optimization using existing optimization methods.

In [55], an approach to load shedding control of voltage instability using sensitivity and simulation is given. The sensitivity is first derived from a Jacobian matrix with respect to control variables, and then the control amount is estimated to satisfy post-disturbance stability based on the sensitivity. The method can be further expanded into the simulations using trial and error method. The basic idea is to reduce the control amount needed through iterations and to use dynamical simulation to verify the control effect. In [56], the sensitivity information is used to rank load buses as candidates for load shedding. Then a binary search relying on the results of time domain simulation is used to determine the minimal amount of load shedding needed at a given time. The binary search continues building a smaller and smaller interval of load shedding amount such that upper bound of the interval is stable system response and lower bound is unstable system response. In the search procedure, the load shedding locations and time are pre-specified, and only the load shedding amounts are the decision variables. At each step, the mid-point of the search interval is tested through dynamical simulations and taken as the new upper or lower bound according to simulation results. A conceptual diagram of the trial and error method is shown in Fig. 4-1. In this figure P1 is the upper bound and P2 the lower bound. In the simulation, first a large load shedding amount P1 is identified through dynamical simulation such that the system equilibrium can be recovered. The lower bound P2 corresponds to load shedding amount which is insufficient

to reach an equilibrium conditions. Therefore, the best load shedding amount should lie in between P2 and P1. In the following iteration, the midpoint amount of the load shedding (P1+P2)/2 is tried, and the range containing the minimum load shedding amount is reduced by half. The search procedure continues until the range is small enough. Trial and error simulation methods can be very time consuming for large power systems, and transient behaviors such as voltage dip or sag are not considered in these methods.

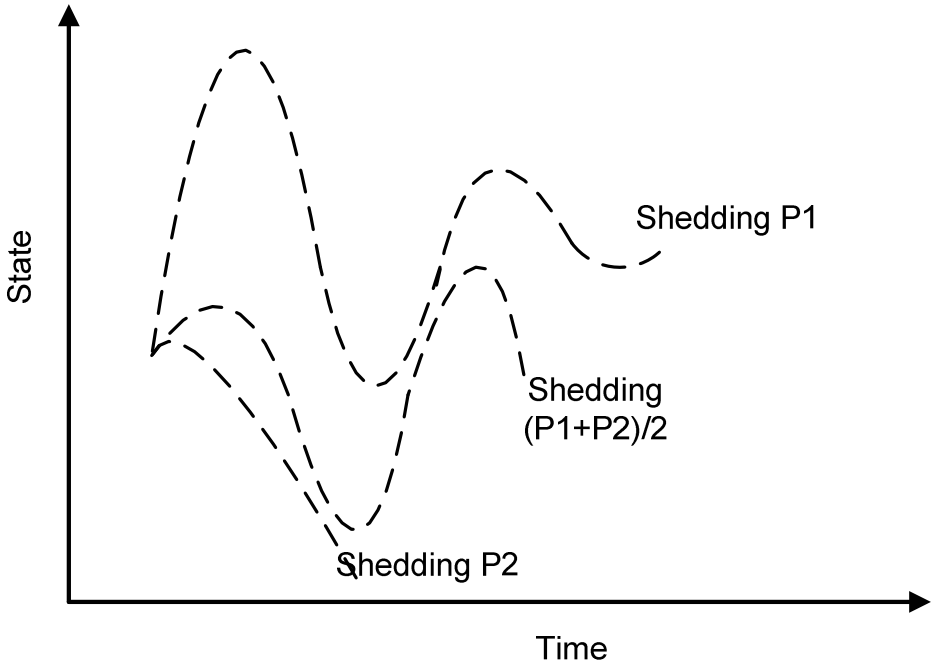

Fig. 4-1. Trial and Error Method

In another approach, search and optimization techniques with modal predictive control are used to determine control strategies as shown in Fig. 4-2. System responses are predicted based on the current state for several different candidate control sequences. For example, the solid line is the actual system trajectory until time T_0, and the dashed lines are the future system trajectories and the corresponding controls. From initial state point A at time T_0, the

future states at T_0+T_p can be predicted as different trajectories under different controls. The predicted trajectories are labeled T1, T2 and T3, with corresponding control outputs are U1, U2 and U3. In [57], a tree-search method is employed to determine the best control strategy among all the control candidates. This tree-search method is similar to those used in chess computers where each node in the tree corresponds to one possible control action. In [58], the selection of the optimum control action in the complex optimization problem is achieved by evolutionary programming. In [59], linear programming techniques are applied in each step to determine the control actions. In modal predictive control, power system dynamic behavior is approximated by simple responses such as straight lines in a discrete time formulation, with a time interval usually set to be quite large, for example, 30-60 seconds in [58]. Because of the large time horizons and straight line approximation, such methods are suitable for system dynamics with relatively long term and monotonic change, but power systems dynamic behaviors in short term cannot be represented and enhanced.

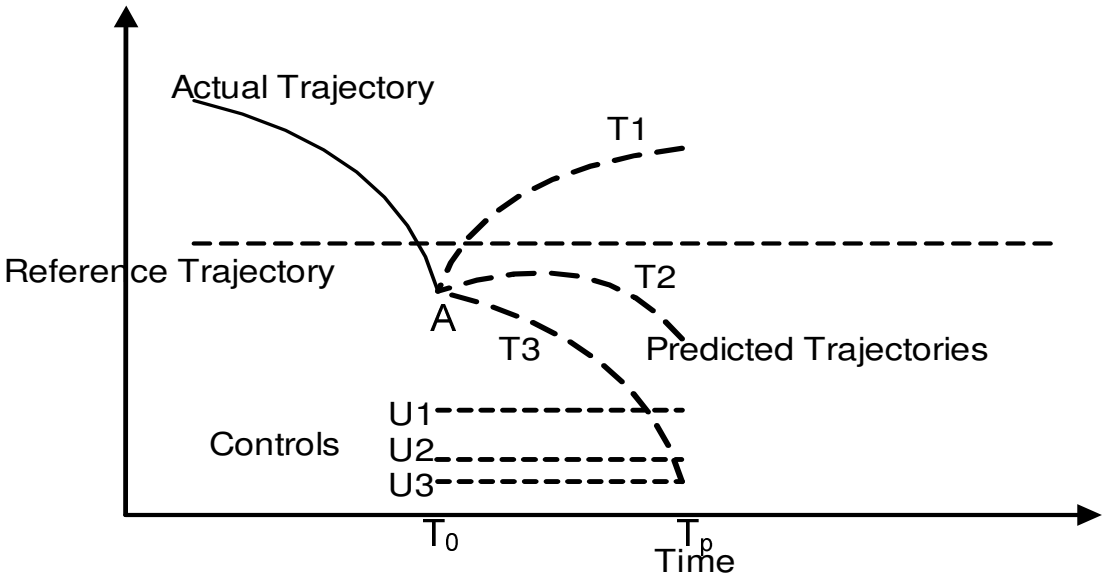

Fig. 4-2. Model Predictive Control

In [60] the difficult problem of control for dynamical system is transformed into a traditional nonlinear optimization problem. The transformation is based on discrete time formulation, with control strategies subsequently obtained from the solution of the transformed problem. However, the transformation tends to give a relatively inaccurate solution compared with the true solution, with the inaccuracy due to the introduction of pseudo minima from the transformation that are not the solutions of the original problem [61].

The control strategies proposed in the power system literature attempt to improve power system dynamic security through simple sensitivity information or complex dynamics transformation. In the simple schemes such as trial and error methods, the coordination between control resources is very difficult, and no power system transitions are considered. In the application of modal predictive control, the system states are predicted based on the linearization, and actual system state trajectories may be different from those predicted. In the method of problem transformation, inaccurate solutions may be reached due to the pseudo minima from the transformation. Therefore, there still a room for improvement in dynamic security analysis with accurate system dynamics representation and accurate solution.

4.1.2 *Trajectory Optimization Problems*

Trajectory optimization problems, or optimal control problems, aim to find the time-optimal solution for dynamical systems [80-83]. The history of trajectory optimization theory can be traced back at least to the late seventeen century when Johann Bernoulli posed a challenge to contemporary mathematicians to solve a simple problem considered from the modern viewpoint. Based on the original works from pioneers such as Leibniz, Newton,

Hospital, Jakob Bernoulli and Johann Bernoulli, the theory of the calculus of variation and trajectory optimization was developed subsequently by mathematicians such as Euler, Lagrange, Hamilton, Pontryagin, and so on. In trajectory optimization problems, the systems in the study are governed by dynamics. Under the effect of control, there may be multiple trajectories for the system state variables. A given performance index is defined for the system trajectories, and, among all possible trajectories, one will have the best performance according to the performance index. The task of trajectory optimization is to find the trajectory with the optimal objective, and to identify the corresponding control actions.

The trajectories of power systems are the movements of power system variables such as bus voltage and generator angles. Power system post-disturbance responses subject to different control strategies can be formulated as trajectory optimization problems, and power system dynamics can be represented in trajectory optimization formulation. In the trajectory optimization problem, a cost function or an objective function associated with trajectories is minimized or maximized under the constraints of dynamical state law, control variables, and boundary conditions. Both power system equilibrium and state constraints such as voltage dip can be considered in a unified way by imposing equality and inequality constraints on the state and control variables. To solve the difficult problems with inequality constraints, the extended penalty function method can be applied by transforming the original problem into a sequence of trajectory optimization problems without inequality constraints.

4.2 Formulation

Dynamical systems can be represented by a set of ordinary differential equations as shown in (4.1) .

$$\dot{x} = f(x) \tag{4.1}$$

Considering the existence of control variables, the system can be reformulated in (4.2)

$$\dot{x} = f(x,u) \tag{4.2}$$

where u is the control vector.

The system may also have initial-time and end-time conditions. For example, the initial time conditions may be the system states subject to disturbances, and the end time conditions may be the post disturbance equilibrium. Initial time and end time conditions can be represented in general form as:

$$b(x_0, u_0, x_T, u_T) = 0 \tag{4.3}$$

Initial time and end time conditions are called boundary conditions. The general form of the boundary conditions is the mixed conditions of initial time and end time, and the boundary conditions of the initial time and the end time may be separable, such as $b_0(x_0, u_0) = 0,\ b_T(x_T, u_T) = 0$. The initial time conditions for given initial conditions can be $b_0(x_0, u_0) = x_0 - x(0) = 0$, and the end time conditions for the post disturbance equilibrium can be written as $b_T(x_T, u_T) = \dot{x}_T = f(x_T, u_T) = 0$

The problem of trajectory optimization is to find the optimal trajectory among all the possible trajectories given the boundary (initial time and end time) conditions. The concept of trajectory optimization is shown in Fig. 4-3. In the figure, there exist different trajectories

connecting power system initial state and final state under different control strategies. The objective of power system trajectory optimization problem is to find the best control strategy and trajectory (for example, the solid line in Fig. 4-3) among all the possible candidates. Conceptual control output from dynamical optimization is illustrated in Fig. 4-4.

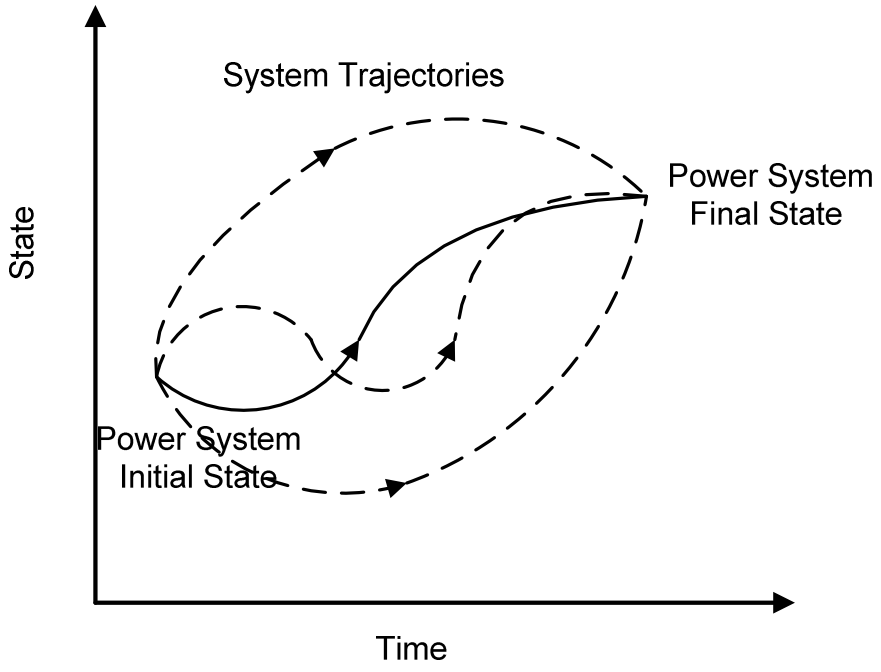

Fig. 4-3. Power System Dynamical Optimization Concept

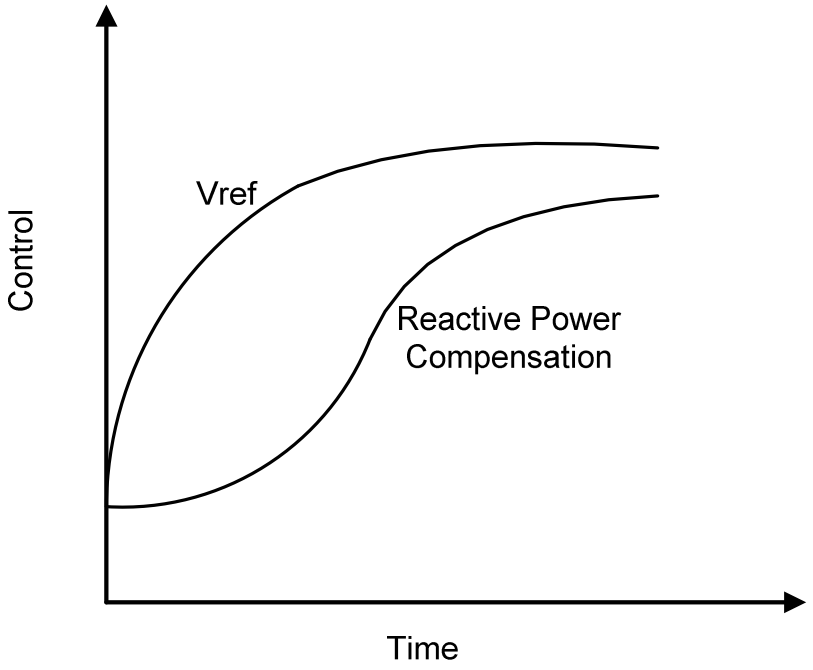

Fig. 4-4. Conceptual Dynamical Optimization Control Action

Control resources may be reactive power support, load, and the reference voltage of the automatic voltage regulator (AVR) as functions of time. Reactive power compensation is a control resource with which to enhance dynamic security by adjusting reactive power support. Reactive power compensation can be achieved through the Flexible AC Transmission Systems (FACTS) devices [84-86]. Through advances in power electronics, reactive power support can be provided continuously for security control from devices such as Static VAR Compensator and Static Synchronous Compensator (STATCOM). Load control such as non-disruptive load is another alternative control resource for dynamic security enhancement. Traditionally load control is achieved by load shedding, which leads to loss of power supply for some customers. In contrast to load shedding, non-disruptive load control schedules load usage for controllable load in the load center through high-speed communication technology.

As a result, load level can be controlled with imperceptible consequence to mitigate system stability by using non-disruptive load control [87-89]. The reference voltage set point control is used in the secondary voltage control scheme in many European countries [90-96]. The reference voltage set point control can adjust the generator terminal voltage through the automatic voltage regulator. Continuous control of the reference voltage set point can adjust the system voltage level in other buses through the generator terminal voltage control. In additional to the control resources of reactive power compensation, load control and reference voltage set point, it is still possible that, in the future, technology improvement in related areas such as electronics and communication may provide even more control resources that can be coordinated by the trajectory optimization method for power system security enhancement.

The objective function measuring the cost of control and the performance is defined as $J = \int_0^T L(x,u)dt$. $L(x,u)$ can include control amount and deviation from desirable states depending on the functional forms along the trajectory. The control amount can be represented as $L = u^T Q u$ with Q as a weighting matrix; deviation from desirable states can be represented as $L = (x - \overline{x})^T S(x - \overline{x})$ with $\overline{x}$ as a desirable state vector and S as a weighting matrix. For example, the desirable value for voltage in power system is about 1 per unit. The closer the actual voltage to the desirable voltage, the better the performance is.

In addition to the constraints of dynamical state law in (4.2), there also exist control and state variables constraints such as control function, and upper and lower limits on control and state variables. These additional constraints can be represented as a set of equalities or

inequalities in the problem formulation. Thus, the mathematical formulation of trajectory optimization is given as:

$$\min \quad J = \int_0^T L(x,u)dt \tag{4.4}$$

subject to

$$\dot{x} = f(x,u)$$

$$0 = c(x,u)$$

$$0 \le d(x,u)$$

where $c(x,u) = 0$ and $d(x,u) \ge 0$ are the equality and inequality constraints respectively.

The necessary conditions for trajectory optimization problems with both equality and inequality constraints are quite complex. Unconstrained trajectory optimization problems with only equality constraints are considered first, and then inequality constraints are incorporated into the formulation for constrained trajectory optimization problems.

Define multiplier λ and μ with the system differential equations $\dot{x} = f(x,u)$ and equality constraints $c(x,u) = 0$, and define a scalar function H (the Hamiltonian) as follows:

$$H(x,u,\lambda,\mu) = \lambda^T f + L + \mu^T c \tag{4.5}$$

The necessary conditions for trajectory optimization problems with only equality constraints are:

$$\begin{cases} \dot{x} = H_{\lambda}^{T} = f(x,u) \\ 0 = c(x,u) \\ \dot{\lambda} = -H_{x}^{T} = -(\dfrac{\partial L}{\partial x})^{T} - (\dfrac{\partial f}{\partial x})^{T}\lambda - (\dfrac{\partial c}{\partial x})^{T}\mu \\ 0 = H_{u}^{T} = (\dfrac{\partial L}{\partial u})^{T} + (\dfrac{\partial f}{\partial u})^{T}\lambda + (\dfrac{\partial c}{\partial u})^{T}\mu \end{cases} \tag{4.6}$$

The end conditions are $b_0(x_0,u_0)=0,\ b_T(x_T,u_T)=0$.

In power system application, algebraic equations in addition to the state law are the power flow equations. The constrained problem formulation in power system is given as:

$$\min \quad J = \int_0^T L(x,y,u)dt \tag{4.7}$$

subject to

$$\dot{x} = f(x,y,u)$$
$$0 = g(x,y,u)$$
$$0 \le d(x,y,u)$$

where x represents the system state variables, corresponding to dynamical states of generators; y corresponds to algebraic variables, usually associated to the transmission system and steady-state element models; vector u is used here to represent system parameters such as reactive power compensation, load level of non-disruptive load control etc, that are directly controllable. The necessary conditions for (4.7) without inequality constraints are similar to the necessary conditions for (4.4) without inequality constraints. The Hamiltonian is defined as:

$$H(x,y,u,\lambda,\mu,\gamma) = \lambda^{T} f + L + \gamma^{T} g \tag{4.8}$$

The necessary conditions for (4.7) without inequality constraints are:

$$\begin{cases} \dot{x} = H_{\lambda}^{T} = f(x, y, u) \\ 0 = g(x, y, u) \\ \dot{\lambda} = -H_{x}^{T} = -(\partial L / \partial x)^{T} - (\partial f / \partial x)^{T} \lambda - (\partial g / \partial x)^{T} \gamma \\ 0 = H_{u}^{T} = (\partial L / \partial u)^{T} + (\partial f / \partial u)^{T} \lambda + (\partial g / \partial u)^{T} \gamma \\ 0 = H_{y}^{T} = (\partial L / \partial y)^{T} + (\partial f / \partial y)^{T} \lambda + (\partial g / \partial y)^{T} \gamma \end{cases} \tag{4.9}$$

4.3 Extended Penalty Function Equivalence

The necessary conditions for trajectory optimization problems with both equality and inequality constraints are given by Pontryagin's Minimum Principle [80, 82]. Considering problem (4.4), the necessary conditions for inequality constraints with only state variables are the requirements that the product of inequality constraints and multipliers must be zero; the necessary conditions for inequality constraints with both state and control variables must satisfy the requirement that specifies that the Hamiltonian must be minimized over the set of all possible control resources. This can be formulated as:

$$\begin{cases} \dot{x} = H_{\lambda}^{T} = f(x, u) \\ 0 = c(x, u) \\ \dot{\lambda} = -H_{x}^{T} = -(\dfrac{\partial L}{\partial x})^{T} - (\dfrac{\partial f}{\partial x})^{T} \lambda - (\dfrac{\partial c}{\partial x})^{T} \mu \\ H(x, u, \lambda, \mu) = \min\limits_{v \in K} H(x, v, \lambda, \mu) \end{cases} \tag{4.10}$$

where K is the feasible set of control variables.

It is very difficult to solve trajectory optimization problems with inequality constraints because Pontryagin's Minimum Principle implies nonlinear optimization problems along the trajectory. It is thus desirable to transform inequality constraints into equality constraints. This transformation can be achieved via extended penalty function equivalence.

The inequality constrained trajectory optimization problem can be transformed into an equality constrained problem using penalty functions [97]. The trajectory optimization problem equivalent to (4.4) but without inequality constraints is as follows:

$$\min \quad J(\rho_k) = \int_0^T [L(x,u) + \rho_k \sum D_i(\rho_k, x, u)]dt \tag{4.11}$$

subject to

$$\dot{x} = f(x,u)$$

$$0 = c(x,u)$$

where penalty parameter $\rho_k > 0$ and D_i denote the penalty function terms that are added to the original cost function. In general these penalty function terms are small if the inequality constraints in the original optimization problem are satisfied and large if the inequality constraints are violated. If the inequality constraints are violated, the cost function is dominated by the penalty term. Therefore the optimization problem will tend to minimize the penalty term and thus the amount of constraint violation. On the other hand, if the constraints are satisfied, the penalty form remains small and makes no significant contribution to the cost function in (4.11). By driving penalty parameter ρ_k to zero, the influence of the penalty term D_i on the cost function becomes smaller and smaller, and the sequence of solution of

penalized optimization problem converges to the solution of the original optimization problem.

Penalty functions are usually classified as interior penalty function, exterior penalty function and extended penalty function. The differences among three categories are shown in Fig. 4-5. In the figure, the feasible region is defined as the domain of all trajectories that satisfy the inequality constraints $d(x,u) \geq 0$. The infeasible region is defined as the domain of all trajectories that violate the inequality constraints $d(x,u) \geq 0$.

A popular exterior function is the quadratic loss function defined as $D_i = (\min(0, d_i) / \rho_k)^2$. This penalty function is zero if the constraint is satisfied and non-zero otherwise. A disadvantage in using this penalty function is that at the constraint boundary $d_i = 0$ the first-order derivatives of the penalty function are discontinuous which makes the necessary conditions difficult to solve. The interior penalty function is defined only in the feasible region and is infinite on the constraint boundary $d_i = 0$. The interior penalty function can be defined as the inverse barrier function given by $D_i = 1/d_i$ or the logarithmic barrier function given by $D_i = \log(d_i)$. A disadvantage of the interior penalty function is that it is not defined for infeasible trajectories. Thus the numerical solution procedure used must be such that all the intermediate solutions satisfy the inequality constraints, a condition often difficult to accomplish in practice.

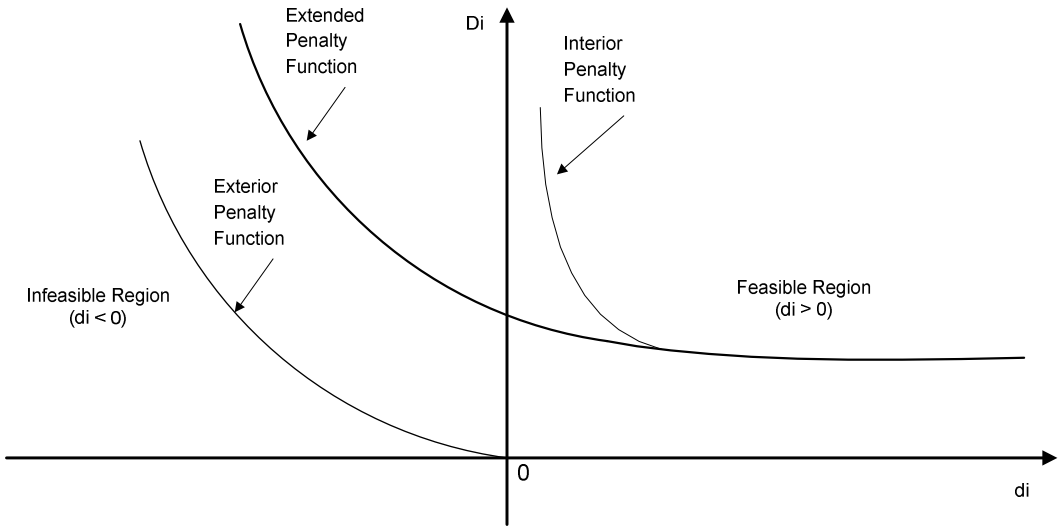

Fig. 4-5. Penalty Functions

The extended penalty function combines the interior and exterior penalty functions. A quadratic extended penalty function is given in [97] by

$$D_i = \begin{cases} 1/d_i & d_i \geq \sqrt{\rho_k} \\ (1/\sqrt{\rho_k})[3 - 3d_i/\sqrt{\rho_k} + (d_i/\sqrt{\rho_k})^2] & d_i \leq \sqrt{\rho_k} \end{cases} \tag{4.12}$$

The extended penalty function uses $\sqrt{\rho_k}$ as a transition point and extends the range from the feasible region to the infeasible region. This allows trajectories that do not satisfy inequality constraints to be treated at intermediate steps of the optimization process. The first and second derivatives of the extended penalty function are continuous at the transition point, which is sufficient for the continuation technique to solve the necessary conditions.

The Hamiltonian of the transformed trajectory optimization problem with equality constraints only is $H(x,u,\lambda,\mu) = \lambda^T f + L + \rho_k \sum D_i(\rho_k, x, u) + \mu^T c$, and the necessary conditions are defined as follows:

$$\begin{cases} \dot{x} = H_{\lambda}^{T} = f(x,u) \\ 0 = c(x,u) \\ \dot{\lambda} = -H_{x}^{T} = -(\dfrac{\partial L}{\partial x})^{T} - (\dfrac{\partial f}{\partial x})^{T}\lambda - \rho_k \sum (\dfrac{\partial D_i}{\partial x}) - (\dfrac{\partial c}{\partial x})^{T}\mu \\ 0 = H_{u}^{T} = (\dfrac{\partial L}{\partial u})^{T} + (\dfrac{\partial f}{\partial u})^{T}\lambda + \rho_k \sum (\dfrac{\partial D_i}{\partial u}) + (\dfrac{\partial c}{\partial u})^{T}\mu \end{cases} \tag{4.13}$$

The constrained trajectory optimization problem for differential and algebraic equations in (4.7) can be formulated in a similar way using the penalty function. For the inequality constraints $0 \le d(x, y, u)$, define the penalty term:

$$D_i = \begin{cases} 1/d_i & d_i \ge \sqrt{\rho_k} \\ (1/\sqrt{\rho_k})[3 - 3d_i/\sqrt{\rho_k} + (d_i/\sqrt{\rho_k})^2] & d_i \le \sqrt{\rho_k} \end{cases}$$

The Hamiltonian is $H(x, y, u, \lambda, \gamma) = \lambda^T f + L + \rho_k \sum D_i(\rho_k, x, y, u) + \gamma^T g$, and the necessary conditions are given in (4.14).

$$\begin{cases} \dot{x} = H_{\lambda}^{T} = f(x, y, u) \\ 0 = g(x, y, u) \\ \dot{\lambda} = -H_{x}^{T} = -(\partial L/\partial x)^{T} - (\partial f/\partial x)^{T}\lambda - (\partial g/\partial x)^{T}\gamma - \rho_k \sum \partial D_i/\partial x \\ 0 = H_{u}^{T} = (\partial L/\partial u)^{T} + (\partial f/\partial u)^{T}\lambda + (\partial g/\partial u)^{T}\gamma + \rho_k \sum \partial D_i/\partial u \\ 0 = H_{y}^{T} = (\partial L/\partial y)^{T} + (\partial f/\partial y)^{T}\lambda + (\partial g/\partial y)^{T}\gamma + \rho_k \sum \partial D_i/\partial y \end{cases} \tag{4.14}$$

The formulation of necessary conditions in (4.13) and (4.14) is a two-point boundary value problem (TPBVP). Such a problem can be solved by finite difference methods or by shooting methods [98, 99]. Solutions of transformed trajectory optimization problems with

equality constraints only will approach the solutions of original trajectory optimization problems with both equality and inequality constraints as the penalty parameter ρ_k goes close to zero.

4.4 Numerical Solution of Boundary Value Problem

The necessary condition of trajectory optimization is a boundary value problem (BVP), more specifically, a two-point boundary value problem (TPBVP) for differential algebraic equations. The boundary value problem in (4.13) and (4.14) can be written in a general form as follows.

$$\dot{x} = f(x, y) \tag{4.15}$$

$$0 = g(x, y) \tag{4.16}$$

$$0 = b(x_0, y_0, x_T, y_T) \tag{4.17}$$

In the formulation of (4.15)-(4.17), the compact forms of system representation and variable representation are used. For example, the variable vector x include both the system differential states and the co-states or the multiplier in the trajectory optimization. The variable vector y represents power flow variables, control variables and the co-states. The power flow variables may be bus voltage magnitude and bus voltage angle, and the control variables may be reactive power compensation, generator reference voltage, and load. The boundary conditions (4.17) are also in a compact form consisting of both initial time and end time conditions for power system differential states and algebraic states.

The boundary value problem can be solved by finite difference methods or by shooting methods [98, 99]. Finite difference methods aim to find a numerical approximation over the

entire time interval, and these methods are thus sometimes referred to as global methods. The shooting methods employ numerical solutions of the initial value problem to find the solution of boundary value problems. In the mathematical literature, both methods are applied to solve the boundary value problem, and there is no well established conclusion as to whether one method is superior to the other. In this section, finite difference methods are applied to solve the boundary value problem from the necessary condition of the trajectory optimization. A survey of some global methods to solve BVP-ODE is shown in [100].

The basic idea of the finite difference methods is to transform a boundary value problem into a set of nonlinear equations in a mesh of the time interval. The differential quotients in the differential equations are replaced by the finite difference quotients. For a time interval defined as [0, T], a mesh or a sequence of steps is defined with N subintervals:

$$0 = t_0 < t_1 < \cdots < t_{N-1} < t_N = T$$

The corresponding differential and algebraic states at the mesh points are denoted as:

$$x_0 < x_1 < \cdots < x_{N-1} < x_N = x_T$$

$$y_0 < y_1 < \cdots < y_{N-1} < y_N = y_T$$

The differential operator $\dot{x} = f(x, y)$ can be numerically approximated by the finite difference $FD(x_0, \cdots, x_N, y_0, \cdots, y_N) = 0$. Then the boundary value problem in (4.15)-(4.17) can be replaced by the nonlinear equation set as:

$$0 = FD_i(x_0, \cdots, x_N, y_0, \cdots, y_N) \qquad 1 \le i \le N \qquad (4.18)$$

$$0 = g(x_i, y_i) \qquad 0 \le i \le N \qquad (4.19)$$

$$0 = b(x_0, y_0, x_N, y_N) \qquad (4.20)$$

By using finite difference methods, a compact form of the finite difference equations can be written as a set of nonlinear equations in (4.21).

$$\Phi(X,Y)=0 \tag{4.21}$$

where

$$X=[x_0{}^T,\cdots,x_N{}^T]^T \qquad\qquad Y=[y_0{}^T,\cdots,y_N{}^T]^T$$

The finite difference quotients may be defined by the trapezoidal method, that is, $FD_i(x_0,\cdots,x_N,y_0,\cdots,y_N)=x_i-x_{i-1}-h[f(x_i,y_i)+f(x_{i-1},y_{i-1})]/2$ for $1\le i\le N$. Thus the general form of nonlinear equations $\Phi(V,W)$ becomes:

$$\Phi_0(X,Y)=\begin{cases} b(x_0,y_0,x_N,y_N) \\ g(x_0,y_0) \end{cases}$$

$$\Phi_i(X,Y)=\begin{cases} x_i-x_{i-1}-h[f(x_i,y_i)+f(x_{i-1},y_{i-1})]/2 \\ g(x_i,y_i) \end{cases} \qquad 1\le i\le N$$

In the trajectory optimization application, the common boundary conditions are the given initial time conditions and the equilibrium conditions at the end time. The general form of nonlinear equations $\Phi(X,Y)=0$ may be written in the expanded form in (4.22)-(4.24) for $x\in R^n$ and $y\in R^m$ with N subintervals.

$$0=b(x_0,y_0,x_N,y_N) \tag{4.22}$$

$$0=x_i-x_{i-1}-h[f(x_i,y_i)+f(x_{i-1},y_{i-1})]/2 \qquad 1\le i\le N \tag{4.23}$$

$$0=g(x_i,y_i) \qquad 0\le i\le N \tag{4.24}$$

For the boundary value problem, there are $(n+m)\times(N+1)$ total unknowns for the differential states $X=[x_0{}^T,\cdots,x_N{}^T]^T$ and the algebraic states $Y=[y_0{}^T,\cdots,y_N{}^T]^T$. In the

expanded form of the finite difference method, there are n equations defined in (4.22) for the boundary value conditions. There are $n \times N$ equations defined in (4.23) for the finite difference operators, and there are $n \times (N+1)$ equations defined in (4.24) for the algebraic equations. Therefore, the total number of equations is $(n+m) \times (N+1)$ for the corresponding $(n+m) \times (N+1)$ unknowns.

By solving the nonlinear equation set $\Phi(X,Y) = 0$, the solution of the two-point boundary value problem for differential algebraic equation can be obtained, which gives the optimal control strategy for power system dynamics.

4.5 Numerical Examples

4.5.1 *Trajectory Optimization Results for Simple Mathematical Example*

A simple mathematical example [97] is shown to demonstrate the trajectory optimization. The problem has two states and one control variable. The objective is to minimize control over the time period from 0 to 1 by moving from a set of initial time state conditions to the specified end time state conditions. The initial time and end state requirements are listed in (4.26). Besides state law, there is an additional inequality constraint of state variable x_1.

$$J = \frac{1}{2}\int_0^1 u^2 dt \tag{4.25}$$

subject to

$$\dot{x}_1 = x_2$$

$$\dot{x}_2 = u$$

$$0 \le 0.1 - x_1$$

$$x_1(0) = 0 \qquad (4.26)$$

$$x_2(0) = 1$$

$$x_1(1) = 0$$

$$x_2(1) = -1$$

The numerical examples of the optimal solution are shown in Fig. 4-6 and Fig. 4-7. It can be observed that both conditions at the initial time and the end time are satisfied. Also there is no violation of the inequality constraint for state variable x_1.

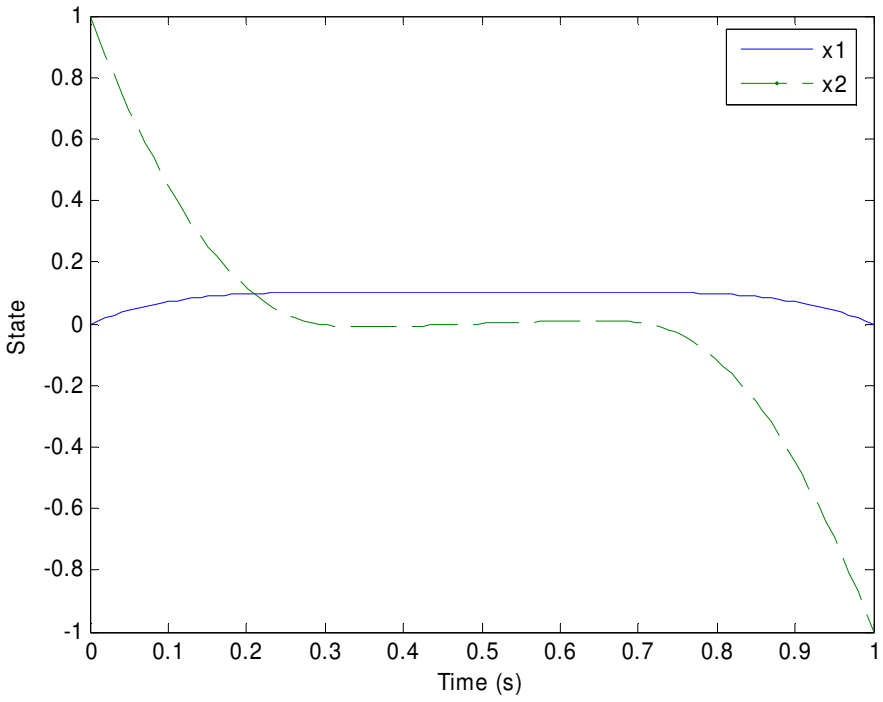

Fig. 4-6. Optimal State Trajectories for Simple Mathematical Example

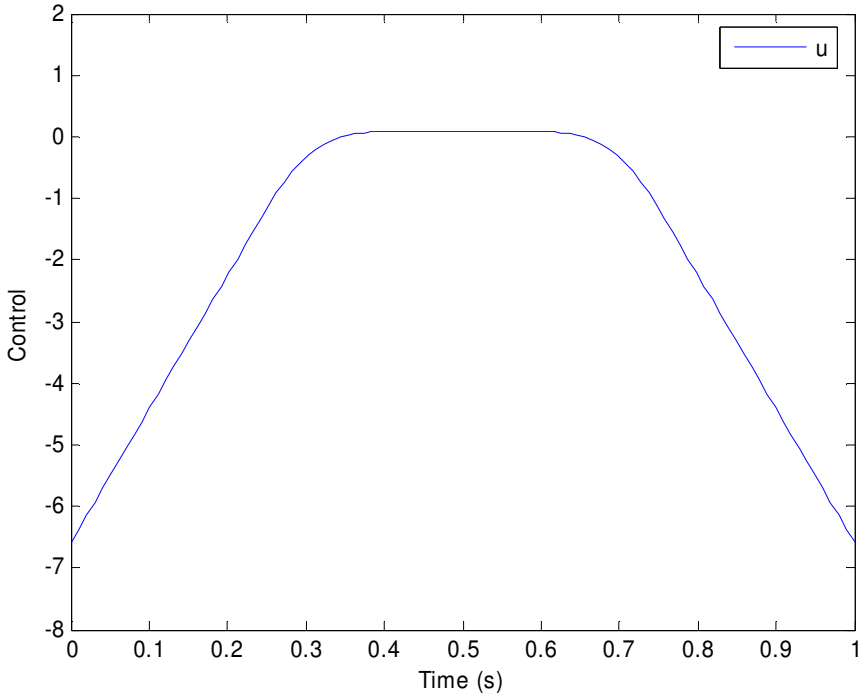

Fig. 4-7. Optimal Control Trajectory for Simple Mathematical Example

4.5.2 *Trajectory Optimization Results for 2-Bus System*

In this section, trajectory optimization is applied to a simple 2-bus power system [15]. In the power system, a load bus is connected with a generator through a transmission line as shown in Fig. 4-8. The control resource is a reactive power compensation device B*c* with continuous output at the load bus.

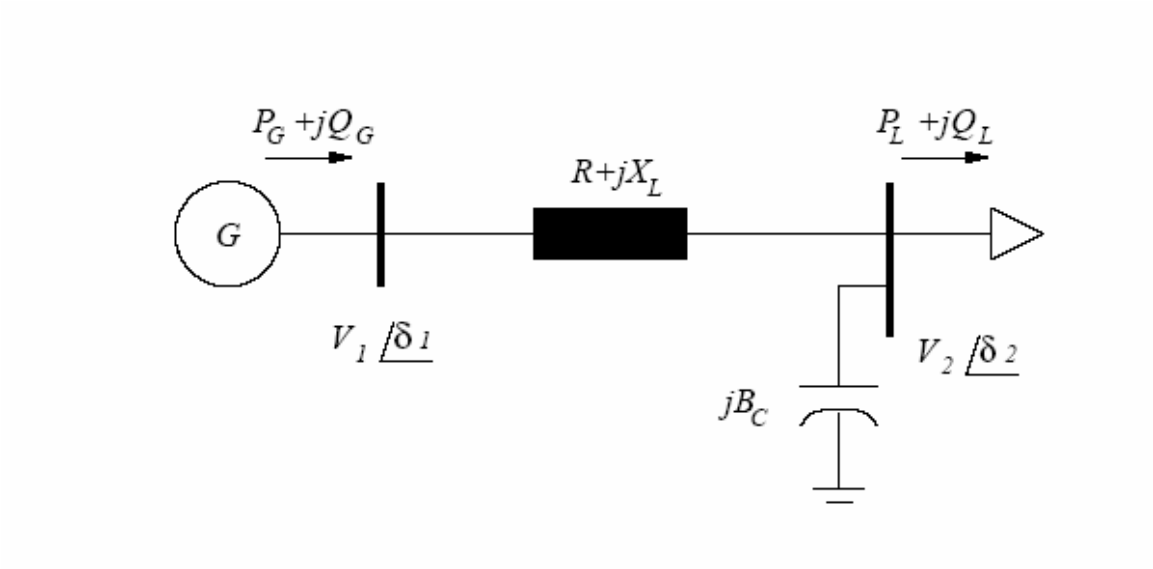

Fig. 4-8. Two-Bus Power System Diagram

The system dynamics are represented by a set of ordinary differential equations in (4.27).

$$\begin{cases} \dot{\omega} = \dfrac{1}{M}[P_m - P_G - D_G\omega] \\ \dot{\delta} = \omega - \dfrac{1}{D_L}[P_L - P_d] \\ \dot{V}_2 = \dfrac{1}{\tau}[Q_L - Q_d] \end{cases} \tag{4.27}$$

where

$$P_G = V_1^2 G - V_1 V_2 (G\cos\delta_{12} - B\sin\delta_{12})$$

$$Q_G = V_1^2 B - V_1 V_2 (G\sin\delta_{12} + B\cos\delta_{12})$$

$$P_L = -V_2^2 G + V_1 V_2 (G\cos\delta_{12} + B\sin\delta_{12})$$

$$Q_L = -V_2^2 (B - B_C) - V_1 V_2 (G\sin\delta_{12} - B\cos\delta_{12})$$

$$G = R/(R^2 + X_L^2) \quad B = X_L/(R^2 + X_L^2)$$

The disturbance of the system is the transmission line impedance change from 0.5 to 0.6. The system will experience collapse if no control is applied, and the collapse trajectory is shown in Fig. 4-9.

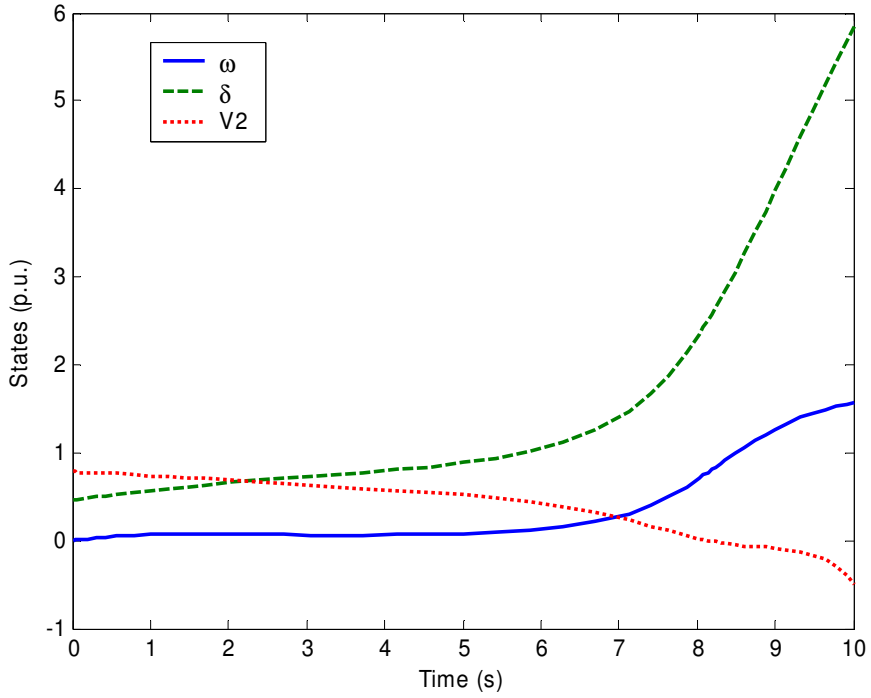

Fig. 4-9. Trajectories after Disturbance without Control

The system can reach post disturbance equilibrium if reactive power compensation is applied at the load bus. The objective chosen is to minimize the cost function $0.5\int_0^T B_C{}^2 dt$ where the end time is specified as 10 seconds, that is, the system will restore to a new operating point after 10 seconds.

The detailed formulation of the trajectory optimization for the 2-bus system is shown as follows in (4.28)-(4.31).

$$\min \qquad \frac{1}{2}\int_0^T B_C{}^2 dt \tag{4.28}$$

subject to:

System Dynamics:

$$\begin{cases} \dot{\omega} = \dfrac{1}{M}[P_m - P_G - D_G\omega] \\ \dot{\delta} = \omega - \dfrac{1}{D_L}[P_L - P_d] \\ \dot{V}_2 = \dfrac{1}{\tau}[Q_L - Q_d] \end{cases} \tag{4.29}$$

Initial time conditions:

$$\begin{cases} \omega_0 = 0 \\ \delta_0 = 0.4636 \\ V_{20} = 0.7826 \end{cases} \tag{4.30}$$

End time conditions:

$$\begin{cases} 0 = \dfrac{1}{M}[P_{mT} - P_{GT} - D_G\omega_T] \\ 0 = \omega_T - \dfrac{1}{D_L}[P_{LT} - P_{dT}] \\ 0 = \dfrac{1}{\tau}[Q_{LT} - Q_{dT}] \end{cases} \tag{4.31}$$

In the formulation, the objective function is given in (4.28), and the system dynamics are represented in (4.29). The initial time conditions for the system are shown in (4.30), and the end time conditions are given in (4.31). The boundary conditions are the combination of (4.30) and (4.31).

Three co-state variables associated with dynamical equations (4.29) are defined as $\lambda_1, \lambda_2, \lambda_3$.

The Hamiltonian associated with the trajectory optimization problem is:

$$H(x,u) = \frac{1}{2} B_c^{\,2} + \lambda^T f(x,u)$$

$$= \frac{1}{2} B_c^{\,2} + \lambda_1 \frac{1}{M}(P_m - P_G - D_G\omega) + \lambda_2(\omega - \frac{1}{D_L}(P_L - P_d)) + \lambda_3 \frac{1}{\tau}(Q_L - Q_d)$$

The derivatives of Hamiltonian with respect to state variables and control variable are:

$$\frac{\partial H}{\partial x_1} = \frac{\partial H}{\partial \omega} = \lambda_1 \frac{1}{M}(-D_g) + \lambda_2$$

$$\frac{\partial H}{\partial x_2} = \frac{\partial H}{\partial \delta} = \lambda_1 \frac{1}{M}(-\frac{\partial P_g}{\partial \delta}) + \lambda_2(-\frac{1}{D_L})\frac{\partial P_l}{\partial \delta} + \lambda_3 \frac{1}{\tau}\frac{\partial Q_l}{\partial \delta}$$

$$= \lambda_1 \frac{1}{M} V_1 V_2(-G\sin\delta - B\cos\delta) + \lambda_2(-\frac{1}{D_L})V_1 V_2(-G\sin\delta + B\cos\delta)$$

$$+ \lambda_3 \frac{1}{\tau}(-V_1 V_2)(G\cos\delta + B\sin\delta)$$

$$\frac{\partial H}{\partial x_3} = \frac{\partial H}{\partial V_2} = \lambda_1 \frac{1}{M}(-\frac{\partial P_g}{\partial V_2}) + \lambda_2(-\frac{1}{D_L})\frac{\partial P_l}{\partial V_2} + \lambda_3 \frac{1}{\tau}\frac{\partial Q_l}{\partial V_2}$$

$$= \lambda_1 \frac{1}{M}(-V_1)(G\cos\delta - B\sin\delta) + \lambda_2(-\frac{1}{D_L})[-2V_2 G + V_1(G\cos\delta + B\sin\delta)]$$

$$+ \lambda_3 \frac{1}{\tau}[-2V_2(B - B_c) - V_1(G\sin\delta - B\cos\delta)]$$

$$\frac{\partial H}{\partial u} = \frac{\partial H}{\partial B_C} = B_C + \lambda_3 \frac{1}{\tau} V_2^2$$

The compact form of the necessary conditions of the trajectory optimization problem is:

$$\begin{cases} \dot{x} = f(x,u) \\ \dot{\lambda} = -\nabla_x H(x,u) \\ 0 = \nabla_u H(x,u) \end{cases}$$

The necessary conditions can be expanded as:

$$\begin{cases} \dot{\omega} = [P_m - P_G - D_G\omega]/M \\ \dot{\delta} = \omega - [P_L - P_d]/D_L \\ \dot{V}_2 = [Q_L - Q_d]/\tau \\ \dot{\lambda}_1 = -(\lambda_1(-D_g)/M + \lambda_2) \\ \dot{\lambda}_2 = -(\lambda_1(-\partial P_g/\partial\delta)/M + \lambda_2(-1)(\partial P/\partial\delta)/D_L + \lambda_3(\partial Q_l/\partial\delta)/\tau) \\ \dot{\lambda}_3 = -(\lambda_1(-\partial P_g/\partial V_2)/M + \lambda_2(-1)(\partial P_l/\partial V_2)/D_L + \lambda_3(\partial Q_l/\partial V_2)/\tau) \\ 0 = B_C + \lambda_3 V_2^2/\tau \end{cases} \tag{4.32}$$

The boundary conditions are:

$$\begin{cases} \omega_0 = 0 \\ \delta_0 = 0.4636 \\ V_{20} = 0.7826 \\ 0 = \dfrac{1}{M}[P_{mT} - P_{GT} - D_G\omega_T] \\ 0 = \omega_T - \dfrac{1}{D_L}[P_{LT} - P_{dT}] \\ 0 = \dfrac{1}{\tau}[Q_{LT} - Q_{dT}] \end{cases} \tag{4.33}$$

By solving the boundary value conditions defined in (4.32) and (4.33), The optimal control action of the reactive power compensation and the corresponding system trajectories are plotted in Fig. 4-9.

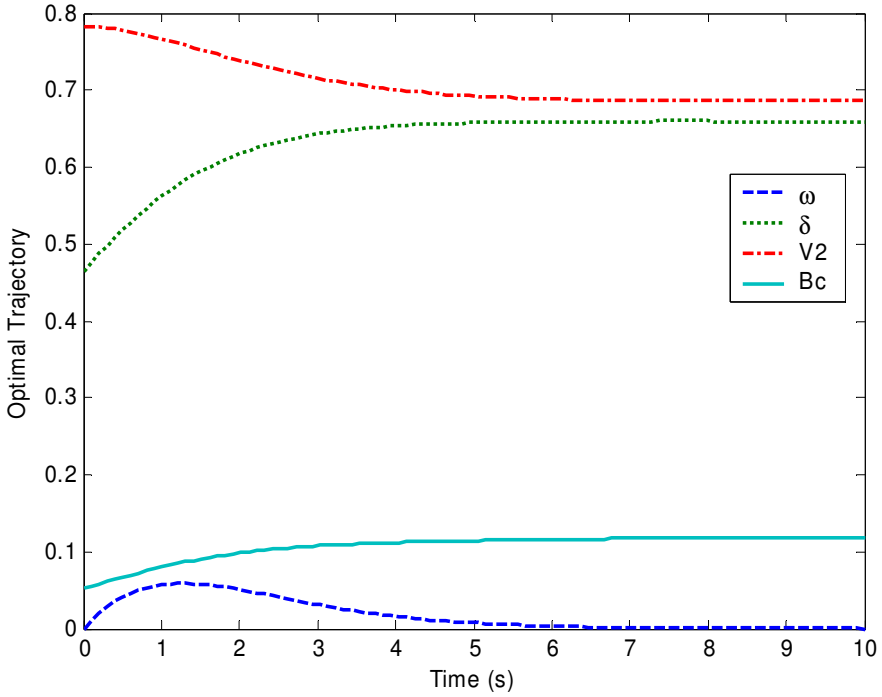

Fig. 4-10. Optimal Trajectories with Reactive Power Compensation

In the second optimization case, a lower limit is imposed on load bus voltage during the transition, and all the other requirements remain the same as in the first optimization case.

The problem can be formulated as follows.

$$\min \qquad \frac{1}{2}\int_0^T B_C{}^2 dt \tag{4.34}$$

subject to:

$$\dot{x} = f(x,u) \tag{4.35}$$

$$r_0(x_0,u_0) = 0 \tag{4.36}$$

$$r_T(x_T,u_T) = 0 \tag{4.37}$$

$$d \geq 0 \tag{4.38}$$

where dynamical equations (4.35) are the same as those in the detailed form in (4.29), and boundary conditions (4.36) and (4.37) are the same as those in the detailed form in (4.30) and (4.31) respectively. The voltage constraint is represented by (4.38), which can be written as $d = V_2 - 0.75 \geq 0$.

The penalty form can be represented as:

$$D = \begin{cases} 1/d & d \geq \sigma = \sqrt{\rho} \\ 1/\sigma(3 - 3d/\sigma + (d/\sigma)^2) & d < \sigma = \sqrt{\rho} \end{cases}$$

The Hamiltonian is defined as:

$$H(x,u) = \frac{1}{2} B_C^2 + \lambda^T f(x,u) + \rho_k D_k$$

Again the necessary conditions can be written in (4.39) for the optimal control solution.

$$\begin{cases} \dot{x} = f(x,u) \\ \dot{\lambda} = -\nabla_x H(x,u) \\ 0 = \nabla_u H(x,u) \end{cases} \tag{4.39}$$

During the numerical experiment, the penalty parameter ρ_k approaches zero. Initially the boundary value problem is solved for a large penalty parameter. Then the penalty parameter is reduced, and the boundary value problem is solved for the new parameter. The procedure continues until the penalty parameter reaches a very small number close to zero. The optimization results are shown in Fig. 4-11, from which it can be observed that load bus voltage satisfied the imposed constraints.

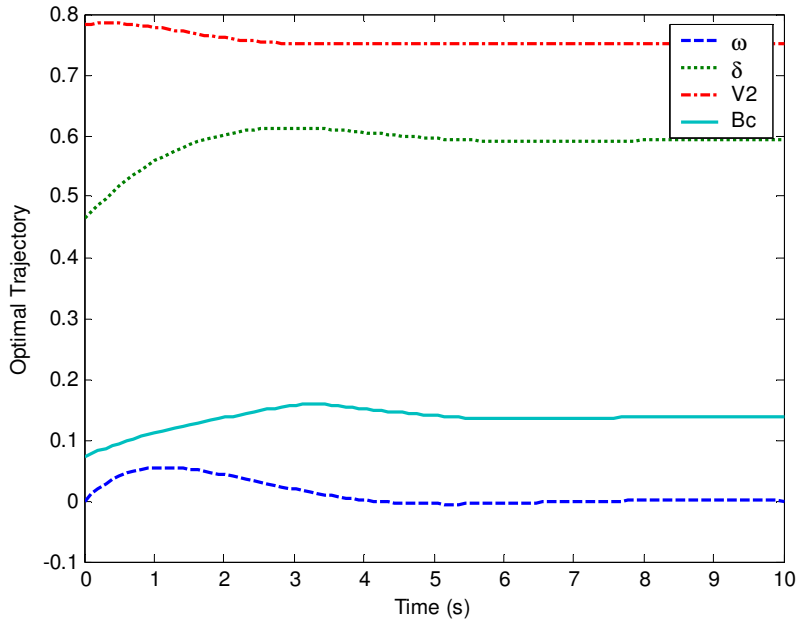

Fig. 4-11. Constrained Optimal Trajectories with Reactive Power Compensation

The trajectory optimization theory can be also applied with a particular time delay with respect to the control actions. If a control delay exists, the system trajectories will remain the same as the uncontrolled post disturbance trajectory during the period of delay, and then the system trajectories and conditions can be changed when control is applied after the delay. In the following example, a two-second reactive power compensation delay is applied, and under the delayed control, the optimal system trajectories and control is shown Fig. 4-12. It can be observed that in the first 2 second period, the control output is zero, and system states such as bus voltage and generator angle is the same as in the post disturbance case without control. The control is activated after 2 seconds, and the system states therefore change correspondingly. It can also be observed that, with the existence of the delay, the maximum amount of reactive compensation is larger than that of the case without delay.

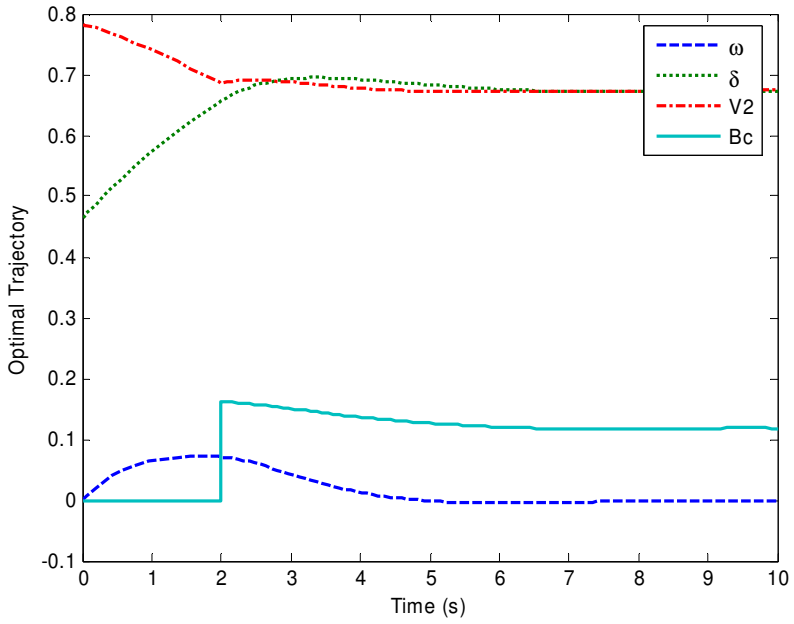

Fig. 4-12. Optimal Trajectories with Delayed Reactive Power Compensation

In the Table 4-1, the maximum reactive compensation amounts are shown with respect to the delay period. It can be shown that the required control amount increases as the control is delayed. The result in Table 4-1 is also plotted in Fig. 4-13.

TABLE 4-1 CONTROL AMOUNT WITH RESPECT TO DELAY

Delay (s)	Maximum Control Amount (p.u.)
0	0.1178
2	0.1612
7	0.2116
8	0.4065

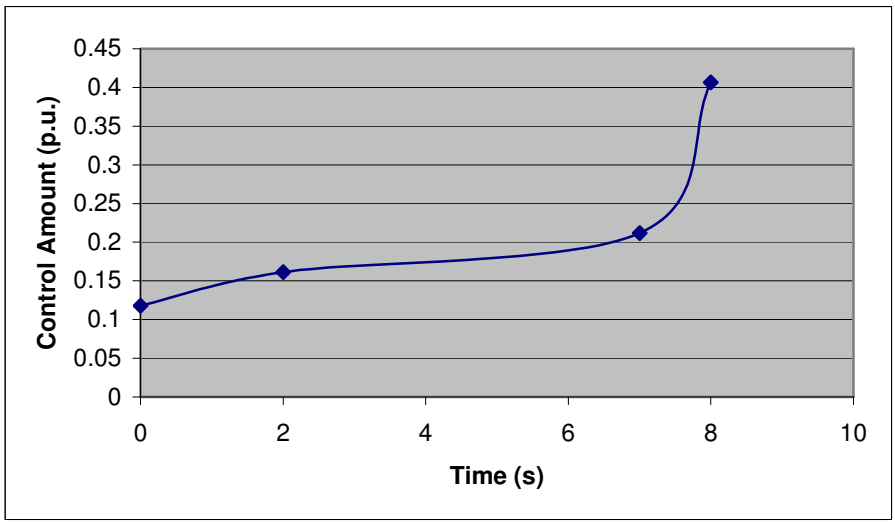

Fig. 4-13. Control Amount with respect to Control Delay

In addition to the reactive power compensation, load control is also a possible control resource with which to mitigate system failure. The effect of load control is shown in Fig. 4-14. The initial load level is 0.7 p.u., and the minimum load level during the control is 0.63 p.u., which is only a 10% load level change. It is thus demonstrated that a slightly reduced load level can save the system from collapse.

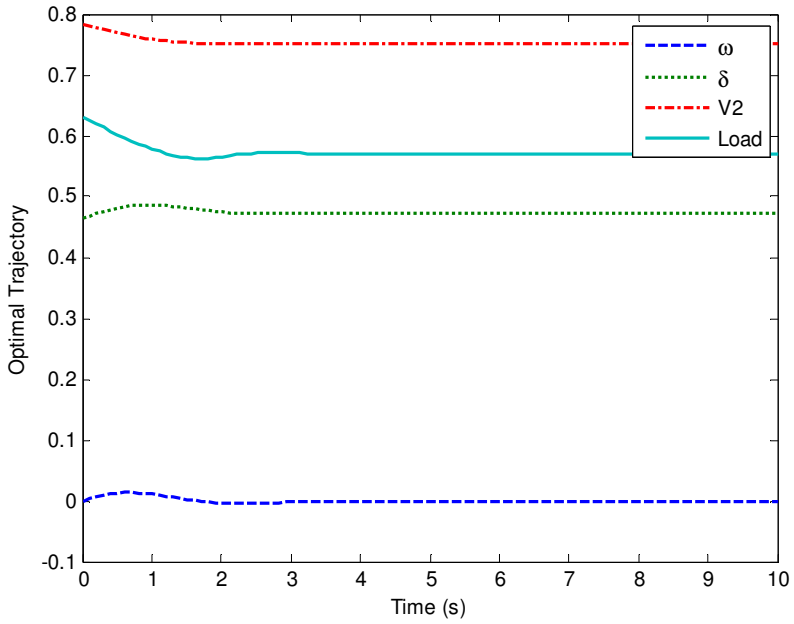

Fig. 4-14. Optimal Trajectories with Load Control

Control resource such as reactive power compensation and load can be used together as a combined control strategy. The effect of such combined control is shown in Fig. 4-15. Compared with the control strategies with only reactive power compensation and only load control shown in Fig. 4-10 and Fig. 4-14, the combined control strategy needs less reactive power compensation and can serve more load. In Table 4-2, a comparison of individual control strategies and combined strategies is given. It can be observed that the combined control strategy requires less individual control resources compared with the individual control actions.

TABLE 4-2 COMPARISON OF CONTROL STRATEGIES

Control	Maximum Bc (p.u.)	Load Variation (%)
Reactive Control Only	0.1588	-
Load Control Only	-	9.94
Combined Control	0.14	0.91

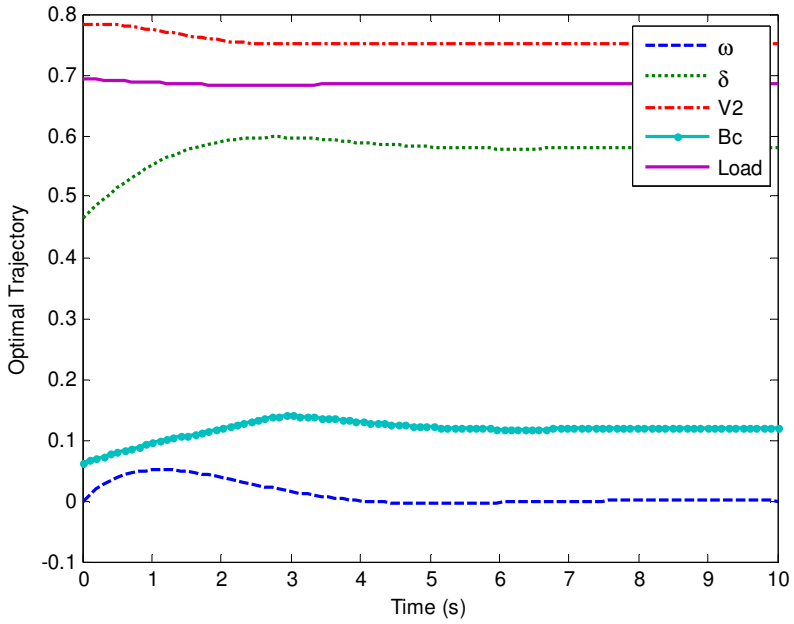

Fig. 4-15. Optimal Trajectories with Combined Control

4.5.3 *Trajectory Optimization Results for 3-Bus System*

A simple three bus power system shown in Fig. 4-16 is used to demonstrate the optimal control effect after the disturbance. There are two generators and one load in the system. In the dynamic security analysis, the disturbance is the branch reactance change of the transmission line between bus 2 and bus 3. Before the disturbance, the reactance is 0.1 p.u., and the reactance becomes 0.125 p.u. after the disturbance. The system experiences an instability problem after the disturbance, as shown in Fig. 4-17.

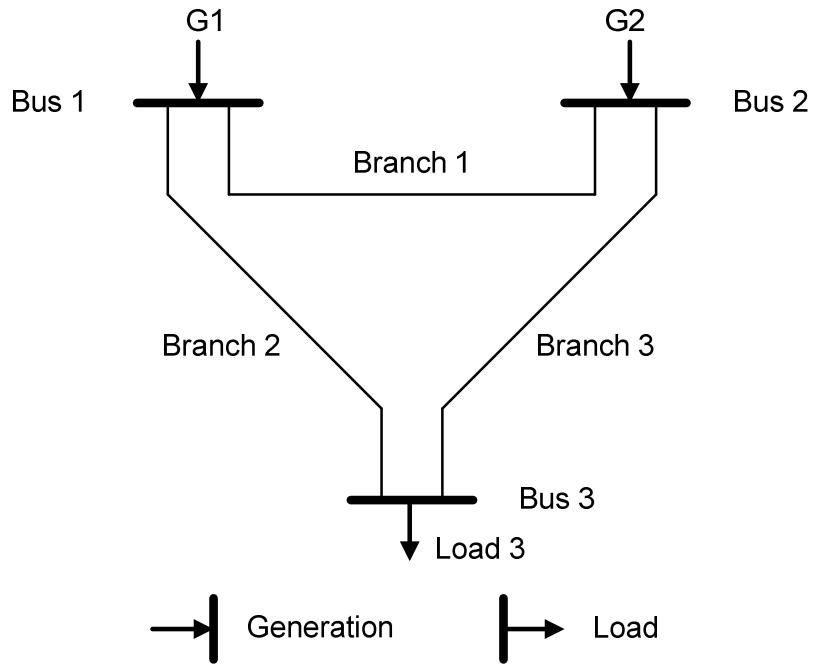

Fig. 4-16. Three-Bus Power System Diagram

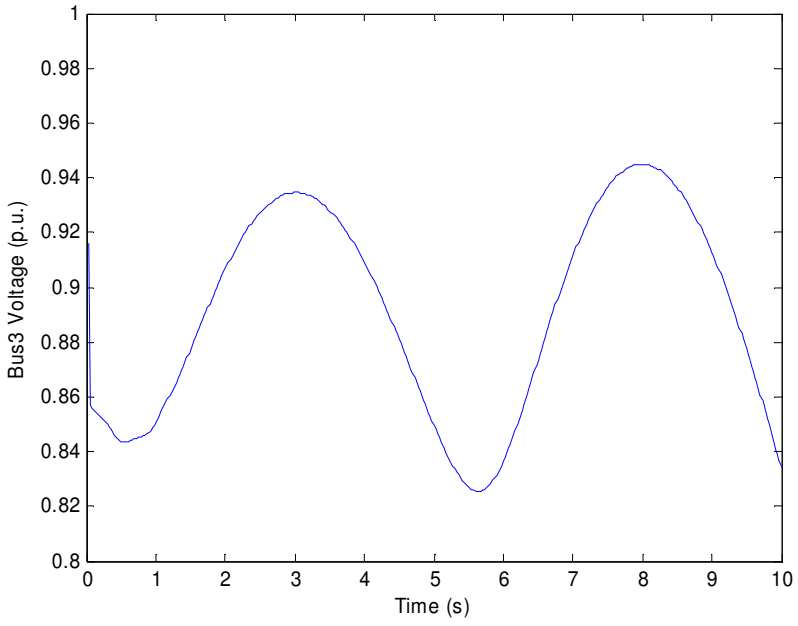

Fig. 4-17. Trajectories after Disturbance without Control

To prevent instability due to the disturbance, several control strategies are applied. In the control cases, an equilibrium condition at the end time is imposed and the bus voltage is set to be no less than 0.85 per unit. In the first numerical experiment, reactive support at bus 3 is chosen as the control resource. Using continuous reactive power compensation, a new equilibrium point with improved voltage profile is reached for all three buses. The bus voltage trajectories, generator relative angle, and control trajectory are shown in Fig. 4-18, Fig. 4-19 and Fig. 4-20 respectively.

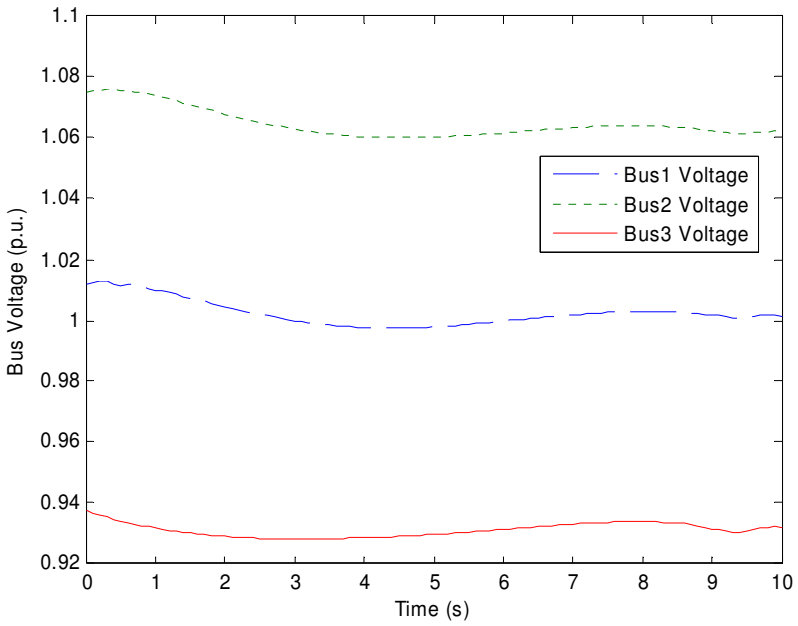

Fig. 4-18. Bus Voltage Trajectories with Reactive Power Compensation

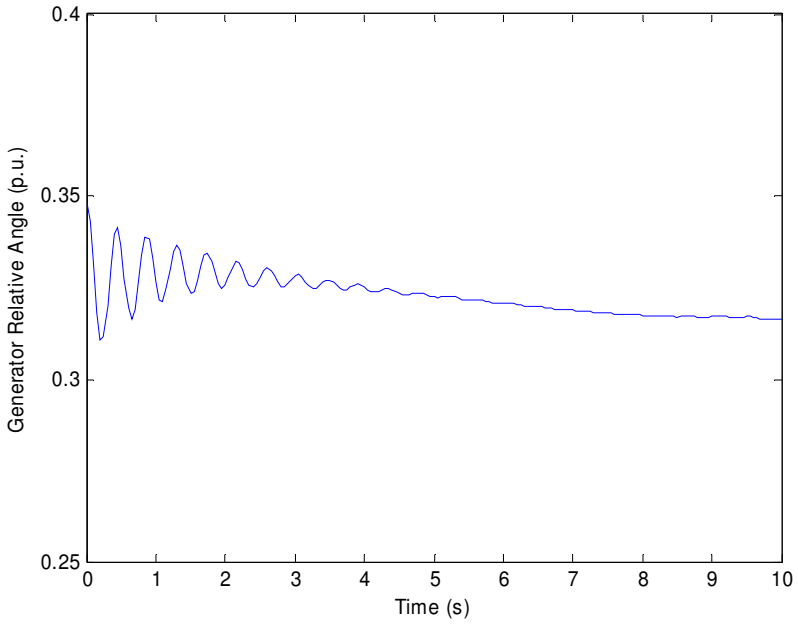

Fig. 4-19. Generator Relative Angle with Reactive Power Compensation

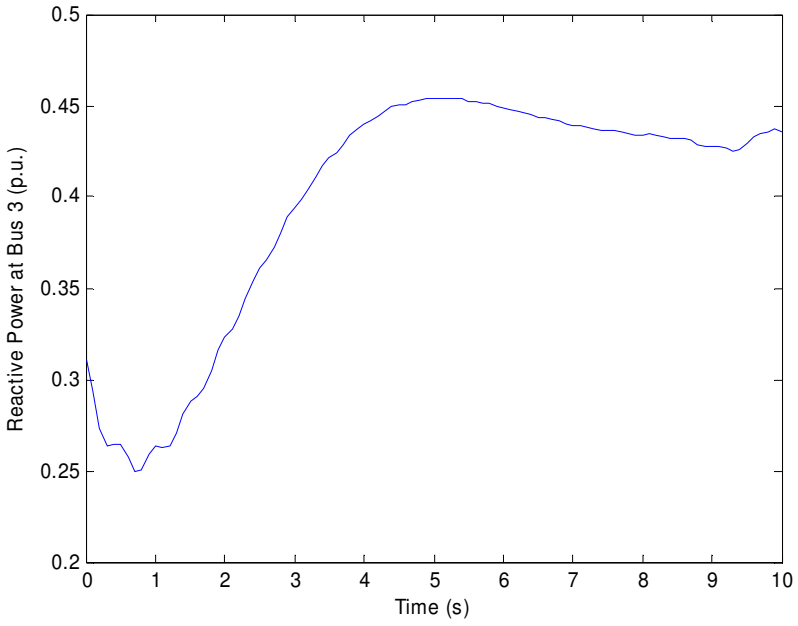

Fig. 4-20. Reactive Power Compensation Trajectory

In the next numerical experiment, the load at bus 3 is chosen as the control resource. Under continuous load control, a new equilibrium point is reached with improved voltage profile for all three buses. The bus voltage trajectories, generator relative angle, and control trajectory are shown in Fig. 4-21, Fig. 4-22 and Fig. 4-23 respectively.

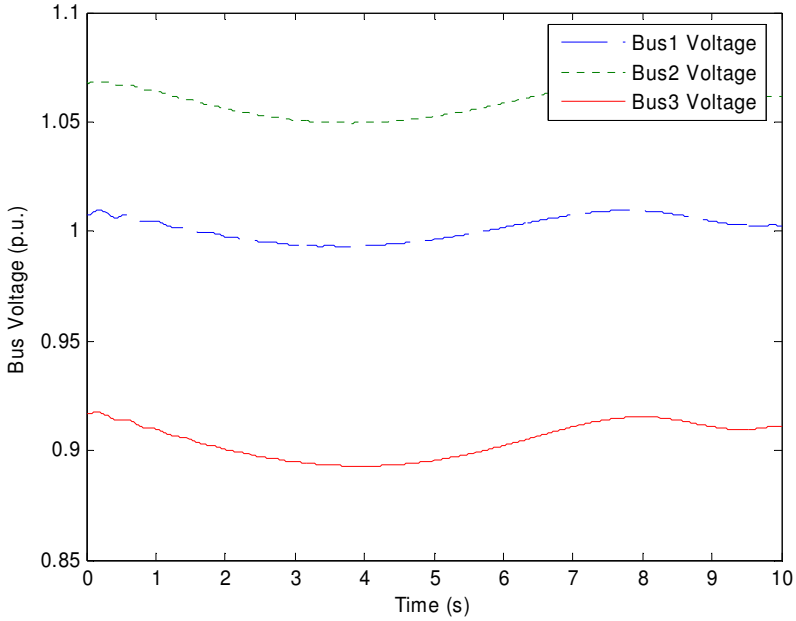

Fig. 4-21. Bus Voltage Trajectories with Load Control

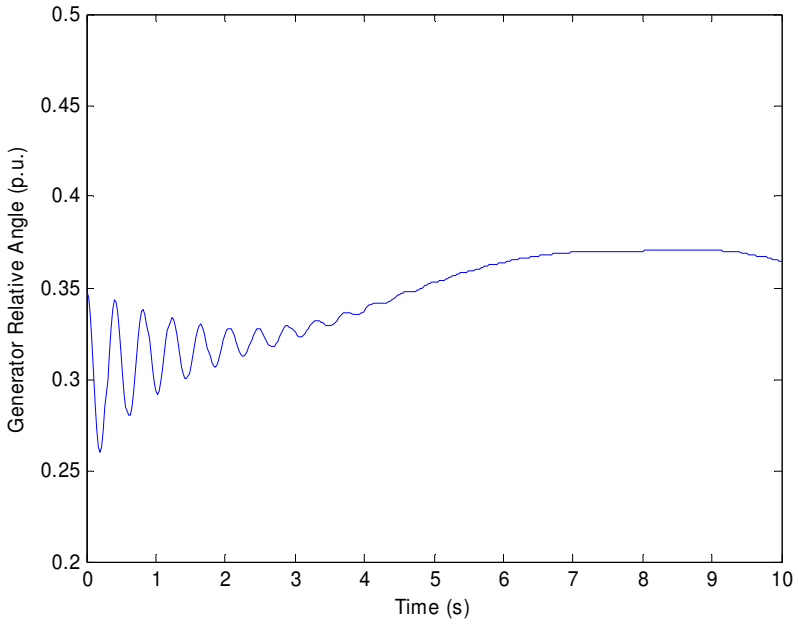

Fig. 4-22. Generator Relative Angle with Load Control

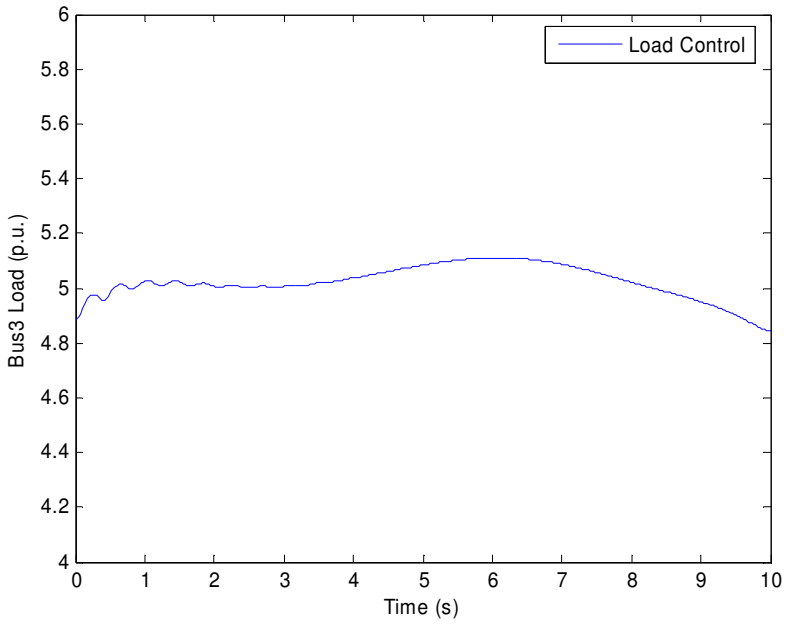

Fig. 4-23. Load Control Trajectory

In the next example for the 3-bus power system, a combined control strategy using reactive power compensation and load control is applied. The bus voltage trajectories and generator relative angle are plotted in Fig. 4-24 and Fig. 4-25 respectively. The control trajectories for combined reactive power compensation and load control are shown in Fig. 4-26 and Fig. 4-27 respectively. It can be observed that the reactive power compensation variation and load variation are reduced under the combined strategy in contrast with the control strategies with single control resource.

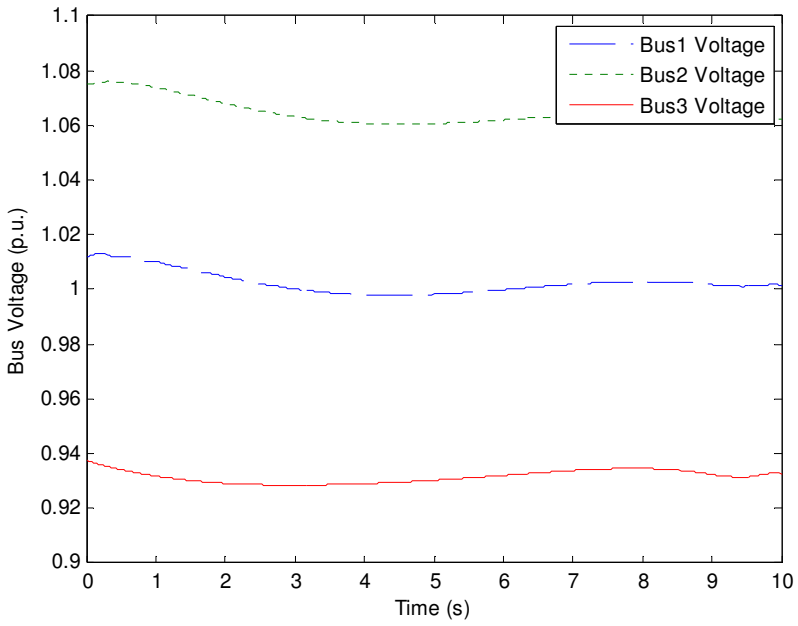

Fig. 4-24. Bus Voltage Trajectories with Combined Control

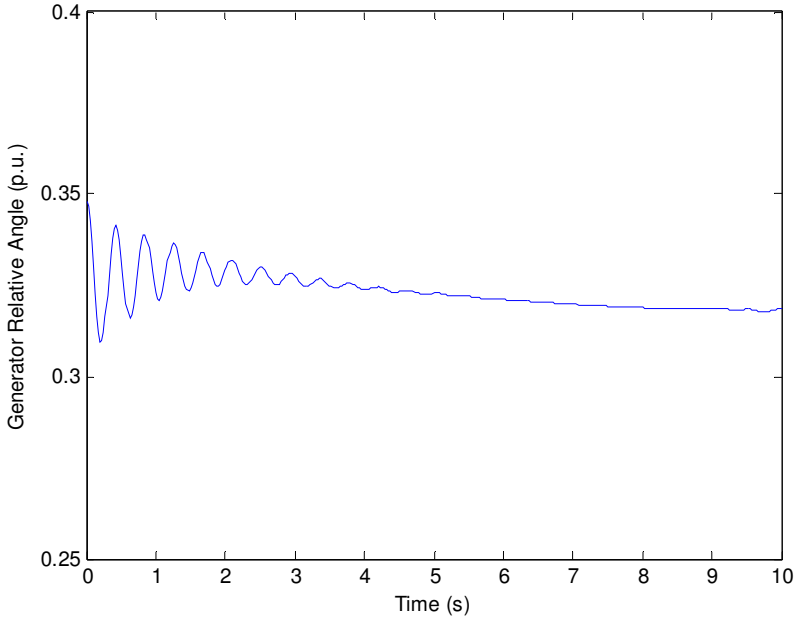

Fig. 4-25. Generator Relative Angle with Combined Control

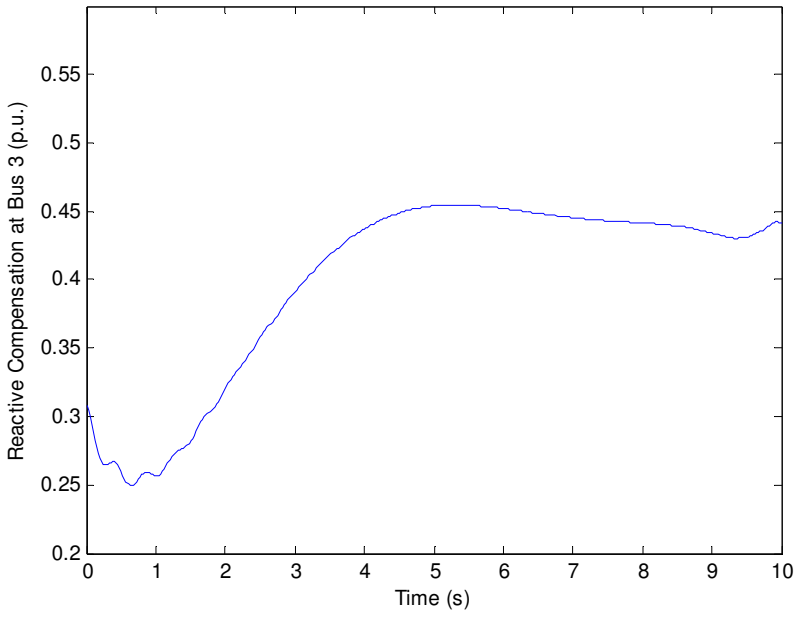

Fig. 4-26. Reactive Power Compensation Trajectory

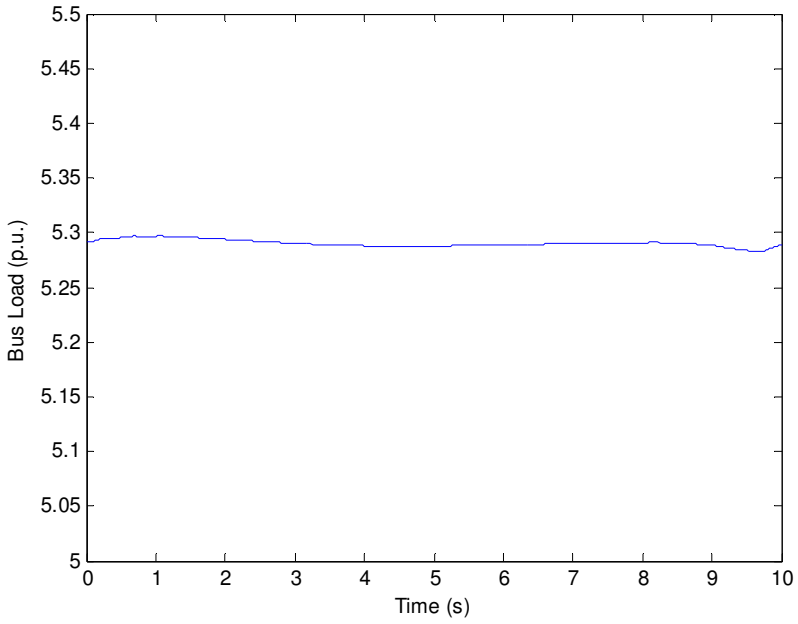

Fig. 4-27. Load Control Trajectory

Control delay can be also applied in the 3-bus system to study the control effect. In Table 4-3, the maximum control amounts for different control resources are listed with respect to delay time. It can be observed that the required control amount generally increases with respect to increased delay.

TABLE 4-3 MAXIMUM CONTROL AMOUNT WITH RESPECT TO DELAY

Delay (s)	Reactive Power (p.u.)	Load Variation (%)
0	0.4546	0.3
2	0.6841	0.58
5	1.1288	3.1

4.5.4 *Trajectory Optimization Results for New England System*

The trajectory optimization method is applied to the New England system using reactive power support and load control. There are 39 buses and 10 generators in the New England system. The disturbance is the loss of two transmission lines, that is, line 6-7 and line 2-25. The system response after line loss is shown in Fig. 4-28 and Fig. 4-29. It is shown that system failure occurs in less than 5 seconds.

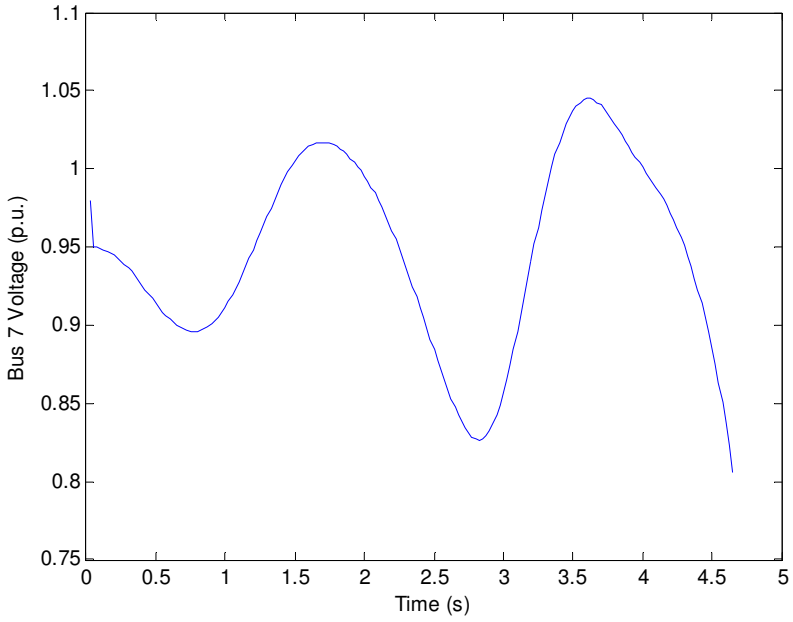

Fig. 4-28. Voltage Trajectory after Disturbance without Control

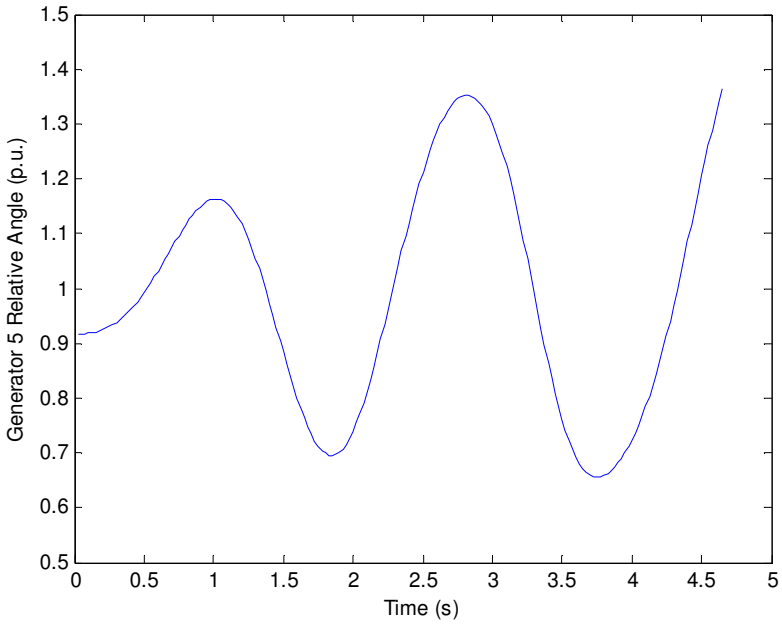

Fig. 4-29. Generator Angle Trajectory after Disturbance without Control

The sudden system failure can be mitigated by applying reactive power compensation control. Since there are 39 buses in the New England system, any bus can be a potential location for the reactive power compensation. There is a tradeoff between possible control candidate location and the optimal control solution. On one hand, the control strategy can benefit from adding more control candidates producing a larger feasible region for the system. On the other hand, having only a limited set of control locations with a relatively narrow feasible region adds implementation convenience. One way to handle the tradeoff between the large feasible region and the limited set of control locations is to consider all the possible location candidates first. Then, from the result produced by trajectory optimization, the locations with relatively large control output can be selected for further analysis. Based on this procedure of location selection, all the buses in the New England system are

considered in the first trajectory optimization application, and subsequently those locations with relatively large control output are selected in order until system failure can be mitigated. The results showing reactive power outputs at all buses are shown in Table 4-4. From the control output at all the locations, locations are selected and added into the list by the order of the output until the trajectory optimization solution is reached. With this selection method, the reactive power compensation can be located at bus 19, 25, 26, 28, 29, 31, 33, 34, 35, 36, 37, 38 to mitigate system failure. This is the minimum set of control locations capable of mitigating system failure in the sense that the control locations are selected in descending order from large output to small output. It is noted that these locations are close to the generator buses, as equilibrium conditions with respect to the generation states are to be reached in the optimization formulation. For example, bus 31, 33, 34, 35, 36, 37, 38 are generation buses, while the remaining buses are near generation buses. The voltage trajectory with the control at limited control locations is shown in Fig. 4-30, demonstrating the transition from the post disturbance state to the new operating state. The generator relative angle showing the synchronized generator angles is plotted in Fig. 4-31. From the control trajectories, it is seen that reactive power compensations vary from positive values to negative values, that means the reactive power compensation devices can either absorb or produce reactive power. The optimal trajectory is achieved by the corresponding optimal control actions, as shown in Fig. 4-32 and Fig. 4-33.

TABLE 4-4 MAXIMUM CONTROL AMOUNT AT ALL BUSES

Bus	Reactive Power	Bus	Reactive Power	Bus	Reactive Power
1	0.0263	14	0.0333	27	0.0680
2	0.0242	15	0.0402	28	0.1688
3	0.0295	16	0.0468	29	0.1891
4	0.0333	17	0.0458	30	0.0155
5	0.0338	18	0.0391	31	0.0793
6	0.0342	19	0.0743	32	0.0373
7	0.0316	20	0.0572	33	0.0738
8	0.0313	21	0.0546	34	0.0637
9	0.0220	22	0.0600	35	0.0626
10	0.0335	23	0.0617	36	0.0631
11	0.0323	24	0.0479	37	0.0983
12	0.0339	25	0.0898	38	0.2009
13	0.0329	26	0.0896	39	0.0257

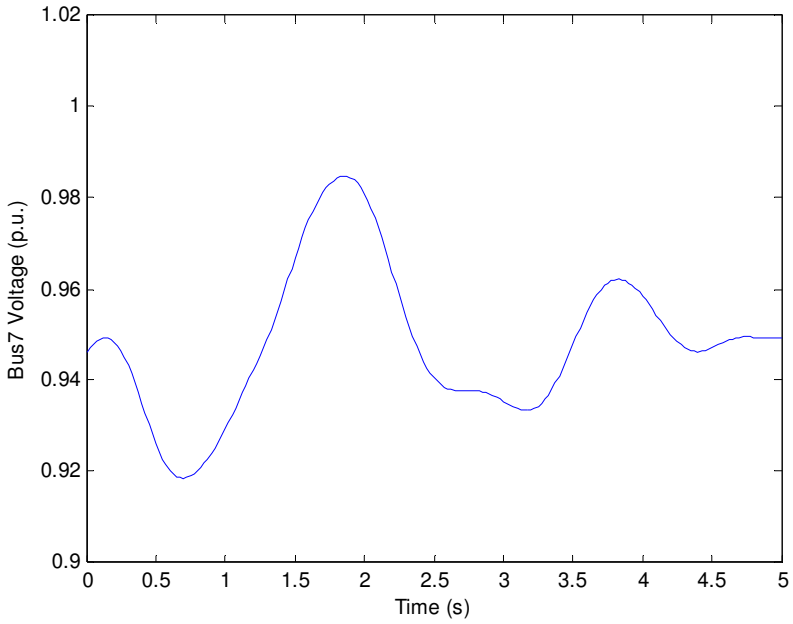

Fig. 4-30. Bus Voltage Trajectory with Reactive Power Compensation

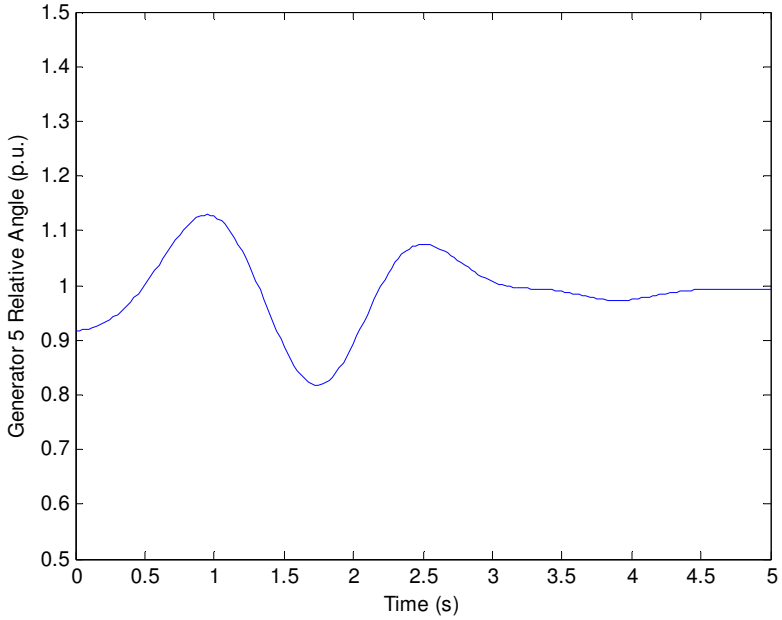

Fig. 4-31. Generator Relative Angle Trajectory with Reactive Power Compensation

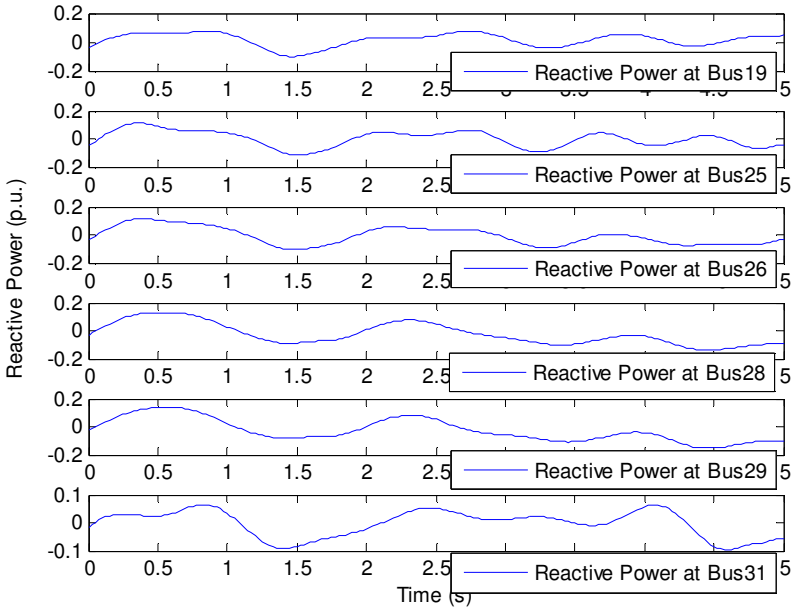

Fig. 4-32. Optimal Reactive Power Support Trajectories

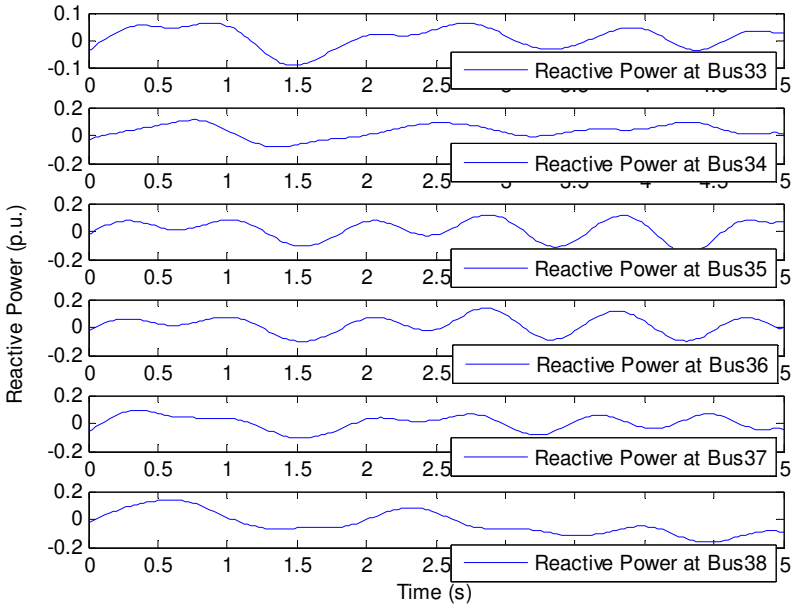

Fig. 4-33. Optimal Reactive Power Support Trajectories

The combined control of reactive power compensation and the non-disruptive load control of real power can also be applied using trajectory optimization theory. Similar to the selection of the reactive power compensation locations, the load control locations are chosen as bus 25, 26, 28, 29, each of which has relative large control output. The system state trajectories and the control trajectories are shown in the following figures.

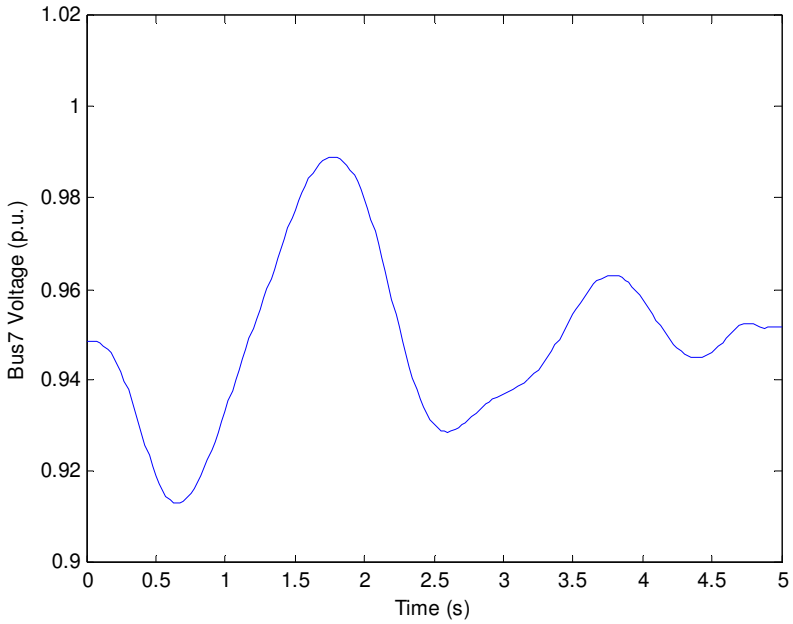

Fig. 4-34. Bus Voltage Trajectory

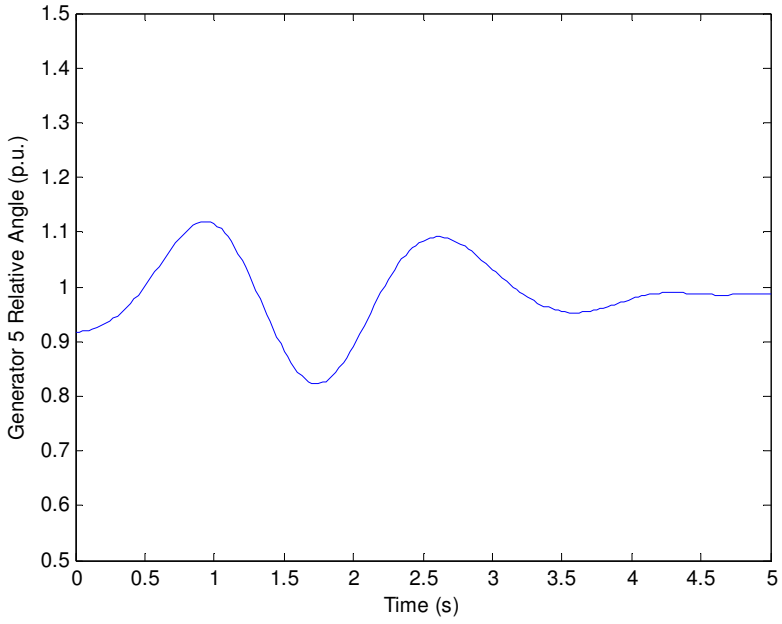

Fig. 4-35. Generator Relative Angle Trajectory

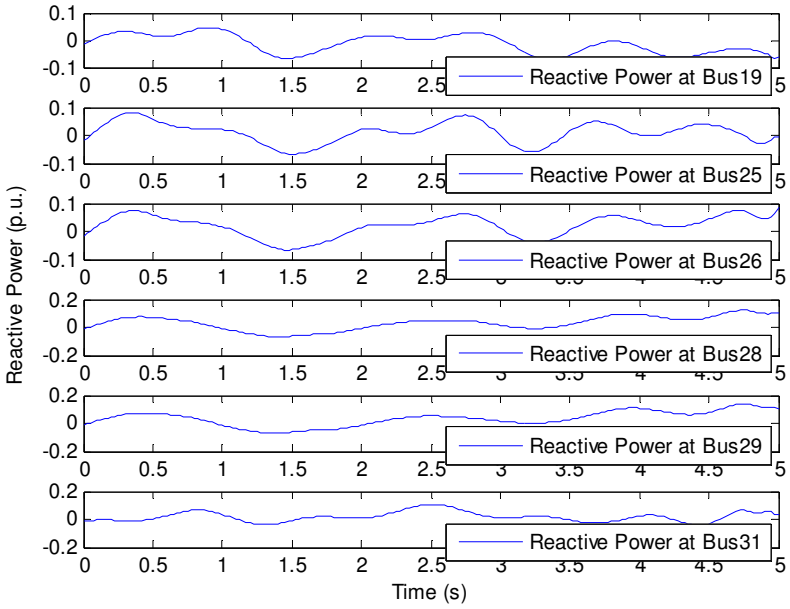

Fig. 4-36. Optimal Reactive Power Support Trajectories

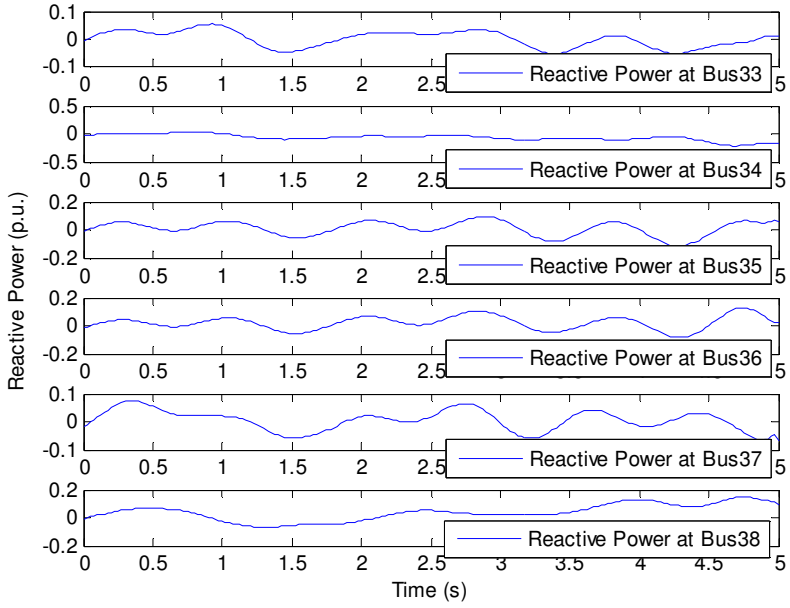

Fig. 4-37. Optimal Reactive Power Support Trajectories

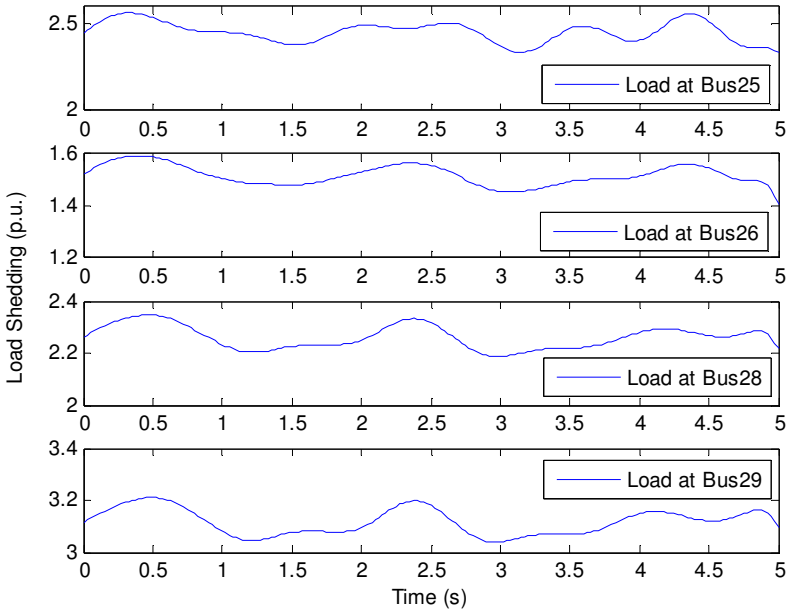

Fig. 4-38. Optimal Load Control Trajectories

The combined control of reactive power compensation and load control can also be applied with a certain time delay. In the delayed example, different delay intervals are shown to demonstrate the relationship between delay and the amount of maximum control. As it is shown in Table 4-5, there is a correlation between the objective value, the maximum control amount and the delay. More delay usually means greater amount of control. Delay also influences system states such as bus voltage. When there is control delay, the system states will not be changed during the delay period. Thus system states such as bus voltage will remain the same as the ones without control actions during the delay period, and an undesirable outcome occurring during the delay period cannot be eliminated. For example, if there is no delay, the lowest bus voltage is 0.9131 per unit under the control. However, if

there is a 2.5 second delay, the lowest bus voltage can drop to 0.8844 per unit. The summary of the delay effects is shown in Table 4-5 and Table 4-6.

TABLE 4-5 MAXIMUM REACTIVE CONTROL AMOUNT WITH RESPECT TO DELAY

Delay (s)	ΔQ19 (p.u.)	ΔQ25 (p.u.)	ΔQ26 (p.u.)	ΔQ28 (p.u.)	ΔQ29 (p.u.)	ΔQ31 (p.u.)
0	0.0710	0.0821	0.0879	0.1224	0.1356	0.1067
0.5	0.1032	0.1033	0.1332	0.1904	0.2104	0.1497
1	0.1559	0.1296	0.1756	0.2648	0.2946	0.2168
2	0.2393	0.1990	0.2091	0.2662	0.2913	0.4302
Delay (s)	ΔQ33 (p.u.)	ΔQ34 (p.u.)	ΔQ35 (p.u.)	ΔQ36 (p.u.)	ΔQ37 (p.u.)	ΔQ38 (p.u.)
0	0.0547	0.2154	0.1141	0.1271	0.0760	0.1494
0.5	0.0752	0.2960	0.1161	0.1634	0.0951	0.2310
1	0.1086	0.4036	0.1404	0.2271	0.1181	0.3272
2	0.1508	0.6003	0.1749	0.2955	0.1707	0.3321

TABLE 4-6 MAXIMUM LOAD CONTROL AMOUNT WITH RESPECT TO DELAY

Delay (s)	ΔP25 (%)	ΔP26 (%)	ΔP28 (%)	ΔP29 (%)
0	5.25	8.04	3.57	2.96
0.5	7.73	9.88	4.25	3.66
1	11.3	14.13	4.7	4.72
2	11.6	11.14	8.08	7.03

4.5.5 *Trajectory Optimization Results for IEEE 118-Bus System*

In the section the trajectory optimization method is applied for the IEEE 118-Bus system. There are 118 buses and 48 generators in this system. The system sustains voltage decline and generator angle increase subject to the disturbance of line 8-9 trip. The bus voltage and generator relative angle following the disturbance are shown in Fig. 4-39 and Fig. 4-40.

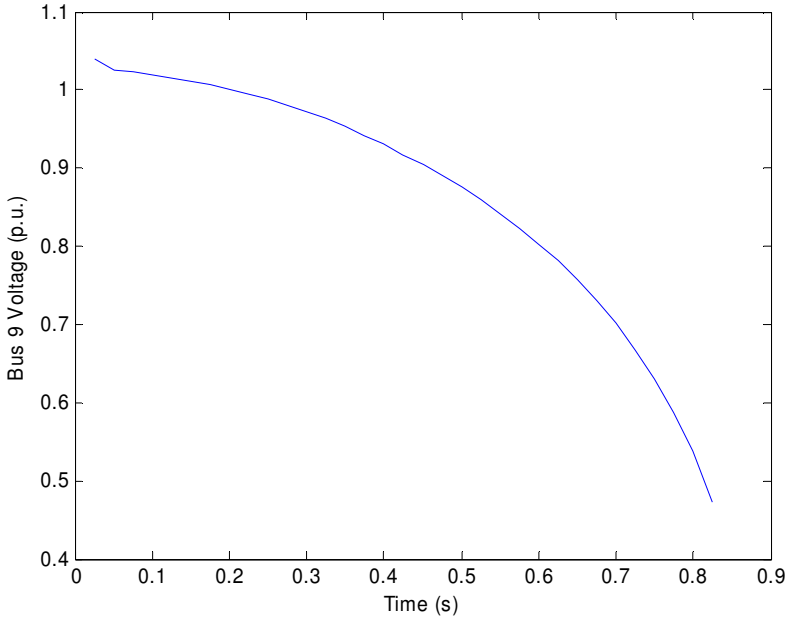

Fig. 4-39. Bus Voltage Trajectory after Disturbance

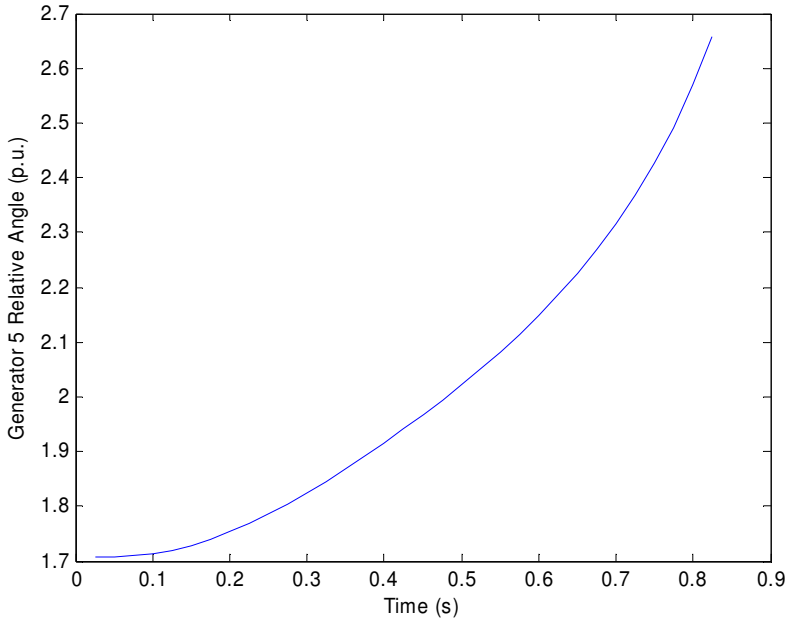

Fig. 4-40. Generator Relative Angle Trajectory after Disturbance

With the application of trajectory optimization theory, system failure of the IEEE 118-bus system can be avoided by reactive power compensation and load control. In the initial optimization run, all control locations are considered, and the control locations with relatively large output are selected to reduce the number of control locations in the subsequent optimization run. The control locations for the reactive power compensation are located from bus 1 to bus 60, and from bus 72 to bus 118. The real power load control locations are from bus 1 and bus 36, and from bus 72 and bus 118. The bus voltage and generator relative angle are shown in Fig. 4-41 and Fig. 4-42. The reactive power and load control trajectories at the buses with relatively large control output are shown in Fig. 4-43 and Fig. 4-44, and among these buses, bus 8, 9, and 10, happen to be the buses very close to the disturbance.

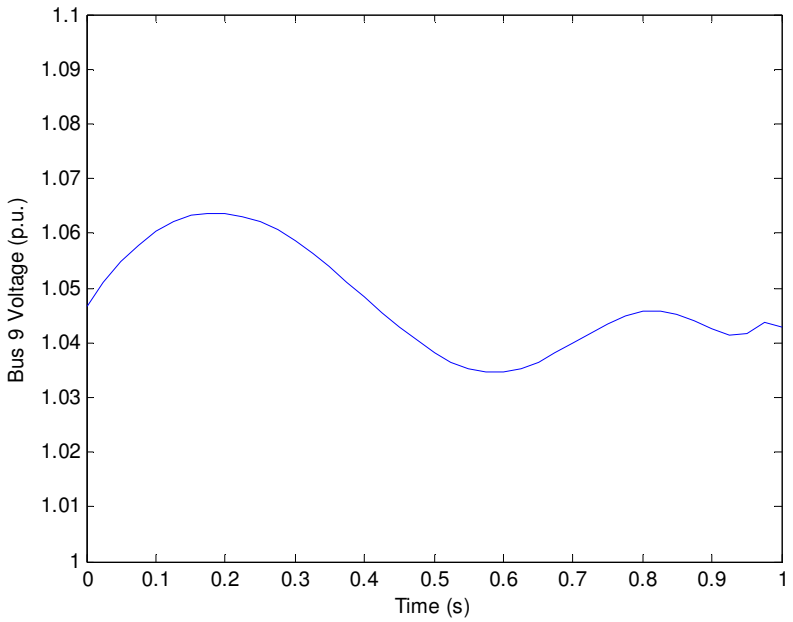

Fig. 4-41. Optimal Bus Voltage Trajectory

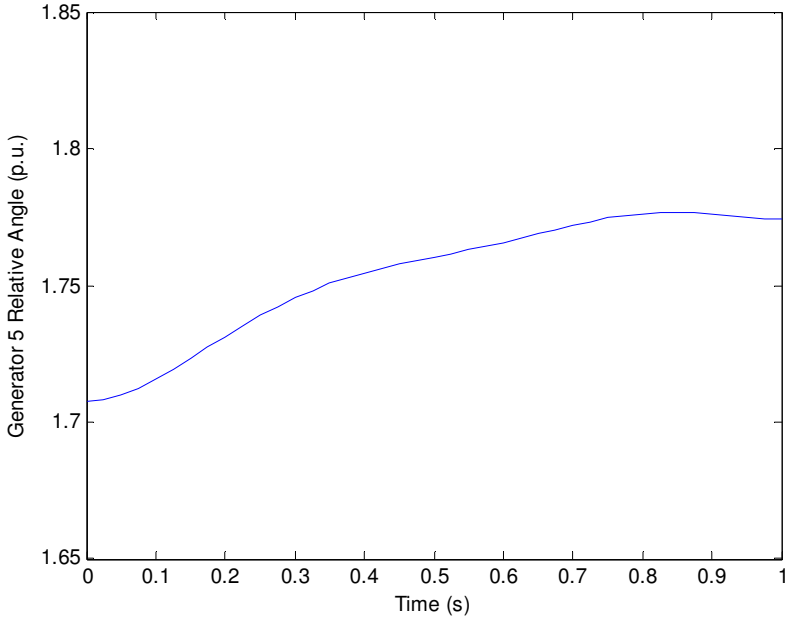

Fig. 4-42. Optimal Generator Relative Angle Trajectory

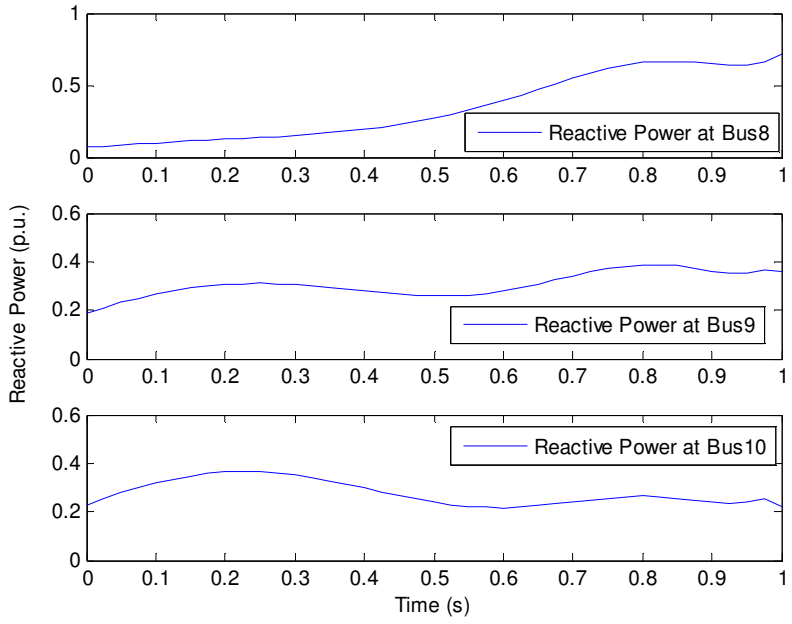

Fig. 4-43. Optimal Reactive Power Compensation Trajectories

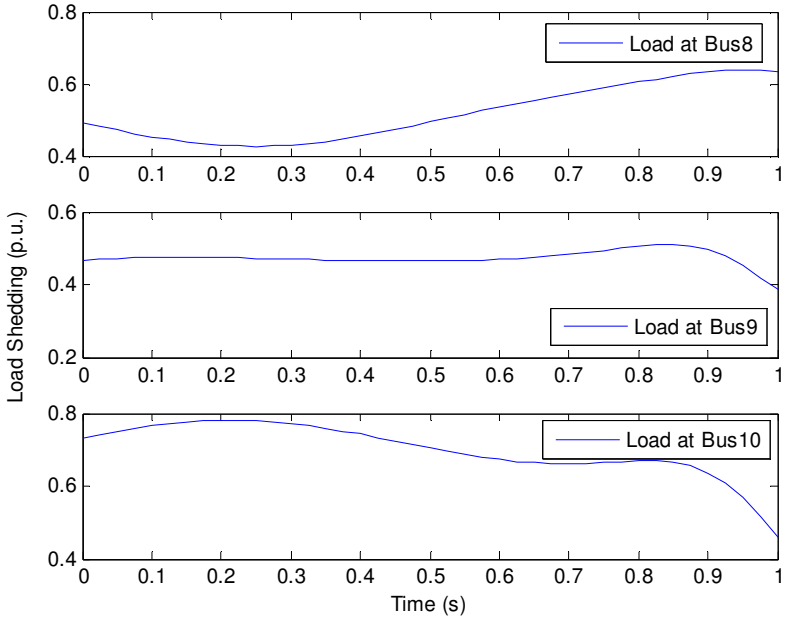

Fig. 4-44. Optimal Load Control Trajectories

The control delay effect is also studied for the IEEE 118-bus system. Different delays are tried to in this study, and it is found that the system failure could be avoided if the delay is less than 0.3 second. The maximum control amount with respect to delay effect is shown in Table 4-7, and generally more control amount is needed as control is increasingly delayed.

TABLE 4-7 MAXIMUM CONTROL AMOUNT WITH RESPECT TO DELAY

Delay (s)	ΔQ8 (p.u.)	ΔQ9 (p.u.)	ΔQ10 (p.u.)	ΔP8 (%)	ΔP9 (%)	ΔP10 (%)
0	0.7201	0.3883	0.3646	51.83	66.75	56.44
0.1	0.7035	0.3782	0.4056	52.48	63.61	61.24
0.2	0.7050	0.4813	0.5752	39.36	73.25	79.60

4.6 Summary

A coordinated control strategy to restore power system operating equilibrium after disturbances has been proposed. In this strategy, both post disturbance equilibrium conditions and dynamic transitions are considered. Power system control strategy is formulated as a trajectory optimization problem with both inequality and equality constraints, and an extended penalty function is applied to transform the original constrained problem into the optimization problem with equality constraints only. The two-point boundary value problem arising from necessary conditions in the trajectory optimization is solved by the finite difference method. As a result, the solution offered by the proposed method provides the optimal control actions consisting of control locations, amount, and time to restore the system operating state and satisfy transitional requirements after disturbances.

CHAPTER 5 CONCLUSION

5.1 Contributions

This dissertation proposes advanced computational and optimization techniques that can be applied to mitigate instabilities in power systems subject to disturbances. The research work has been integrated into a general framework for power system dynamic security analysis. The proposed methods cover strategies for both power system instability identification and control, and provide a fast simulation algorithm and coordinated optimization techniques to improve power system security.

The main contributions of the dissertation can be summarized as:

- Fast algorithm is proposed to identify power system dynamic behavior using the decoupled time domain simulation method. The computational efficiency of the dynamic equations is improved through decoupled time domain simulation method. For the large power systems, there may be tens of equations for each generator, and the total number of dynamic equations may be quite large. Thus the application of the decoupled time domain simulation method for the large system is promising.
- A coordinated control strategy combining control amount of a variety of control locations over time with the incorporation of power system dynamics is presented as a method for mitigation of power system instability by trajectory optimization.

- Power system dynamic performance is improved by the proposed method within the constraints imposed on system transition. In addition to the equilibrium conditions, the inequality constraints can also be considered. As one of the applications, power quality such as voltage dip in power system dynamics can be improved by imposing the inequality constraints. Cascading events may also be prevented by including transitional constraints in the trajectory optimization.

5.2 Further Research Directions

Based on the proposed research work in the dissertation, further research might be done in a variety of directions. Potential research focus could include the following areas:

- Inclusion of explicitly stability index in combination with equilibrium condition (as boundary conditions) in trajectory optimization
- Trajectory optimization with a mixture of continuous and discrete variables for better coordination of available control resources
- Global solution of trajectory optimization for better performance
- Power market related issues for dynamic security resources such as prices, allocation, etc

REFERENCES

[1] Vijay Vittal, "The future power engineering professor," in *Proc.2003 IEEE Power Engineering Society General Meeting*, pp. 127-129.

[2] G. S. Vassell, "Northeast Blackout of 1965," *IEEE Power Engineering Review*, vol. 11, pp. 4-8, Jan. 1991.

[3] U.S.-Canada Power System Outage Task Force, "Final Report on the August 14, 2003, Blackout in the United States and Canada: Causes and Recommendations," U.S. Department of Energy, Washington, D.C. April 2004.

[4] P. Fairley, "The unruly power grid," *IEEE Spectrum*, vol. 41, pp. 22-27, August 2004.

[5] Y. V. Makarov, V. I. Reshetov, A. Stroev, and I. Voropai, "Blackout prevention in the united states, Europe, and Russia," *Proceedings of the IEEE*, vol. 93, pp. 1942-1955, Nov. 2005.

[6] Richard J. Gilbert and Edward Kahn, *International comparisons of electricity regulation*. Cambridge ; New York: Cambridge University Press, 1996.

[7] P. Kundur, J. Paserba, V. Ajjarapu, G. Andersson, A. Bose, C. Canizares, N. Hatziargyriou, D. Hill, A. Stankovic, C. Taylor, T. Van Cutsem, and V. Vittal, "Definition and classification of power system stability IEEE/CIGRE joint task force on stability terms and definitions," *IEEE Transactions on Power Systems*, vol. 19, pp. 1387-1401, 2004.

[8] P. Kundur, *Power system stability and control*. New York: McGraw-Hill, 1994.

[9] Allen J. Wood and Bruce F. Wollenberg, *Power generation, operation, and control*. New York: Wiley, 1984.

[10] M. Huneault and F. D. Galiana, "A survey of the optimal power flow literature," *IEEE Transactions on Power Systems*, vol. 6, pp. 762-770, May 1991.

[11] T. Van Cutsem, "Voltage instability: phenomena, countermeasures, and analysis methods," *Proceedings of the IEEE*, vol. 88, pp. 208-227, Feb. 2000.

[12] Stephen Wiggins, *Introduction to applied nonlinear dynamical systems and chaos*, 2nd ed. New York: Springer, 2003.

[13] John Guckenheimer and Philip Holmes, *Nonlinear oscillations, dynamical systems and bifurcations of vector fields*. New York: Springer-Verlag, 1983.

[14] Thierry Van Cutsem and Costas Vournas, *Voltage stability of electric power systems*. Boston: Kluwer Academic Publishers, 1998.

[15] Claudio Canizares, "Voltage stability assessment: concepts, practices and tools," IEEE/Power Eng. Soc. Power Syst. Stability Subcommittee Special Publication, 2003.

[16] E. L. Allgower and Kurt Georg, *Numerical continuation methods : an introduction*. Berlin ; New York: Springer-Verlag, 1990.

[17] K. Iba, H. Suzuki, M. Egawa, and T. Watanabe, "Calculation of critical loading condition with nose curve using homotopy continuation method," *Power Systems, IEEE Transactions on*, vol. 6, pp. 584-593, May 1991.

[18] V. Ajjarapu and C. Christy, "The continuation power flow: a tool for steady state voltage stability analysis," *IEEE Transactions on Power Systems*, vol. 7, pp. 416-423, Feb. 1992.

[19] C. A. Canizares and F. L. Alvarado, "Point of collapse and continuation methods for large AC/DC systems," *IEEE Transactions on Power Systems*, vol. 8, pp. 1-8, Feb. 1993.

[20] Chiang Hsiao-Dong, A. J. Flueck, K. S. Shah, and N. Balu, "CPFLOW: a practical tool for tracing power system steady-state stationary behavior due to load and generation variations," *IEEE Transactions on Power Systems*, vol. 10, pp. 623-634, May 1995.

[21] A. J. Flueck and J. R. Dondeti, "A new continuation power flow tool for investigating the nonlinear effects of transmission branch parameter variations," *IEEE Transactions on Power Systems*, vol. 15, pp. 223-227, Feb. 2000.

[22] A. J. Flueck, Chiang Hsiao-Dong, and K. S. Shah, "Investigating the installed real power transfer capability of a large scale power system under a proposed multiarea interchange schedule using CPFLOW," *IEEE Transactions on Power Systems*, vol. 11, pp. 883-889, May 1996.

[23] Z. Feng, V. Ajjarapu, and B. Long, "Identification of voltage collapse through direct equilibrium tracing," *IEEE Transactions on Power Systems*, vol. 15, pp. 342-349, Feb. 2000.

[24] V. Ajjarapu, "Identification of steady-state voltage stability in power systems," *Proceedings of Third IASTED International Conference on High Technology in the Power Industry, pp. 244-247, Phoenix, Arizona, March 1988. International Journal of Energy Systems*, vol. 11, pp. 43-46, 1991.

[25] Lu Jin, Liu Chih-Wen, and J. S. Thorp, "New methods for computing a saddle-node bifurcation point for voltage stability analysis," *IEEE Transactions on Power Systems*, vol. 10, pp. 978-989, May 1995.

[26] K. Kim, H. Schattler, V. Venkatasubramanian, J. Zaborszky, and P. Hirsch, "Methods for calculating oscillations in large power systems," *IEEE Transactions on Power Systems*, vol. 12, pp. 1639-1648, Nov. 1997.

[27] I. Dobson and L. Lu, "New methods for computing a closest saddle node bifurcation and worst case load power margin for voltage collapse," *IEEE Transactions on Power Systems*, vol. 8, pp. 905-913, August 1993.

[28] P. A. Lof, T. Smed, G. Andersson, and D. J. Hill, "Fast calculation of a voltage stability index," *IEEE Transactions on Power Systems*, vol. 7, pp. 54-64, Feb. 1992.

[29] Hong Young-Huei, Pan Ching-Tsai, and Lin Wen-Wei, "Fast calculation of a voltage stability index of power systems," *IEEE Transactions on Power Systems*, vol. 12, pp. 1555-1560, Nov. 1997.

[30] Chiang Hsiao-Dong and R. Jean-Jumeau, "Toward a practical performance index for predicting voltage collapse in electric power systems," *IEEE Transactions on Power Systems*, vol. 10, pp. 584-592, May 1995.

[31] C. A. Canizares, A. C. Z. De Souza, and V. H. Quintana, "Comparison of performance indices for detection of proximity to voltage collapse," *IEEE Transactions on Power Systems*, vol. 11, pp. 1441-1450, August 1996.

[32] A. C. Z. de Souza, C. A. Canizares, and V. H. Quintana, "New techniques to speed up voltage collapse computations using tangent vectors," *IEEE Transactions on Power Systems*, vol. 12, pp. 1380-1387, August 1997.

[33] C. D. Vournas, "Voltage stability and controllability indices for multimachine power systems," *IEEE Transactions on Power Systems*, vol. 10, pp. 1183-1194, August 1995.

[34] A. Tiranuchit and R. J. Thomas, "A posturing strategy against voltage instabilities in electric power systems," *IEEE Transactions on Power Systems*, vol. 3, pp. 87-93, Feb. 1988.

[35] I. Dobson and L. Lu, "Computing an optimum direction in control space to avoid stable node bifurcation and voltage collapse in electric power systems," *IEEE Transactions on Automatic Control*, vol. 37, pp. 1616-1620, 1992.

[36] S. Greene, I. Dobson, and F. L. Alvarado, "Sensitivity of the loading margin to voltage collapse with respect to arbitrary parameters," *IEEE Transactions on Power Systems*, vol. 12, pp. 262-272, Feb. 1997.

[37] S. Greene, I. Dobson, and F. L. Alvarado, "Contingency ranking for voltage collapse via sensitivities from a single nose curve," *IEEE Transactions on Power Systems*, vol. 14, pp. 232-240, Feb. 1999.

[38] I. Dobson, F. Alvarado, and C. L. DeMarco, "Sensitivity of Hopf bifurcations to power system parameters," in *Proc.1992 31st IEEE Conference on Decision and Control*, pp. 2928-2933 vol.3.

[39] C. A. Cafizares, "Calculating optimal system parameters to maximize the distance to saddle-node bifurcations," *IEEE Transactions on Circuits and Systems I: Fundamental Theory and Applications* vol. 45, pp. 225-237, March 1998.

[40] Wu Qiang, D. H. Popovic, D. J. Hill, and C. J. Parker, "Voltage security enhancement via coordinated control," *IEEE Transactions on Power Systems*, vol. 16, pp. 127-135, Feb. 2001.

[41] Yuan Zhou and V. Ajjarapu, "Identification and tracing of voltage and oscillatory stability margins," in *Proc.2002 IEEE Power Engineering Society Winter Meeting* pp. 250-255 vol.1.

[42] J. Y. Astic, A. Bihain, and M. Jerosolimski, "The mixed Adams-BDF variable step size algorithm to simulate transient and long term phenomena in power systems," *IEEE Transactions on Power Systems*, vol. 9, pp. 929-935, May 1994.

[43] F. Iavernaro, M. La Scala, and F. Mazzia, "Boundary values methods for time-domain simulation of power system dynamic behavior," *IEEE Transactions on Circuits and Systems I: Fundamental Theory and Applications*, vol. 45, pp. 50-63, 1998.

[44] Liu Chih-Wen and J. S. Thorp, "New methods for computing power system dynamic response for real-time transient stability prediction," *IEEE Transactions on Circuits and Systems I: Fundamental Theory and Applications*, vol. 47, pp. 324-337, March 2000.

[45] H. R. Fankhauser, K. Aneros, A. A. Edris, and S. Torseng, "Advanced simulation techniques for the analysis of power system dynamics," *IEEE Computer Applications in Power*, vol. 3, pp. 31-36, October 1990.

[46] A. Kurita, H. Okubo, K. Oki, S. Agematsu, D. B. Klapper, N. W. Miller, W. W. Price, Jr., J. J. Sanchez-Gasca, K. A. Wirgau, and T. D. Younkins, "Multiple time-scale power system dynamic simulation," *IEEE Transactions on Power Systems*, vol. 8, pp. 216-223, Feb. 1993.

[47] M. Stubbe, A. Bihain, J. Deuse, and J. C. Baader, "STAG-a new unified software program for the study of the dynamic behaviour of electrical power systems," *IEEE Transactions on Power Systems*, vol. 4, pp. 129-138, Feb. 1989.

[48] Yuan Zhou and V. Ajjarapu, "Local parameterization approach for unified time domain simulation of power system dynamics," in *Proc.2002 IEEE Power Engineering Society Winter Meeting*, pp. 244-249.

[49] M. A. Pai, *Energy function analysis for power system stability*. Boston: Kluwer Academic Publishers, 1989.

[50] A. A. Fouad and Vijay Vittal, *Power system transient stability analysis using the transient energy function method*. Englewood Cliffs, N.J.: Prentice Hall, 1992.

[51] H. D. Chiang, "The BCU method for direct stability analysis of electric power systems: theory and applications," in *Systems and control theory for power systems*, *IMA volumes in mathematics and its applications v. 64*, J. H. Chow, P. V. Kokotoviâc, and R. J. Thomas, Eds. New York: Springer-Verlag, 1995, pp. 39-94.

[52] T. J. Overbye and C. L. De Marco, "Voltage security enhancement using energy based sensitivities," *IEEE Transactions on Power Systems*, vol. 6, pp. 1196-1202, August 1991.

[53] C. L. DeMarco and C. A. Canizares, "A vector energy function approach for security analysis of AC/DC systems," *IEEE Transactions on Power Systems*, vol. 7, pp. 1001-1011, August 1992.

[54] C. W. Taylor, "Concepts of undervoltage load shedding for voltage stability," *IEEE Transactions on Power Delivery,*, vol. 7, pp. 480-488, April 1992.

[55] T. Van Cutsem, "An approach to corrective control of voltage instability using simulation and sensitivity," *IEEE Transactions on Power Systems*, vol. 10, pp. 616-622, 1995.

[56] C. Moors and T. Van Cutsem, "Determination of optimal load shedding against voltage instability," in *Proc.1999 the 13th Power Systems Computation Conference*, Trondheim, Norway, pp. 993-1000.

[57] M Larsson, D. J. Hill, and G Olsson, "Emergency voltage control using search and predictive control," *International Journal of Electric Power and Energy Systems*, vol. 24, pp. 121-130, February 2002.

[58] J. Y. Wen, Q. H. Wu, D. R. Turner, S. J. Cheng, and J. Fitch, "Optimal coordinated voltage control for power system voltage stability," *IEEE Transactions on Power Systems*, vol. 19, pp. 1115-1122, May 2004.

[59] I.A. Hiskens and B. Gong, "Voltage stability enhancement via model predictive control of load," in *Proc.2004 the Symposium on Bulk Power System Dynamics and Control VI*, Cortina d'Ampezzo, Italy.

[60] E. De Tuglie, M. Dicorato, M. La Scala, and P. Scarpellini, "A corrective control for angle and voltage stability enhancement on the transient time-scale," *IEEE Transactions on Power Systems*, vol. 15, pp. 1345-1353, Nov. 2000.

[61] O. von Stryk and R. Bulirsch, "Direct and indirect methods for trajectory optimization," *Annals of Operations Research*, vol. 37, pp. 357-373, 1992.

[62] T. Van Cutsem and C. D. Vournas, "Voltage stability analysis in transient and mid-term time scales," *IEEE Transactions on Power Systems*, vol. 11, pp. 146-154, 1996.

[63] Dan Yang and V. Ajjarapu, "A decoupled method for power system time domain simulation via invariant subspace partition," in *Proc.2005 IEEE Power Engineering Society General Meeting*, pp. 1225-1230.

[64] Dan Yang and V. Ajjarapu, "A decoupled time-domain simulation method via invariant subspace partition for power system analysis," *IEEE Transactions on Power Systems*, vol. 21, pp. 11-18, Feb. 2006.

[65] P. M. Anderson and A. A. Fouad, *Power system control and stability*, Rev. printing. ed. New York: IEEE Press, 1994.

[66] Bo Long, "The detection of dynamic voltage collapse and transfer margin estimation," M.S. thesis, Iowa State University, 1997.

[67] Yuan Zhou, "Manifold based voltage stability boundary tracing, margin control optimization and time domain simulation," Ph.D. dissertation, Iowa State University, 2001.

[68] Xiaoyu Wen, "A novel approach for identification and tracing of oscillatory stability and damping ratio margin boundaries," Ph.D. dissertation, Iowa State University 2005.

[69] P. W. Sauer and M. A. Pai, "Power system steady-state stability and the load-flow Jacobian," *IEEE Transactions on Power Systems*, vol. 5, pp. 1374-1383, Nov. 1990.

[70] U. M. Ascher and Linda Ruth Petzold, *Computer methods for ordinary differential equations and differential-algebraic equations*. Philadelphia: Society for Industrial and Applied Mathematics, 1998.

[71] E. Hairer and G. Wanner, *Solving ordinary differential equations II: stiff and differential-algebraic problems*: Springer-Verlag, 1991.

[72] J. D. Lambert, *Numerical methods for ordinary differential systems : the initial value problem*. Chichester ; New York: Wiley, 1991.

[73] A. Iserles, *A first course in the numerical analysis of differential equations*. Cambridge ; New York: Cambridge University Press, 1996.

[74] P. Deuflhard and Folkmar Bornemann, *Scientific computing with ordinary differential equations*. New York: Springer, 2002.

[75] J.C. Butcher, "Numerical methods for ordinary differential equations in the 20th century," in *Numerical analysis: historical developments in the 20th century*, C. Brezinski and L. Wuytack, Eds.: Elsevier, 2001, pp. 449-477.

[76] Gene H. Golub and Charles F. Van Loan, *Matrix Computations*. Baltimore: Johns Hopkins University Press, 1983.

[77] G.M. Shroff and H.B. Keller, "Stabilization of unstable procedures: the recursive projection method," *SIAM Journal on Numerical Analysis*, vol. 30, pp. 1099-1120, August 1993.

[78] V. Janovsky and O. Liberda, "Continuation of invariant subspaces via the recursive projection method," *Applications of Mathematics*, vol. 48, pp. 241-255, 2003.

[79] Jorge Nocedal and Stephen J. Wright, *Numerical optimization*. New York: Springer, 1999.

[80] Arthur E. Bryson and Yu-Chi Ho, *Applied optimal control : optimization, estimation, and control*. New York: Hemisphere Pub. Corp., 1975.

[81] H. J. Sussmann and J. C. Willems, "300 years of optimal control: from the brachystochrone to the maximum principle," *IEEE Control Systems Magazine*, vol. 17, pp. 32-44, June 1997.

[82] Pablo Pedregal, *Introduction to optimization*. Berlin ; New York: Springer, 2004.

[83] John T. Betts, "Survey of numerical methods for trajectory optimization," *Journal of Guidance, Control, and Dynamics*, vol. 21, pp. 193-207, 1998.

[84] Narain G. Hingorani and Lazlo Gyugyi, *Understanding FACTS : concepts and technology of flexible AC transmission systems*. New York: IEEE Press, 2000.

[85] Yong-Hua Song and Allan Johns, *Flexible ac transmission systems (FACTS)*. London: Institution of Electrical Engineers, 1999.

[86] Enrique Acha, *FACTS : modelling and simulation in power networks*. Chichester ; Hoboken, NJ: Wiley, 2004.

[87] J. Eto, C. Goldman, G. Heffner, B. Kirby, J. Kueck, M. Kintner-Meyer, J. Dagle, T. Mount, W. Schultze, R. Thomas, and R. Zimmerman, "Innovative developments in load as a reliability resource," in *Proc.2002 IEEE Power Engineering Society Winter Meeting*, pp. 1002-1004.

[88] D. Backer, "Technologies for fast load control," in *Proc.2002 IEEE Power Engineering Society Winter Meeting*, pp. 999-1000.

[89] Ian A. Hiskens, "Load as a controllable resource for dynamic security enhancement," in *Proc.2006 IEEE Power Engineering Society General Meeting*.

[90] P. Lagonotte, J. C. Sabonnadiere, J. Y. Leost, and J. P. Paul, "Structural analysis of the electrical system: application to secondary voltage control in France," *IEEE Transactions on Power Systems*, vol. 4, pp. 479-486, May 1989.

[91] M. D. Ilic, Liu Xiaojun, G. Leung, M. Athans, C. Vialas, and P. Pruvot, "Improved secondary and new tertiary voltage control," *IEEE Transactions on Power Systems*, vol. 10, pp. 1851-1862, Nov. 1995.

[92] H. Lefebvre, D. Fragnier, J. Y. Boussion, P. Mallet, and M. Bulot, "Secondary coordinated voltage control system: feedback of EDF," in *Proc.2000 IEEE Power Engineering Society Summer Meeting*, pp. 290-295.

[93] S. Corsi, P. Marannino, N. Losignore, G. Moreschini, and G. Piccini, "Coordination between the reactive power scheduling function and the hierarchical voltage control

of the EHV ENEL system," *IEEE Transactions on Power Systems*, vol. 10, pp. 686-694, May 1995.

[94] J. L. Sancha, J. L. Fernandez, A. Cortes, and J. T. Abarca, "Secondary voltage control: analysis, solutions and simulation results for the Spanish transmission system," *IEEE Transactions on Power Systems*, vol. 11, pp. 630-638, May 1996.

[95] S. Corsi, M. Pozzi, C. Sabelli, and A. Serrani, "The coordinated automatic voltage control of the Italian transmission Grid-part I: reasons of the choice and overview of the consolidated hierarchical system," *IEEE Transactions on Power Systems*, vol. 19, pp. 1723-1732, November 2004.

[96] S. Corsi, M. Pozzi, M. Sforna, and G. Dell'Olio, "The coordinated automatic voltage control of the Italian transmission Grid-part II: control apparatuses and field performance of the consolidated hierarchical system," *IEEE Transactions on Power Systems*, vol. 19, pp. 1733-1741, November 2004.

[97] Brian C. Fabien, "An extended penalty function approach to the numerical solution of constrained optimal control problems," *Optimal Control Applications & Methods*, vol. 17, pp. 341-355, 1996.

[98] U. M. Ascher, Robert M. M. Mattheij, and R. D. Russell, *Numerical solution of boundary value problems for ordinary differential equations*. Englewood Cliffs, N.J.: Prentice Hall, 1988.

[99] Josef Stoer and Roland Bulirsch, *Introduction to numerical analysis*, 3rd ed. New York: Springer, 2002.

[100] J. R. Cash, "A survey of some global methods for solving two-point BVPs," *Applied Numerical Analysis and Computational Mathematics*, vol. 1, pp. 7-17, 2004.

APPENDIX A: TRAJECTORY OPTIMIZATION WITH Vref CONTROL

In addition to the reactive power compensation control and load control, generator reference voltage set point control of the exciter can also be applied as the control resource in the trajectory optimization. In this section, generator Vref control is demonstrated in the 3-bus power system. The voltage reference set points of the two generators are used to mitigate the instability. The results show that a new equilibrium can be restored by adjusting voltage reference set points. The bus voltage trajectories, the relative generator angle, and the control trajectories are shown in the following figures.

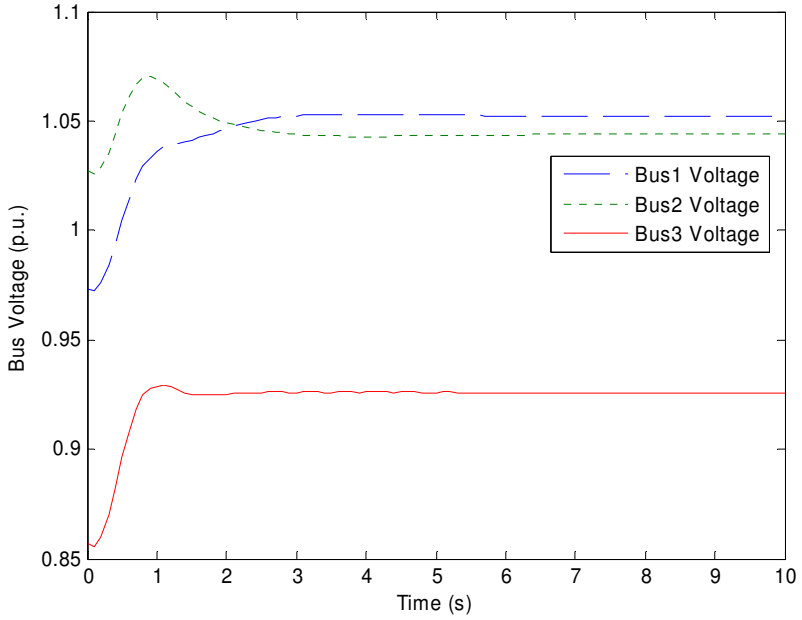

Fig. A-1. Bus Voltage Trajectories with Vref Control

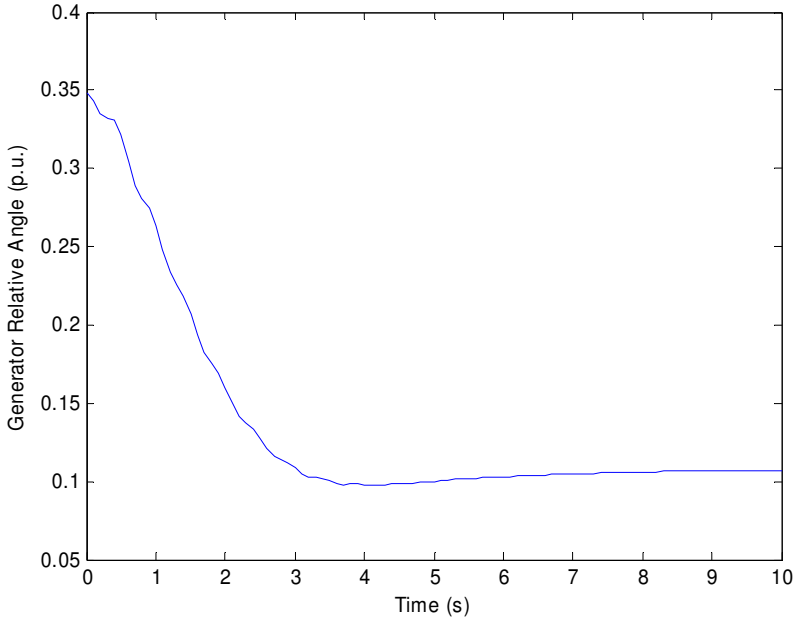

Fig. A-2. Generator Relative Angle with Vref Control

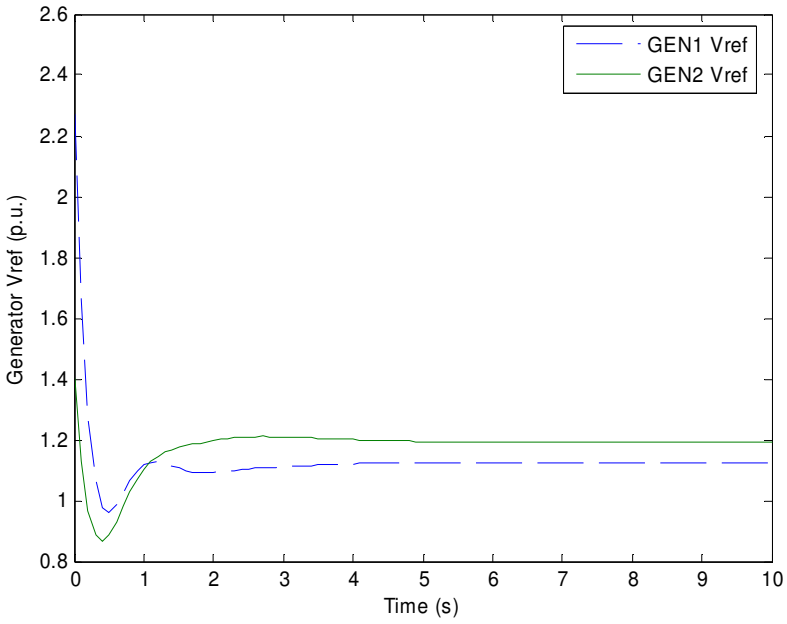

Fig. A-3. Generator Vref Control Trajectories

APPENDIX B: SYSTEM DATA

System Data for New England Power System:

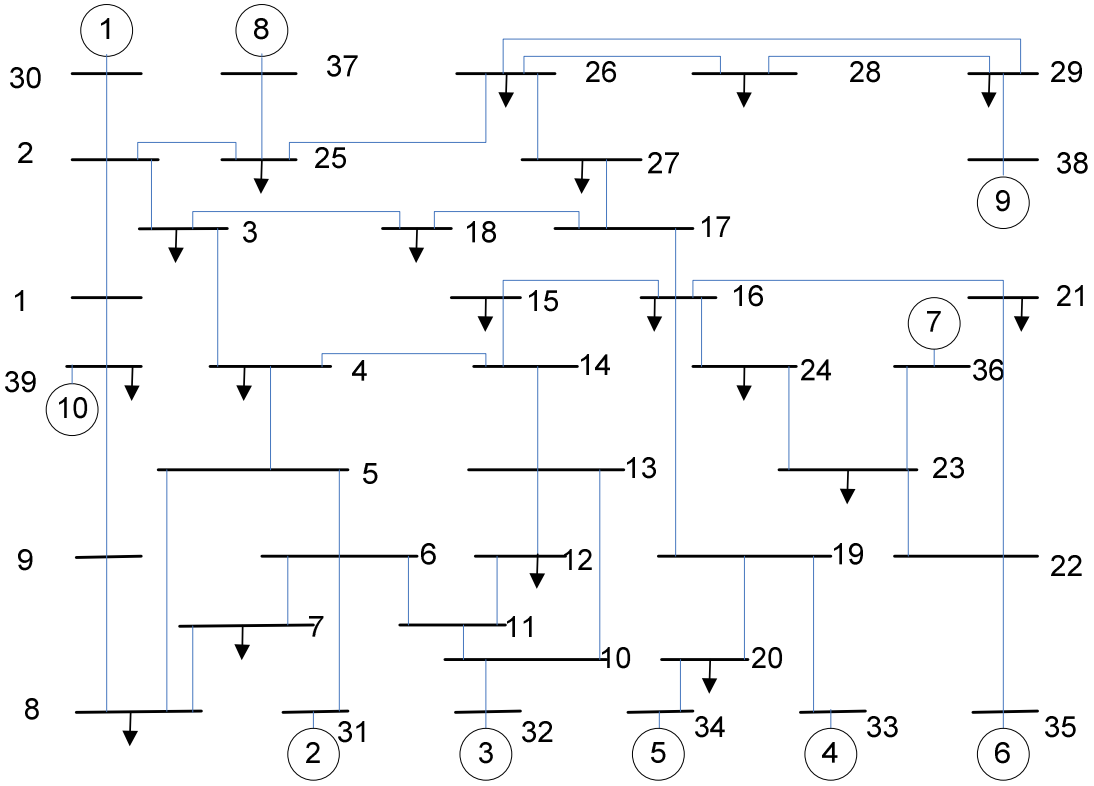

Fig. B-1. New England 39-Bus System One-Line Diagram

TABLE B-1 NEW ENGLAND SYSTEM POWER FLOW DATA I

Bus #	Voltage (p.u.)	Angle (degree)	P_{load} (MW)	Q_{load} (MVAR)	P_{gen} (MW)	Q_{gen} (MVAR)
1	1.0436	-13.39	0.00	0.00	0.00	0.00
2	1.0378	-11.21	0.00	0.00	0.00	0.00
3	1.0056	-13.87	322.00	122.40	0.00	0.00
4	0.9864	-14.01	500.00	184.00	0.00	0.00
5	0.9924	-12.24	0.00	0.00	0.00	0.00
6	0.9956	-11.40	0.00	0.00	0.00	0.00
7	0.9851	-13.75	233.80	84.00	0.00	0.00
8	0.9843	-14.32	522.00	176.00	0.00	0.00
9	1.0233	-14.58	0.00	0.00	0.00	0.00
10	1.0060	-9.41	0.00	0.00	0.00	0.00
11	1.0013	-10.10	0.00	0.00	0.00	0.00
12	0.9876	-10.23	8.50	88.00	0.00	0.00
13	1.0014	-10.23	0.00	0.00	0.00	0.00
14	0.9947	-12.18	0.00	0.00	0.00	0.00
15	0.9909	-13.33	320.00	153.00	0.00	0.00
16	1.0043	-12.16	329.40	132.30	0.00	0.00
17	1.0076	-13.11	0.00	0.00	0.00	0.00
18	1.0055	-13.85	158.00	30.00	0.00	0.00
19	1.0432	-7.90	0.00	0.00	0.00	0.00
20	0.9938	-9.51	680.00	103.00	0.00	0.00
21	1.0122	-9.83	274.00	115.00	0.00	0.00
22	1.0387	-5.44	0.00	0.00	0.00	0.00
23	1.0322	-5.65	247.50	84.60	0.00	0.00
24	1.0029	-12.07	308.60	92.20	0.00	0.00
25	1.0461	-10.01	224.00	47.20	0.00	0.00
26	1.0299	-11.38	139.00	47.00	0.00	0.00
27	1.0136	-13.39	281.00	75.50	0.00	0.00
28	1.0308	-8.00	206.00	27.60	0.00	0.00
29	1.0318	-5.22	283.50	126.90	0.00	0.00
30	1.0475	-8.96	0.00	0.00	230.00	206.87
31	0.9820	0.00	0.00	0.00	722.53	274.61
32	0.9831	-1.58	0.00	0.00	630.00	254.00
33	0.9972	-2.84	0.00	0.00	612.00	152.86
34	1.0123	-4.50	0.00	0.00	488.00	236.74
35	1.0493	-0.58	0.00	0.00	630.00	290.62
36	1.0635	2.00	0.00	0.00	540.00	148.33
37	1.0278	-3.42	0.00	0.00	520.00	48.40
38	1.0265	1.74	0.00	0.00	810.00	138.33

39	1.0300	-14.68	1104.00	250.00	1000.00	123.30

TABLE B-2 NEW ENGLAND SYSTEM POWER FLOW DATA II

From Bus	To Bus	Resistance (p.u.)	Reactance (p.u.)	Line Charge (p.u.)	Tap Ratio
1	2	0.003500	0.041100	0.69870	0.0000
1	39	0.002000	0.050000	0.37500	0.0000
1	39	0.002000	0.050000	0.37500	0.0000
2	3	0.001300	0.015100	0.25720	0.0000
2	25	0.007000	0.008600	0.14600	0.0000
3	4	0.001300	0.021300	0.22140	0.0000
3	18	0.001100	0.013300	0.21380	0.0000
4	5	0.000800	0.012800	0.13420	0.0000
4	14	0.000800	0.012900	0.13820	0.0000
5	6	0.000200	0.002600	0.04340	0.0000
5	8	0.000800	0.011200	0.14760	0.0000
6	7	0.000600	0.009200	0.11300	0.0000
6	11	0.000700	0.008200	0.13890	0.0000
7	8	0.000400	0.004600	0.07800	0.0000
8	9	0.002300	0.036300	0.38040	0.0000
9	39	0.001000	0.025000	1.20000	0.0000
10	11	0.000400	0.004300	0.07290	0.0000
10	13	0.000400	0.004300	0.07290	0.0000
13	14	0.000900	0.010100	0.17230	0.0000
14	15	0.001800	0.021700	0.36600	0.0000
15	16	0.000900	0.009400	0.17100	0.0000
16	17	0.000700	0.008900	0.13420	0.0000
16	19	0.001600	0.019500	0.30400	0.0000
16	21	0.000800	0.013500	0.25480	0.0000
16	24	0.000300	0.005900	0.06800	0.0000
17	18	0.000700	0.008200	0.13190	0.0000
17	27	0.001300	0.017300	0.32160	0.0000
21	22	0.000800	0.014000	0.25650	0.0000
22	23	0.000600	0.009600	0.18460	0.0000
23	24	0.002200	0.035000	0.36100	0.0000
25	26	0.003200	0.032300	0.51300	0.0000
26	27	0.001400	0.014700	0.23960	0.0000
26	28	0.004300	0.047400	0.78020	0.0000
26	29	0.005700	0.062500	1.02900	0.0000
28	29	0.001400	0.015100	0.24900	0.0000

2	30	0.000000	0.018100	0.00000	1.0250
6	31	0.000000	0.050000	0.00000	1.0700
6	31	0.000000	0.050000	0.00000	1.0700
10	32	0.000000	0.020000	0.00000	1.0700
12	11	0.001600	0.043500	0.00000	1.0060
12	13	0.001600	0.043500	0.00000	1.0060
19	20	0.000700	0.013800	0.00000	1.0600
19	33	0.000700	0.014200	0.00000	1.0700
20	34	0.000900	0.018000	0.00000	1.0250
22	35	0.000000	0.014300	0.00000	1.0250
23	36	0.000500	0.027200	0.00000	1.0000
25	37	0.000600	0.023200	0.00000	1.0250
29	38	0.000800	0.015600	0.00000	1.0250

TABLE B-3 NEW ENGLAND SYSTEM GENERATOR DATA I

Bus #	Xd	Xq	X'd	X'q	Rs	T'do	T'qo	Mg	Dg
30	0.1000	0.0690	0.0310	0.0690	0.0002	10.200	0.010	84.000	5.000
31	0.2590	0.2820	0.0700	0.1700	0.0002	6.5600	1.5000	60.600	5.000
32	0.2500	0.2370	0.0530	0.0880	0.0002	5.7000	1.5000	71.600	5.000
33	0.2620	0.2580	0.0440	0.1660	0.0002	5.6900	1.5000	57.200	5.000
34	0.6700	0.6200	0.1320	0.1660	0.0002	5.4000	0.4400	52.000	5.000
35	0.2540	0.2410	0.0500	0.0810	0.0002	7.3000	0.4000	69.600	5.000
36	0.2950	0.2920	0.0490	0.1860	0.0002	5.6600	1.5000	52.800	5.000
37	0.2900	0.2800	0.0570	0.0910	0.0010	6.7000	0.4100	48.600	5.000
38	0.2110	0.2050	0.0570	0.0590	0.0002	4.7900	1.9600	69.000	5.000
39	0.0200	0.0190	0.0060	0.0080	0.0002	7.0000	0.7000	1000.0	10.000

TABLE B-4 NEW ENGLAND SYSTEM GENERATOR DATA II

Bus #	Ke	Te	Se	Ka	Ta	Kf	Tf	Tch	Tg	Rg
30	1.0000	0.2500	0.0000	20.000	0.0600	0.0400	1.0000	1.6000	0.2000	0.0500
31	1.0000	0.4100	0.0000	40.000	0.0500	0.0600	0.5000	54.100	0.4500	0.0500
32	1.0000	0.5000	0.0000	40.000	0.0600	0.0800	1.0000	10.000	3.0000	0.0500
33	1.0000	0.5000	0.0000	40.000	0.0600	0.0800	1.0000	10.180	0.2400	0.0500
34	1.0000	0.7900	0.0000	30.000	0.0200	0.0300	1.0000	9.7900	0.1200	0.0500
35	1.0000	0.4700	0.0000	40.000	0.0200	0.0800	1.2500	10.000	3.0000	0.0500
36	1.0000	0.7300	0.0000	30.000	0.0200	0.0300	1.0000	7.6800	0.2000	0.0500
37	1.0000	0.5300	0.0000	40.000	0.0200	0.0900	1.2600	7.0000	3.0000	0.0500
38	1.0000	1.4000	0.0000	20.000	0.0200	0.0300	1.0000	6.1000	0.3800	0.0500
39	1.0000	1.0000	0.0000	20.000	0.0200	0.0300	1.0000	10.000	2.0000	0.0500

System Data for IEEE 118-Bus Power System:

TABLE B-5 IEEE 118-BUS SYSTEM POWER FLOW DATA I

Bus #	Voltage (p.u.)	Angle (degree)	P_{load} (MW)	Q_{load} (MVAR)	P_{gen} (MW)	Q_{gen} (MVAR)
1	0.9550	0.98	61.20	27.00	0.00	2.21
2	0.9708	1.81	24.00	9.00	0.00	0.00
3	0.9670	2.05	46.80	10.00	0.00	0.00
4	0.9980	6.38	36.00	12.00	-9.00	-13.69
5	1.0021	6.87	0.00	0.00	0.00	0.00
6	0.9900	3.81	62.40	22.00	0.00	19.19
7	0.9892	3.38	22.80	2.00	0.00	0.00
8	1.0150	12.45	42.00	5.00	-28.00	97.46
9	1.0399	19.88	30.50	10.00	0.00	0.00
10	1.0500	28.15	50.00	5.00	540.00	-33.99
11	0.9843	3.61	84.00	23.00	0.00	0.00
12	0.9900	3.11	56.40	10.00	102.00	98.60
13	0.9665	2.34	40.80	16.00	0.00	0.00
14	0.9831	2.68	16.80	1.00	0.00	0.00
15	0.9700	3.55	108.00	30.00	0.00	19.67
16	0.9822	3.28	30.00	10.00	0.00	0.00
17	0.9933	6.64	13.20	3.00	0.00	0.00
18	0.9730	4.02	72.00	34.00	0.00	35.09
19	0.9621	3.56	54.00	25.00	0.00	-8.00
20	0.9532	4.82	21.60	3.00	0.00	0.00
21	0.9523	6.88	16.80	8.00	0.00	0.00
22	0.9633	10.16	12.00	5.00	0.00	0.00
23	0.9972	16.41	8.40	3.00	0.00	0.00
24	0.9920	16.83	0.00	0.00	-13.00	-12.66
25	1.0500	24.32	0.00	0.00	264.00	53.31
26	1.0150	26.24	0.00	0.00	376.80	22.75
27	0.9680	8.99	74.40	13.00	-9.00	14.90
28	0.9608	6.84	20.40	7.00	0.00	0.00
29	0.9627	5.58	28.80	4.00	0.00	0.00
30	0.9806	12.52	0.00	0.00	0.00	0.00
31	0.9670	5.70	51.60	27.00	8.40	37.76
32	0.9630	8.33	70.80	23.00	0.00	-5.31
33	0.9693	3.82	27.60	9.00	0.00	0.00

34	0.9840	5.71	70.80	26.00	0.00	-4.09
35	0.9801	5.17	39.60	9.00	0.00	0.00
36	0.9800	5.16	37.20	17.00	0.00	12.74
37	0.9896	6.32	0.00	0.00	0.00	0.00
38	0.9537	12.38	0.00	0.00	0.00	0.00
39	0.9690	3.04	32.40	11.00	0.00	0.00
40	0.9700	2.22	24.00	23.00	-46.00	33.52
41	0.9658	1.94	44.40	10.00	0.00	0.00
42	0.9850	4.59	44.40	23.00	-59.00	50.55
43	0.9721	6.40	21.60	7.00	0.00	0.00
44	0.9763	10.54	19.20	8.00	0.00	0.00
45	0.9792	13.15	63.60	22.00	0.00	0.00
46	1.0050	16.75	33.60	10.00	22.80	3.60
47	1.0156	19.58	40.80	0.00	0.00	0.00
48	1.0199	18.79	24.00	11.00	0.00	0.00
49	1.0250	20.06	104.40	30.00	244.80	137.34
50	0.9997	17.62	20.40	4.00	0.00	0.00
51	0.9638	14.45	20.40	8.00	0.00	0.00
52	0.9532	13.30	21.60	5.00	0.00	0.00
53	0.9436	12.14	27.60	11.00	0.00	0.00
54	0.9550	13.28	135.60	32.00	57.60	11.30
55	0.9520	12.95	75.60	22.00	0.00	8.58
56	0.9540	13.16	100.80	18.00	0.00	8.18
57	0.9693	14.59	14.40	3.00	0.00	0.00
58	0.9569	13.55	14.40	3.00	0.00	0.00
59	0.9850	18.59	332.40	113.00	186.00	84.34
60	0.9927	23.26	93.60	3.00	0.00	0.00
61	0.9950	24.35	0.00	0.00	192.00	-40.23
62	0.9980	23.58	92.40	14.00	0.00	6.96
63	0.9671	22.78	0.00	0.00	0.00	0.00
64	0.9826	24.99	0.00	0.00	0.00	0.00
65	1.0050	28.96	0.00	0.00	469.20	137.36
66	1.0500	28.44	46.80	18.00	470.40	-8.02
67	1.0187	25.26	33.60	7.00	0.00	0.00
68	0.9996	29.66	0.00	0.00	0.00	0.00
69	1.0350	30.00	0.00	0.00	437.65	-73.43
70	0.9840	20.79	79.20	20.00	0.00	21.36
71	0.9868	20.16	0.00	0.00	0.00	0.00
72	0.9800	17.99	0.00	0.00	-12.00	-10.71
73	0.9910	19.95	0.00	0.00	-6.00	9.81
74	0.9580	20.06	81.60	27.00	0.00	2.92
75	0.9657	21.80	56.40	11.00	0.00	0.00

76	0.9430	20.95	81.60	36.00	0.00	14.32
77	1.0060	28.03	73.20	28.00	0.00	35.20
78	1.0028	27.74	85.20	26.00	0.00	0.00
79	1.0082	28.25	46.80	32.00	0.00	0.00
80	1.0400	31.40	156.00	26.00	572.40	104.03
81	0.9946	30.34	0.00	0.00	0.00	0.00
82	0.9846	29.68	64.80	27.00	0.00	0.00
83	0.9802	31.34	24.00	10.00	0.00	0.00
84	0.9774	34.73	13.20	7.00	0.00	0.00
85	0.9850	36.77	28.80	15.00	0.00	4.09
86	0.9858	35.15	25.20	10.00	0.00	0.00
87	1.0150	35.50	0.00	0.00	4.80	11.37
88	0.9853	40.91	57.60	10.00	0.00	0.00
89	1.0050	46.05	0.00	0.00	728.40	-13.34
90	0.9850	38.85	93.60	42.00	-85.00	65.53
91	0.9800	38.69	0.00	0.00	-10.00	-13.11
92	0.9900	38.95	78.00	10.00	0.00	1.92
93	0.9828	35.12	14.40	7.00	0.00	0.00
94	0.9867	32.37	36.00	16.00	0.00	0.00
95	0.9761	30.87	50.40	31.00	0.00	0.00
96	0.9884	30.33	45.60	15.00	0.00	0.00
97	1.0089	30.44	18.00	9.00	0.00	0.00
98	1.0224	30.26	40.80	8.00	0.00	0.00
99	1.0100	30.76	0.00	0.00	-42.00	-17.53
100	1.0170	32.26	44.40	18.00	302.40	125.05
101	0.9902	34.02	26.40	15.00	0.00	0.00
102	0.9884	37.18	6.00	3.00	0.00	0.00
103	0.9938	28.65	27.60	16.00	48.00	40.00
104	0.9710	25.47	45.60	25.00	0.00	15.01
105	0.9650	24.39	37.20	26.00	0.00	21.66
106	0.9599	24.22	51.60	16.00	0.00	0.00
107	0.9503	22.42	33.60	12.00	0.00	0.00
108	0.9473	23.32	2.40	1.00	0.00	0.00
109	0.9404	22.92	9.60	3.00	0.00	0.00
110	0.9266	22.27	46.80	30.00	0.00	0.00
111	0.9273	22.26	0.00	0.00	0.00	0.00
112	0.9110	21.14	30.00	13.00	0.00	0.00
113	0.9902	6.84	0.00	0.00	0.00	0.00
114	0.9596	7.92	9.60	3.00	0.00	0.00
115	0.9595	7.91	26.40	7.00	0.00	0.00
116	0.9999	29.66	0.00	0.00	0.00	0.00
117	0.9723	1.23	24.00	8.00	0.00	0.00

118	0.9480	20.84	39.60	15.00	0.00	0.00

TABLE B-6 IEEE 118-BUS SYSTEM POWER FLOW DATA II

From Bus	To Bus	Resistance (p.u.)	Reactance (p.u.)	Line Charge (p.u.)	Tap Ratio
1	2	0.030300	0.099900	0.02540	0.0000
1	3	0.012900	0.042400	0.01082	0.0000
2	12	0.018700	0.061600	0.01572	0.0000
3	5	0.024100	0.108000	0.02840	0.0000
3	12	0.048400	0.160000	0.04060	0.0000
4	5	0.001760	0.007980	0.00210	0.0000
4	11	0.020900	0.068800	0.01748	0.0000
5	6	0.011900	0.054000	0.01426	0.0000
8	5	0.000000	0.026700	0.00000	0.9850
5	11	0.020300	0.068200	0.01738	0.0000
6	7	0.004590	0.020800	0.00550	0.0000
7	12	0.008620	0.034000	0.00874	0.0000
8	9	0.002440	0.030500	1.16200	0.0000
8	30	0.004310	0.050400	0.51400	0.0000
9	10	0.002580	0.032200	1.23000	0.0000
11	12	0.005950	0.019600	0.00502	0.0000
11	13	0.022250	0.073100	0.01876	0.0000
12	14	0.021500	0.070700	0.01816	0.0000
12	16	0.021200	0.083400	0.02140	0.0000
12	117	0.032900	0.140000	0.03580	0.0000
13	15	0.074400	0.244400	0.06268	0.0000
14	15	0.059500	0.195000	0.05020	0.0000
15	17	0.013200	0.043700	0.04440	0.0000
15	19	0.012000	0.039400	0.01010	0.0000
15	33	0.038000	0.124400	0.03194	0.0000
16	17	0.045400	0.180100	0.04660	0.0000
17	18	0.012300	0.050500	0.01298	0.0000
30	17	0.000000	0.038800	0.00000	0.9600
17	31	0.047400	0.156300	0.03990	0.0000
17	113	0.009130	0.030100	0.00768	0.0000
18	19	0.011190	0.049300	0.01142	0.0000
19	20	0.025200	0.117000	0.02980	0.0000
19	34	0.075200	0.247000	0.06320	0.0000
20	21	0.018300	0.084900	0.02160	0.0000
21	22	0.020900	0.097000	0.02460	0.0000
22	23	0.034200	0.159000	0.04040	0.0000
23	24	0.013500	0.049200	0.04980	0.0000

23	25	0.015600	0.080000	0.08640	0.0000
23	32	0.031700	0.115300	0.11730	0.0000
24	70	0.002210	0.411500	0.10198	0.0000
24	72	0.048800	0.196000	0.04880	0.0000
26	25	0.000000	0.038200	0.00000	0.9600
25	27	0.031800	0.163000	0.17640	0.0000
26	30	0.007990	0.086000	0.90800	0.0000
27	28	0.019130	0.085500	0.02160	0.0000
27	32	0.022900	0.075500	0.01926	0.0000
27	115	0.016400	0.074100	0.01972	0.0000
28	29	0.023700	0.094300	0.02380	0.0000
29	31	0.010800	0.033100	0.00830	0.0000
30	38	0.004640	0.054000	0.42200	0.0000
31	32	0.029800	0.098500	0.02510	0.0000
32	113	0.061500	0.203000	0.05180	0.0000
32	114	0.013500	0.061200	0.01628	0.0000
33	37	0.041500	0.142000	0.03660	0.0000
34	36	0.008710	0.026800	0.00568	0.0000
34	37	0.002560	0.009400	0.00984	0.0000
34	43	0.041300	0.168100	0.04226	0.0000
35	36	0.002240	0.010200	0.00268	0.0000
35	37	0.011000	0.049700	0.01318	0.0000
38	37	0.000000	0.037500	0.00000	0.9350
37	39	0.032100	0.106000	0.02700	0.0000
37	40	0.059300	0.168000	0.04200	0.0000
38	65	0.009010	0.098600	1.04600	0.0000
39	40	0.018400	0.060500	0.01552	0.0000
40	41	0.014500	0.048700	0.01222	0.0000
40	42	0.055500	0.183000	0.04660	0.0000
41	42	0.041000	0.135000	0.03440	0.0000
42	49	0.071500	0.323000	0.08600	0.0000
42	49	0.071500	0.323000	0.08600	0.0000
43	44	0.060800	0.245400	0.06068	0.0000
44	45	0.022400	0.090100	0.02240	0.0000
45	46	0.040000	0.135600	0.03320	0.0000
45	49	0.068400	0.186000	0.04440	0.0000
46	47	0.038000	0.127000	0.03160	0.0000
46	48	0.060100	0.189000	0.04720	0.0000
47	49	0.019100	0.062500	0.01604	0.0000
47	69	0.084400	0.277800	0.07092	0.0000
48	49	0.017900	0.050500	0.01258	0.0000
49	50	0.026700	0.075200	0.01874	0.0000

49	51	0.048600	0.137000	0.03420	0.0000
49	54	0.073000	0.289000	0.07380	0.0000
49	54	0.086900	0.291000	0.07300	0.0000
49	66	0.018000	0.091900	0.02480	0.0000
49	66	0.018000	0.091900	0.02480	0.0000
49	69	0.098500	0.324000	0.08280	0.0000
50	57	0.047400	0.134000	0.03320	0.0000
51	52	0.020300	0.058800	0.01396	0.0000
51	58	0.025500	0.071900	0.01788	0.0000
52	53	0.040500	0.163500	0.04058	0.0000
53	54	0.026300	0.122000	0.03100	0.0000
54	55	0.016900	0.070700	0.02020	0.0000
54	56	0.002750	0.009550	0.00732	0.0000
54	59	0.050300	0.229300	0.05980	0.0000
55	56	0.004880	0.015100	0.00374	0.0000
55	59	0.047390	0.215800	0.05646	0.0000
56	57	0.034300	0.096600	0.02420	0.0000
56	58	0.034300	0.096600	0.02420	0.0000
56	59	0.082500	0.251000	0.05690	0.0000
56	59	0.080300	0.239000	0.05360	0.0000
59	60	0.031700	0.145000	0.03760	0.0000
59	61	0.032800	0.150000	0.03880	0.0000
63	59	0.000000	0.038600	0.00000	0.9600
60	61	0.002640	0.013500	0.01456	0.0000
60	62	0.012300	0.056100	0.01468	0.0000
61	62	0.008240	0.037600	0.00980	0.0000
64	61	0.000000	0.026800	0.00000	0.9850
62	66	0.048200	0.218000	0.05780	0.0000
62	67	0.025800	0.117000	0.03100	0.0000
63	64	0.001720	0.020000	0.21600	0.0000
64	65	0.002690	0.030200	0.38000	0.0000
65	66	0.000000	0.037000	0.00000	0.9350
65	68	0.001380	0.016000	0.63800	0.0000
66	67	0.022400	0.101500	0.02682	0.0000
68	69	0.000000	0.037000	0.00000	0.9350
68	81	0.001750	0.020200	0.80800	0.0000
68	116	0.000340	0.004050	0.16400	0.0000
69	70	0.030000	0.127000	0.12200	0.0000
69	75	0.040500	0.122000	0.12400	0.0000
69	77	0.030900	0.101000	0.10380	0.0000
70	71	0.008820	0.035500	0.00878	0.0000
70	74	0.040100	0.132300	0.03368	0.0000

70	75	0.042800	0.141000	0.03600	0.0000
71	72	0.044600	0.180000	0.04444	0.0000
71	73	0.008660	0.045400	0.01178	0.0000
74	75	0.012300	0.040600	0.01034	0.0000
75	77	0.060100	0.199900	0.04978	0.0000
75	118	0.014500	0.048100	0.01198	0.0000
76	77	0.044400	0.148000	0.03680	0.0000
76	118	0.016400	0.054400	0.01356	0.0000
77	78	0.003760	0.012400	0.01264	0.0000
77	80	0.017000	0.048500	0.04720	0.0000
77	80	0.029400	0.105000	0.02280	0.0000
77	82	0.029800	0.085300	0.08174	0.0000
78	79	0.005460	0.024400	0.00648	0.0000
79	80	0.015600	0.070400	0.01870	0.0000
81	80	0.000000	0.037000	0.00000	0.9350
80	96	0.035600	0.182000	0.04940	0.0000
80	97	0.018300	0.093400	0.02540	0.0000
80	98	0.023800	0.108000	0.02860	0.0000
80	99	0.045400	0.206000	0.05460	0.0000
82	83	0.011200	0.036650	0.03796	0.0000
82	96	0.016200	0.053000	0.05440	0.0000
83	84	0.062500	0.132000	0.02580	0.0000
83	85	0.043000	0.148000	0.03480	0.0000
84	85	0.030200	0.064100	0.01234	0.0000
85	86	0.035000	0.123000	0.02760	0.0000
85	88	0.020000	0.102000	0.02760	0.0000
85	89	0.023900	0.173000	0.04700	0.0000
86	87	0.028280	0.207400	0.04450	0.0000
88	89	0.013900	0.071200	0.01934	0.0000
89	90	0.051800	0.188000	0.05280	0.0000
89	90	0.023800	0.099700	0.10600	0.0000
89	92	0.009900	0.050500	0.05480	0.0000
89	92	0.039300	0.158100	0.04140	0.0000
90	91	0.025400	0.083600	0.02140	0.0000
91	92	0.038700	0.127200	0.03268	0.0000
92	93	0.025800	0.084800	0.02180	0.0000
92	94	0.048100	0.158000	0.04060	0.0000
92	100	0.064800	0.295000	0.04720	0.0000
92	102	0.012300	0.055900	0.01464	0.0000
93	94	0.022300	0.073200	0.01876	0.0000
94	95	0.013200	0.043400	0.01110	0.0000
94	96	0.026900	0.086900	0.02300	0.0000

94	100	0.017800	0.058000	0.06040	0.0000
95	96	0.017100	0.054700	0.01474	0.0000
96	97	0.017300	0.088500	0.02400	0.0000
98	100	0.039700	0.179000	0.04760	0.0000
99	100	0.018000	0.081300	0.02160	0.0000
100	101	0.027700	0.126200	0.03280	0.0000
100	103	0.016000	0.052500	0.05360	0.0000
100	104	0.045100	0.204000	0.05410	0.0000
100	106	0.060500	0.229000	0.06200	0.0000
101	102	0.024600	0.112000	0.02940	0.0000
103	104	0.046600	0.158400	0.04070	0.0000
103	105	0.053500	0.162500	0.04080	0.0000
103	110	0.039060	0.181300	0.04610	0.0000
104	105	0.009940	0.037800	0.00986	0.0000
105	106	0.014000	0.054700	0.01434	0.0000
105	107	0.053000	0.183000	0.04720	0.0000
105	108	0.026100	0.070300	0.01844	0.0000
106	107	0.053000	0.183000	0.04720	0.0000
108	109	0.010500	0.028800	0.00760	0.0000
109	110	0.027800	0.076200	0.02020	0.0000
110	111	0.022000	0.075500	0.02000	0.0000
110	112	0.024700	0.064000	0.06200	0.0000
114	115	0.002300	0.010400	0.00276	0.0000

TABLE B-7 IEEE 118-BUS SYSTEM GENERATOR DATA I

Bus #	Xd	Xq	X'd	X'q	Rs	T'do	T'qo	Mg	Dg
1	0.1000	0.0690	0.0310	0.0690	0.0002	10.200	0.010	84.000	5.000
4	1.2590	1.2820	0.0700	0.1700	0.0002	6.5600	1.5000	60.600	5.000
6	1.2500	1.2370	0.0530	0.0880	0.0002	5.7000	1.5000	71.600	5.000
8	1.2620	1.2580	0.0440	0.1660	0.0002	5.6900	1.5000	57.200	5.000
10	1.6700	1.6200	0.1320	0.1660	0.0002	5.4000	0.4400	52.000	5.000
12	1.2540	1.2410	0.0500	0.0810	0.0002	7.3000	0.4000	69.600	5.000
15	1.2950	1.2920	0.0490	0.1860	0.0002	5.6600	1.5000	52.800	5.000
18	1.2900	1.2800	0.0570	0.0910	0.0010	6.7000	0.4100	48.600	5.000
19	1.2110	1.2050	0.0570	0.0590	0.0002	4.7900	1.9600	69.000	5.000
24	0.0200	0.0190	0.0060	0.0080	0.0002	7.0000	0.7000	1000.0	10.00
25	0.1000	0.0690	0.0310	0.0690	0.0002	10.200	0.010	84.000	5.000
26	1.2590	1.2820	0.0700	0.1700	0.0002	6.5600	1.5000	60.600	5.000
27	1.2500	1.2370	0.0530	0.0880	0.0002	5.7000	1.5000	71.600	5.000
31	1.2620	1.2580	0.0440	0.1660	0.0002	5.6900	1.5000	57.200	5.000

32	1.6700	1.6200	0.1320	0.1660	0.0002	5.4000	0.4400	52.000	5.000
34	1.2540	1.2410	0.0500	0.0810	0.0002	7.3000	0.4000	69.600	5.000
36	1.2950	1.2920	0.0490	0.1860	0.0002	5.6600	1.5000	52.800	5.000
40	1.2900	1.2800	0.0570	0.0910	0.0010	6.7000	0.4100	48.600	5.000
42	1.2110	1.2050	0.0570	0.0590	0.0002	4.7900	1.9600	69.000	5.000
46	0.0200	0.0190	0.0060	0.0080	0.0002	7.0000	0.7000	1000.0	10.00
49	0.1000	0.0690	0.0310	0.0690	0.0002	10.200	0.010	84.000	5.000
54	1.2590	1.2820	0.0700	0.1700	0.0002	6.5600	1.5000	60.600	5.000
55	1.2500	1.2370	0.0530	0.0880	0.0002	5.7000	1.5000	71.600	5.000
56	1.2620	1.2580	0.0440	0.1660	0.0002	5.6900	1.5000	57.200	5.000
59	1.6700	1.6200	0.1320	0.1660	0.0002	5.4000	0.4400	52.000	5.000
61	1.2540	1.2410	0.0500	0.0810	0.0002	7.3000	0.4000	69.600	5.000
62	1.2950	1.2920	0.0490	0.1860	0.0002	5.6600	1.5000	52.800	5.000
65	1.2900	1.2800	0.0570	0.0910	0.0010	6.7000	0.4100	48.600	5.000
66	1.2110	1.2050	0.0570	0.0590	0.0002	4.7900	1.9600	69.000	5.000
69	0.0200	0.0190	0.0060	0.0080	0.0002	7.0000	0.7000	1000.0	10.00
70	0.1000	0.0690	0.0310	0.0690	0.0002	10.200	0.010	84.000	5.000
72	1.2590	1.2820	0.0700	0.1700	0.0002	6.5600	1.5000	60.600	5.000
73	1.2500	1.2370	0.0530	0.0880	0.0002	5.7000	1.5000	71.600	5.000
74	1.2620	1.2580	0.0440	0.1660	0.0002	5.6900	1.5000	57.200	5.000
76	1.6700	1.6200	0.1320	0.1660	0.0002	5.4000	0.4400	52.000	5.000
77	1.2540	1.2410	0.0500	0.0810	0.0002	7.3000	0.4000	69.600	5.000
80	1.2950	1.2920	0.0490	0.1860	0.0002	5.6600	1.5000	52.800	5.000
85	1.2900	1.2800	0.0570	0.0910	0.0010	6.7000	0.4100	48.600	5.000
87	1.2110	1.2050	0.0570	0.0590	0.0002	4.7900	1.9600	69.000	5.000
89	0.0200	0.0190	0.0060	0.0080	0.0002	7.0000	0.7000	1000.0	10.00
90	0.1000	0.0690	0.0310	0.0690	0.0002	10.200	0.010	84.000	5.000
91	1.2590	1.2820	0.0700	0.1700	0.0002	6.5600	1.5000	60.600	5.000
92	1.2500	1.2370	0.0530	0.0880	0.0002	5.7000	1.5000	71.600	5.000
99	1.2620	1.2580	0.0440	0.1660	0.0002	5.6900	1.5000	57.200	5.000
100	1.6700	1.6200	0.1320	0.1660	0.0002	5.4000	0.4400	52.000	5.000
103	1.2540	1.2410	0.0500	0.0810	0.0002	7.3000	0.4000	69.600	5.000
104	1.2950	1.2920	0.0490	0.1860	0.0002	5.6600	1.5000	52.800	5.000
105	1.2900	1.2800	0.0570	0.0910	0.0010	6.7000	0.4100	48.600	5.000

TABLE B-8 IEEE 118-BUS SYSTEM GENERATOR DATA II

Bus #	Ke	Te	Se	Ka	Ta	Kf	Tf	Tch	Tg	Rg
1	1.0000	0.2500	0.0000	20.000	0.0600	0.0400	1.0000	1.6000	0.2000	0.0500
4	1.0000	0.4100	0.0000	40.000	0.0500	0.0600	0.5000	54.100	0.4500	0.0500
6	1.0000	0.5000	0.0000	40.000	0.0600	0.0800	1.0000	10.000	3.0000	0.0500

8	1.0000	0.5000	0.0000	40.000	0.0600	0.0800	1.0000	10.180	0.2400	0.0500
10	1.0000	0.7900	0.0000	30.000	0.0200	0.0300	1.0000	9.7900	0.1200	0.0500
12	1.0000	0.4700	0.0000	40.000	0.0200	0.0800	1.2500	10.000	3.0000	0.0500
15	1.0000	0.7300	0.0000	30.000	0.0200	0.0300	1.0000	7.6800	0.2000	0.0500
18	1.0000	0.5300	0.0000	40.000	0.0200	0.0900	1.2600	7.0000	3.0000	0.0500
19	1.0000	1.4000	0.0000	20.000	0.0200	0.0300	1.0000	6.1000	0.3800	0.0500
24	1.0000	1.0000	0.0000	20.000	0.0200	0.0300	1.0000	10.000	2.0000	0.0500
25	1.0000	0.2500	0.0000	20.000	0.0600	0.0400	1.0000	1.6000	0.2000	0.0500
26	1.0000	0.4100	0.0000	40.000	0.0500	0.0600	0.5000	54.100	0.4500	0.0500
27	1.0000	0.5000	0.0000	40.000	0.0600	0.0800	1.0000	10.000	3.0000	0.0500
31	1.0000	0.5000	0.0000	40.000	0.0600	0.0800	1.0000	10.180	0.2400	0.0500
32	1.0000	0.7900	0.0000	30.000	0.0200	0.0300	1.0000	9.7900	0.1200	0.0500
34	1.0000	0.4700	0.0000	40.000	0.0200	0.0800	1.2500	10.000	3.0000	0.0500
36	1.0000	0.7300	0.0000	30.000	0.0200	0.0300	1.0000	7.6800	0.2000	0.0500
40	1.0000	0.5300	0.0000	40.000	0.0200	0.0900	1.2600	7.0000	3.0000	0.0500
42	1.0000	1.4000	0.0000	20.000	0.0200	0.0300	1.0000	6.1000	0.3800	0.0500
46	1.0000	1.0000	0.0000	20.000	0.0200	0.0300	1.0000	10.000	2.0000	0.0500
49	1.0000	0.2500	0.0000	20.000	0.0600	0.0400	1.0000	1.6000	0.2000	0.0500
54	1.0000	0.4100	0.0000	40.000	0.0500	0.0600	0.5000	54.100	0.4500	0.0500
55	1.0000	0.5000	0.0000	40.000	0.0600	0.0800	1.0000	10.000	3.0000	0.0500
56	1.0000	0.5000	0.0000	40.000	0.0600	0.0800	1.0000	10.180	0.2400	0.0500
59	1.0000	0.7900	0.0000	30.000	0.0200	0.0300	1.0000	9.7900	0.1200	0.0500
61	1.0000	0.4700	0.0000	40.000	0.0200	0.0800	1.2500	10.000	3.0000	0.0500
62	1.0000	0.7300	0.0000	30.000	0.0200	0.0300	1.0000	7.6800	0.2000	0.0500
65	1.0000	0.5300	0.0000	40.000	0.0200	0.0900	1.2600	7.0000	3.0000	0.0500
66	1.0000	1.4000	0.0000	20.000	0.0200	0.0300	1.0000	6.1000	0.3800	0.0500
69	1.0000	1.0000	0.0000	20.000	0.0200	0.0300	1.0000	10.000	2.0000	0.0500
70	1.0000	0.2500	0.0000	20.000	0.0600	0.0400	1.0000	1.6000	0.2000	0.0500
72	1.0000	0.4100	0.0000	40.000	0.0500	0.0600	0.5000	54.100	0.4500	0.0500
73	1.0000	0.5000	0.0000	40.000	0.0600	0.0800	1.0000	10.000	3.0000	0.0500
74	1.0000	0.5000	0.0000	40.000	0.0600	0.0800	1.0000	10.180	0.2400	0.0500
76	1.0000	0.7900	0.0000	30.000	0.0200	0.0300	1.0000	9.7900	0.1200	0.0500
77	1.0000	0.4700	0.0000	40.000	0.0200	0.0800	1.2500	10.000	3.0000	0.0500
80	1.0000	0.7300	0.0000	30.000	0.0200	0.0300	1.0000	7.6800	0.2000	0.0500
85	1.0000	0.5300	0.0000	40.000	0.0200	0.0900	1.2600	7.0000	3.0000	0.0500
87	1.0000	1.4000	0.0000	20.000	0.0200	0.0300	1.0000	6.1000	0.3800	0.0500
89	1.0000	1.0000	0.0000	20.000	0.0200	0.0300	1.0000	10.000	2.0000	0.0500
90	1.0000	0.2500	0.0000	20.000	0.0600	0.0400	1.0000	1.6000	0.2000	0.0500
91	1.0000	0.4100	0.0000	40.000	0.0500	0.0600	0.5000	54.100	0.4500	0.0500
92	1.0000	0.5000	0.0000	40.000	0.0600	0.0800	1.0000	10.000	3.0000	0.0500
99	1.0000	0.5000	0.0000	40.000	0.0600	0.0800	1.0000	10.180	0.2400	0.0500
100	1.0000	0.7900	0.0000	30.000	0.0200	0.0300	1.0000	9.7900	0.1200	0.0500

103	1.0000	0.4700	0.0000	40.000	0.0200	0.0800	1.2500	10.000	3.0000	0.0500
104	1.0000	0.7300	0.0000	30.000	0.0200	0.0300	1.0000	7.6800	0.2000	0.0500
105	1.0000	0.5300	0.0000	40.000	0.0200	0.0900	1.2600	7.0000	3.0000	0.0500

ACKNOWLEDGEMENTS

This dissertation is accomplished under the help of many people whom I am greatly indebted to. I would like to thank major professor, Dr. Ajjarapu, for help and support. I would like to thank my committee members, Dr. Zhijun Wu, Dr. James D. McCalley, Dr. Zhengdao Wang, and Dr. Arne Hallam for all the comments, discussions, and encouragement on the research work. I am grateful to Dr. Wu for his knowledge, patience, and inspiration.

I am grateful to Tao Jin from University of Rochester for the valuable help and discussions on mathematical ideas, concepts and theories. I appreciate very much the help on the numerical algorithm from Dr. René Lamour in Berlin.

I want to thank all the friends in electrical engineering department for the kindly help, and for the great atmosphere in the research and in the life.

Finally, I wish to express my gratitude to my family. My late grandma always takes care of her eldest grandson, and my parents give me great support all the time. My brother brings a lot of joy and fun. At last, I want to thank my wife Yanni for her love, for her understanding, for her sacrifices, and for sharing the lovely life with me.